Integrated Ocean Drilling Program
Expedition 319 Preliminary Report

NanTroSEIZE Stage 2:
NanTroSEIZE riser/riserless observatory

10 May–31 August 2009

Demian Saffer, Lisa McNeill, Eiichiro Araki, Tim Byrne,
Nobuhisa Eguchi, Sean Toczko, Kyoma Takahashi, and the
Expedition 319 Scientists

Published by
Integrated Ocean Drilling Program Management International, Inc.,
for the Integrated Ocean Drilling Program

Publisher's notes

Material in this publication may be copied without restraint for library, abstract service, educational, or personal research purposes; however, this source should be appropriately acknowledged. Core samples and the wider set of data from the science program covered in this report are under moratorium and accessible only to Science Party members until 31 August 2010.

Citation:
Saffer, D., McNeill, L., Araki, E., Byrne, T., Eguchi, N., Toczko, S., Takahashi, K., and the Expedition 319 Scientists, 2009. NanTroSEIZE Stage 2: NanTroSEIZE riser/riserless observatory. *IODP Prel. Rept.,* 319. doi:10.2204/iodp.pr.319.2009

Distribution:
Electronic copies of this series may be obtained from the Integrated Ocean Drilling Program (IODP) Scientific Publications homepage on the World Wide Web at **www.iodp.org/scientific-publications/.**

This publication was prepared by the Japanese Implementing Organization, Center for Deep Earth Exploration (CDEX) at the Japan Agency for Marine-Earth Science and Technology (JAMSTEC), as an account of work performed under the international Integrated Ocean Drilling Program (IODP), which is managed by IODP Management International (IODP-MI), Inc. Funding for the program is provided by the following agencies:

National Science Foundation (NSF), United States

Ministry of Education, Culture, Sports, Science and Technology (MEXT), Japan

European Consortium for Ocean Research Drilling (ECORD)

Ministry of Science and Technology (MOST), People's Republic of China

Korea Institute of Geoscience and Mineral Resources (KIGAM)

Australian Research Council (ARC) and New Zealand Institute for Geological and Nuclear Sciences (GNS), Australian/New Zealand Consortium

Ministry of Earth Sciences (MoES), India

Disclaimer

Any opinions, findings, and conclusions or recommendations expressed in this publication are those of the author(s) and do not necessarily reflect the views of the participating agencies, IODP Management International, Inc., or Japan Agency for Marine-Earth Science and Technology.

November 2009

Expedition 319 participants

Expedition 319 scientists

Eiichiro Araki (4–25 June, 17–27 July, and 9–31 August 2009)
Co-Chief Scientist/VSP Specialist
Earthquake and Tsunami Research Project for Disaster Prevention
Japan Agency for Marine-Earth Science and Technology
2-15 Natsushima-cho, Yokosuka
Kanagawa 237-0061
Japan
araki@jamstec.go.jp

Tim Byrne (4 June–17 July 2009)
Co-Chief Scientist
Center for Integrative Geosciences
University of Connecticut
U-2045, 354 Mansfield Road
Storrs CT 06269
USA
tim.byrne@uconn.edu

Lisa McNeill (25 June–9 August 2009)
Co-Chief Scientist
School of Ocean and Earth Science
National Oceanography Centre, Southampton
University of Southampton
Southampton SO14 3ZH
United Kingdom
lcmn@noc.soton.ac.uk

Demian Saffer (17 July–31 August 2009)
Co-Chief Scientist
The Pennsylvania State University
0310 Deike Building
University Park PA 16802
USA
dsaffer@geosc.psu.edu

Nobuhisa Eguchi (5 May–8 June and 25 June–17 July 2009)
Expedition Project Manager
Center for Deep Earth Exploration
Japan Agency for Marine-Earth Science and Technology
3173-25 Showa-machi
Kanazawa-ku, Yokohama
Kanagawa 236-0001
Japan
neguchi@jamtec.go.jp

Kyoma Takahashi (4 June–25 June 2009)
Expedition Project Manager
Center for Deep Earth Exploration
Japan Agency for Marine-Earth Science and Technology
3173-25 Showa-machi
Kanazawa-ku, Yokohama
Kanagawa 236-0001
Japan
kyoma@jamstec.go.jp

Sean Toczko (17 July–31 August 2009)
Expedition Project Manager
Center for Deep Earth Exploration
Japan Agency for Marine-Earth Science and Technology
3173-25 Showa-machi
Kanazawa-ku, Yokohama
Kanagawa 236-0001
Japan
sean@jamstec.go.jp

Moe Kyaw Thu
Logging Staff Scientist
Center for Deep Earth Exploration
Japan Agency for Marine-Earth Science and Technology
3173-25 Showa-machi
Kanazawa-ku, Yokohama
Kanagawa 236-0001
Japan
moe@jamstec.go.jp

Yoshinori Sanada
Logging Staff Scientist/VSP Coordinator
Center for Deep Earth Exploration
Japan Agency for Marine-Earth Science and Technology
3173-25 Showa-machi
Kanazawa-ku, Yokohama
Kanagawa 236-0001
Japan
sanada@jamstec.go.jp

David Boutt (4 June–20 July 2009)
Physical Properties/Downhole Measurements Specialist
Department of Geosciences
University of Massachusetts, Amherst
611 North Pleasant Street, 233 Morrill Center
Amherst MA 01002
USA
dboutt@geo.umass.edu

David Buchs (17 July–31 August 2009)
Sedimentologist
Australian National University
Research School of Earth Sciences
61 Mills Road, Building J1
0200 Canberra
Australia
david.buchs@anu.edu.au

Christophe Buret (4 June–17 July 2009)
Sedimentologist
Universite de Picardie Jules Verne
33 rue Saint Leu
80000 Amiens
France
christophe.buret@u-picardie.fr

Marianne Conin (20 July–31 August 2009)
Physical Properties/Downhole Measurements Specialist
CEREGE—College de France
Europole de l'Arbois, Bat Trocadero
BP 80
13545 Aix en Provence Cedex 04
France
mconin@crpg.cnrs-nancy.fr

Deniz Cukur (20 July–31 August 2009)
Logging Specialist
Pukyong National University
Department of Energy Resources Engineering
599-1, Daeyeon 3-Dong, Nam-Gu
608-737 Busan
Korea
cukurdeniz@hotmail.com

Mai-Linh Doan (4 June–20 July 2009)
Physical Properties/Logging Specialist
Laboratoire de Géophysique et Tectonophysique
Université Grenoble 1 (Joseph Fourier)
BP53, 1381, rue de la Piscine
38041 Grenoble Cedex 9
France
Mai-Linh.Doan@obs.ujf-grenoble.fr

Natalia Efimenko (4 June–20 July 2009)
Sedimentologist
Institut de Géologie et Paléontologie
Université de Lausanne
Amphipôle
1015 Lausanne-Dorigny
Switzerland
natalia.efimenko@unil.ch

Peter Flemings (17 July–31 August 2009)
Physical Properties/Downhole Measurements Specialist
Institute for Geophysics
Jackson School of Geosciences
University of Texas at Austin
10100 Burnet Road (R2200)
Austin TX 78758-4445
USA
pflemings@jsg.utexas.edu

Nicholas Hayman (4 June–20 July 2009)
Structural Geologist
Institute for Geophysics
Jackson School of Geosciences
University of Texas at Austin
10100 Burnet Road (R2200)
Austin TX 78758-4445
USA
hayman@ig.utexas.edu

Keika Horiguchi (4 June–17 July 2009)
Geochemist
Department of Earth and Space Sciences
Osaka University
1-1 Machikaneyama, Toyonaka
Osaka 560-0043
Japan
keika@ess.sci.osaka-u.ac.jp

Gary Huftile (17 July–31 August 2009)
Structural Geologist
Queensland University of Technology
GPO Box 2434
Brisbane Qld 4001
Australia
g.huftile@qut.edu.au

Takatoshi Ito (4 June–20 July 2009)
Physical Properties/Downhole Measurements Specialist
Institute of Fluid Science
Tohoku University
2-1-1 Katahira, Aoba-ku
Sendai, Miyagi 980-8577
Japan
ito@ifs.tohoku.ac.jp

Shijun Jiang (4 June–17 July 2009)
Micropaleontologist (calcareous nannofossils)
Geological Sciences
Florida State University
108 Carraway Building
Tallahassee FL 32306
USA
jiang@gly.fsu.edu

Koji Kameo (6 August–31 August 2009)
Micropaleontologist
Department of Earth Sciences
Chiba University
1-33, Yayoi, Inage, Chiba
263-8522, Chiba
Japan
kameo@faculty.chiba-u.jp

Yasuyuki Kano (17 July–31 August 2009)
Logging Specialist
Disaster Prevention Research Institute
Kyoto University
Gokasho, Uji 611-0011
Japan
kano@rcep.dpri.kyoto-u.ac.jp

Kuniyo Kawabata (17 July–31 August 2009)
Sedimentologist
National Central University (TWN)
Institute of Geophysics
300 Chung-Da Road, Chung Li City
Taoyuan 32001
Taiwan
kuniyo@eqkc.earth.ncu.edu.tw

Kazuya Kitada (20 July–31 August 2009)
Observatory Specialist
Institute for Research on Earth Evolution
Japan Agency for Marine-Earth Science and Technology
2-15 Natsushima-cho, Yokosuka
Kanagawa 237-0061
Japan
kkitada@jamstec.go.jp

Achim Kopf (6 August–31 August 2009)
Observatory Specialist
Marum Research Centre
Bremen University
Leobener Strasse, MARUM Building
28359 Bremen
Germany
akopf@uni-bremen.de

Weiren Lin (4 June–17 July 2009)
Physical Properties/Downhole Measurements Specialist (hydrogeology)
Kochi Institute for Core Sample Research
Japan Agency for Marine-Earth Science and Technology
200 Monobe-Otsu, Nankoku
Kochi 783-8502
Japan
lin@jamstec.go.jp

J. Casey Moore (20 July–31 August 2009)
Logging Specialist
University of California, Santa Cruz
1156 High Street
Santa Cruz CA 95064
USA
casey@pmc.ucsc.edu

Anja Schleicher (4 June–17 July 2009)
Sedimentologist
Department of Geological Sciences
University of Michigan
1100 North University Avenue
Ann Arbor MI 48109
USA
aschleic@umich.edu

Roland von Huene (20–26 July 2009)
VSP Specialist
Department of Geology
University of California, Davis
2910 North Canyon Road
Camino CA 95709
USA
rhuene@mindspring.com

Thomas Wiersberg (4 June–6 August 2009)
Geochemist
GFZ German Research Center for Geosciences
Section 4.2
Telegrafenberg
14479 Potsdam
Germany
wiers@gfz-potsdam.de

Chief Project Scientists

Masataka Kinoshita (10 May–27 May 2009)
Chief Project Scientist
Institute for Research on Earth Evolution
Japan Agency for Marine-Earth Science and Technology
2-15 Natsushima-cho, Yokosuka
Kanagawa 237-0061
Japan
masa@jamstec.go.jp

Harold Tobin (22 May–4 June 2009)
Chief Project Scientist
Department of Geology and Geophysics
University of Wisconsin-Madison
1215 West Dayton Street
Madison WI 53706
USA
htobin@wisc.edu

NanTroSEIZE specialty coordinators

Toshiya Kanamatsu
Paleomagnetism/Biostratigraphy
Institute for Research on Earth Evolution
Japan Agency for Marine-Earth Science and Technology
2-15 Natsushima-cho
Yokosuka
Kanagawa 237-0061
Japan
toshiyak@jamstec.go.jp

Gaku Kimura
Structural Geology
Department of Earth and Planetary Science
Graduate School of Science
University of Tokyo
7-3-1 Hongo, Bunkyo-ku
Tokyo 113-0033
Japan
gaku@eps.s.u-tokyo.ac.jp

Gregory Moore
Core-Log-Seismic Integration
Department of Geology and Geophysics
University of Hawaii
1680 East-West Road
Honolulu HI 96822
USA
gmoore@hawaii.edu

Demian Saffer
Physical Properties
The Pennsylvania State University
0310 Deike Building
University Park PA 16802
USA
dsaffer@geosc.psu.edu

Michael B. Underwood
Sedimentology
University of Missouri
307 Geology Building
Columbia MO 65211
USA
underwoodm@missouri.edu

Geoff Wheat
Geochemistry
School of Fisheries and Ocean Sciences
University of Alaska Fairbanks
PO Box 475
Moss Landing CA 99775
USA
wheat@mbari.org

Shipboard personnel and technical representatives

Captains (Mantle Quest Japan)
Yasushi Minoura
Yuji Onda

Offshore Installation Managers (Mantle Quest Japan)
Seizaburo Higuchi
Stephen Krukowski

Operations Superintendents (CDEX)
Tsuyoshi Abe
Ikuo Sawada

Curators (Marine Works Japan)
Yohei Arakawa
Satoshi Hirano
Masaru Yasunaga

Assistant Curators (Marine Works Japan)
Toru Fujiki
Tatsuya Kawai
Lena Maeda

Coring Supervisor (AAI)
Jim Aumann

Downhole Tools Engineers
Tan Ting Cheng, Baker Oil Tools
Yu Ito, Schlumberger
Yang Ning, Schlumberger

Drilling Engineers (CDEX)
Daiji Ikenomoto
Yasuhiro Kawano
Yoshinori Masumoto
Tomokazu Saruhashi

Information Technology Manager (Marine Works Japan)
Yukari Kido
Shigemi Matsuda

Laboratory Officers (Marine Works Japan)
Hiroaki Muraki
Toshikatsu Kuramoto

Assistant Laboratory Officers (Marine Works Japan)
Toru Fujiki
Soichi Moriya
Tomoyuki Tanaka

Laboratory Technicians (Marine Works Japan)
Akihiko Fujihara
Yuji Fuwa
Yasushi Hashimoto
Kentaro Hatakeda
Yoko Isoda
Yoshiki Kido
Ryo Kurihara
Yutaka Matsuura
Shunsuke Miyabe
Kazuki Harumoto
Hiroyuki Hayashi
Yuya Hitomi
Stomi Kame
Tatsuya Kawai
Sayaka Kawamura
Toru Koizumi
Yuki Miyajima
Soichi Moriya
Hideki Mukoyoshi
Yukihiko Nakano
Masahiro Nishimura
Tetsuhara Nishino
Toshikatsu Sugawara
Tomohiko Sugiyama
Takahiro Suzuki
Yohei Taketomo
Naotaka Togashi
Hiroki Ushiromura

Publication Assistants (USIO)
Ginny Lowe
Lorri Peters

Operations Geologists (CDEX)
Kyo Furuya
Takayasu Honda
Atsushi Ibusuki
Toshiro Kaminishi
Kiyoshi Koide
Kazuhiro Takahashi
Shigenobu Uraki

Abstract

The Nankai Trough Seismogenic Zone Experiment (NanTroSEIZE) is a coordinated, multiexpedition drilling project designed to investigate fault mechanics and seismogenesis along subduction megathrusts through direct sampling, in situ measurements, and long-term monitoring in conjunction with allied laboratory and numerical modeling studies. The fundamental scientific objectives of the NanTroSEIZE project include characterizing the nature of fault slip and strain accumulation, fault and wall rock composition, fault architecture, and state variables throughout the active plate boundary system. As part of the NanTroSEIZE program, operations during Integrated Ocean Drilling Program (IODP) Expedition 319 included riser drilling, analyses of cuttings and core samples, downhole measurements and logging, and casing at Site C0009 in the Kumano forearc basin as well as riserless drilling, logging while drilling (LWD), casing, and observatory operations at Site C0010 across a major splay fault (termed the "megasplay") that bounds the seaward edge of the forearc basin near its updip terminus. In addition, we drilled at contingency Site C0011 to collect logging-while-drilling data in advance of planned coring operations scheduled as part of IODP Expedition 322.

Site C0009 marked the first riser drilling in IODP history. This allowed several scientific operations unprecedented in IODP, including carefully controlled measurements of in situ pore pressure, permeability and minimum principal stress magnitude, real-time mud gas analysis, and laboratory analyses of cuttings throughout the entire riser-drilled depth range (~700–1600 meters below seafloor [mbsf]). We conducted a leak-off test at one depth interval and successfully deployed the wireline Modular Formation Dynamics Tester 12 times to directly measure in situ stress magnitude, formation pore pressure, and permeability. During all phases of riser drilling, we collected mud gas for geochemical analyses and cuttings samples were collected throughout the entire riser-drilled depth range. Integration of data from cuttings, wireline logging, and cores (from a limited depth interval) allowed definition of a single integrated set of lithologic units and comparison with previously drilled IODP Site C0002 to determine the evolutionary history of the forearc basin. After casing the borehole, we conducted a long-offset (up to 30 km) two-ship active seismic experiment, recording shots within the borehole to image the megasplay and master décollement beneath the borehole, and to evaluate seismic velocity and anisotropy of the forearc basin and accretionary prism sediments around the borehole.

At riserless Site C0010, operations included drilling with measurement while drilling (MWD)/LWD across the megasplay fault to 555 mbsf, casing the borehole with screens at the depth of the fault, conducting an observatory dummy run to test future strainmeter and seismometer deployment procedures, and installation of a temporary pore pressure and temperature monitoring system in advance of planned future permanent observatory emplacement. The observatory system (termed a "smart plug") marks the first observatory installation of the NanTroSEIZE program. MWD/LWD data at this site were used to define unit boundaries and the fault zone target interval for placement of the casing screens. Through comparison with previously drilled Site C0004 these data also provide insights into along-strike differences in the architecture of the megasplay fault and hanging wall.

Introduction

Overview of the NanTroSEIZE complex drilling project

Subduction zones account for 90% of global seismic moment release, generating damaging earthquakes and tsunamis with potentially disastrous effects on heavily populated coastal areas (e.g., Lay et al., 2005). Understanding the processes that govern the strength, nature, and distribution of slip along these plate boundary fault systems is a crucial step toward evaluating earthquake and tsunami hazards. More generally, characterizing fault slip behavior and mechanical state at all plate boundary types through direct sampling, near-field geophysical observations, and measurement of in situ conditions is a fundamental and societally relevant goal of modern earth science. To this end, several recent and ongoing drilling programs have targeted portions of active plate boundary faults that have either slipped coseismically during large earthquakes or nucleated smaller events. These efforts include the San Andreas Fault Observatory at Depth (SAFOD) (Hickman et al., 2004), the Taiwan-Chelungpu Drilling Project (Ma, 2005), and Integrated Ocean Drilling Program (IODP) Nankai Trough Seismogenic Zone Experiment (NanTroSEIZE) drilling (Tobin and Kinoshita, 2006a, 2006b).

The NanTroSEIZE project is a multiexpedition, multistage IODP drilling program focused on understanding the mechanics of seismogenesis and rupture propagation along subduction plate boundary faults. The drilling program includes a coordinated effort to characterize, sample, and instrument the plate boundary system at several locations offshore the Kii Peninsula culminating in drilling, sampling, and instrumenting the plate boundary fault system near the updip limit of inferred coseismic slip, at ~6.2 km below seafloor (Tobin and Kinoshita, 2006b) (Figs. F1, F2, F3). The main objectives are to understand:

- The mechanisms controlling the updip aseismic–seismic transition along the megathrust fault system,
- Processes of earthquake and tsunami generation and strain accumulation and release,
- The absolute mechanical strength of the plate boundary fault, and
- The potential role of a major upper plate fault system (termed the "megasplay" fault) in seismogenesis and tsunamigenesis.

The drilling program will evaluate a set of core hypotheses through a combination of riser and riserless drilling, long-term observatories, and associated geophysical, laboratory, and numerical modeling efforts. The following hypotheses are paraphrased from the original IODP proposals and outlined in Tobin and Kinoshita (2006a, 2006b):

1. Systematic, progressive material and state changes control the onset of seismogenic behavior on subduction thrust faults.
2. Subduction megathrusts are weak faults.
3. Plate motion is accommodated primarily by coseismic frictional slip in a concentrated zone (i.e., the fault is locked during the interseismic period).
4. Physical properties of the plate boundary system (including the fault system and its hanging wall and footwall) change with time during the earthquake cycle.
5. A significant, laterally extensive upper plate fault system (the megasplay fault; Park et al., 2002) slips in discrete events that may include tsunamigenic slip during great earthquakes. It remains locked during the interseismic period and accumulates strain.

Sediment-dominated subduction zones such as the East Aleutian, Cascadia, Sumatra, and Nankai margins are characterized by repeated great earthquakes of ~M 8.0+ (Ruff and Kanamori, 1983). Although the causative mechanisms are not well understood (e.g., Byrne et al., 1988; Moore and Saffer, 2001; Saffer and Marone, 2003), the updip limit of the seismogenic zones at these margins is thought to correlate with a topographic break, often associated with the outer rise (e.g., Byrne et al., 1988; Wang and Hu, 2006). At Nankai, high-resolution seismic reflection profiles across the outer rise clearly document a large out-of-sequence thrust fault system (the megasplay fault, after Park et al., 2002) that branches from the plate boundary décollement close to the updip limit of inferred coseismic rupture in the 1944 Tonankai M 8.2 earthquake (Figs. **F1B, F2**). Several lines of evidence indicate that the megasplay system is active and may accommodate a significant fraction of plate boundary motion (Moore et al., 2007). However, the partitioning of strain between the lower plate interface (the décollement zone) and the megasplay system and the nature and mechanisms of fault slip as a function of depth and time on the megasplay are not understood. One of the first-order goals in characterizing the seismogenic zone along the Nankai Trough—and which bears both on understanding subduction zone megathrust behavior globally and on defining tsunami hazards—is to document the role of the megasplay fault in accommodating plate motion (both seismically and interseismically) and to characterize its mechanical and hydrologic behavior.

In late 2007 through early 2008, IODP Expeditions 314, 315, and 316 were carried out as a unified program of drilling collectively known as NanTroSEIZE Stage 1. A transect of eight sites was selected for riserless drilling to target the frontal thrust region, the midslope megasplay fault region, and the Kumano forearc basin region (Fig. **F3**). Two of these sites were preparatory pilot holes for planned deeper riser drilling operations, and the others primarily targeted fault zones in the shallow, presumed aseismic portions of the accretionary complex (Kinoshita, Tobin, Ashi, Kimura, Lallemant, Screaton, Curewitz, Masago, Moe, and the Expedition 314/315/316 Scientists, 2009). Expedition 314 was dedicated to in situ measurement of physical properties and borehole imaging through logging while drilling (LWD) (Kinoshita et al., 2008). Expedition 315 was devoted to core sampling and downhole temperature measurements at a site in the megasplay region and one in the forearc basin (Ashi et al., 2008). Expedition 316 targeted the frontal thrust and megasplay fault in their shallow, aseismic portions (Ashi et al., 2008; Kimura et al., 2008).

NanTroSEIZE Stage 2 includes two expeditions (319 and 322), with the aims of building on the results of Stage 1 and preparing for later observatory installations for long-term monitoring of deformation at the updip limit of the seismogenic zone. IODP Expedition 319 investigated the properties, structure, and state of stress within the hanging wall above the locked plate boundary at Site C0009 and across the shallow megasplay at Site C0010 and prepared boreholes for the future installation of observatories. IODP Expedition 322 will sample and characterize the properties of sediments on the subducting Philippine Sea plate. The initial results from Expedition 319, described in detail here, include data and operations for two sites: Site C0009, a riser drilling site in the Kumano Basin above the portion of the plate boundary thrust that slips coseismically, and Site C0010, a riserless site into the shallow megasplay fault near its updip terminus. Both sites have also been selected for future installation of long-term observatories.

In future IODP expeditions, long-term borehole observatories will be installed in the boreholes drilled during Expedition 319. The boreholes are located within and above regions of contrasting behavior of the megasplay fault zone and plate boundary as a whole (i.e., a site ~6–7 km above the locked seismogenic plate boundary [Site C0009] and a shallow site in the megasplay fault zone and footwall where slip is presumed to be aseismic [Site C0010]). These observatories have the potential of capturing seismic activity, slow slip behavior, hydraulic transients, and possibly interseismic strain accumulation on the plate boundary and megasplay faults. Currently, the planned observation system for the boreholes consists of an array of sensors designed to monitor slow crustal deformation (e.g., strain, tilt, and pore pressure as a proxy for strain), seismic events including very low frequency (VLF) earthquakes, hydrologic transients associated with strain events, ambient pore pressure, and temperature. To ensure the long-term and continuous monitoring necessary to capture events occurring over a wide range of timescales, these borehole observatories will be connected to submarine cabled observation network called Dense Oceanfloor Network System for Earthquakes and Tsunamis (DONET) (**www.jamstec.go.jp/jamstec-e/maritec/donet/**), which will be constructed in and around the drilling target area.

Background

Geological setting

The Nankai Trough is formed by northwestward subduction of the Philippine Sea plate beneath the Eurasian plate at a rate of ~40–65 mm/y (Seno et al., 1993; Miyazaki and Heki, 2001). The convergence direction is slightly oblique to the trench, and sediments of the Shikoku Basin are actively accreting at the deformation front. The Nankai Trough is among the most extensively studied subduction zones in the world, and great earthquakes during the past 3000 or more years are well documented in historical and archeological records (e.g., Ando, 1975). The Nankai Trough has been selected as a focus site for studies of seismogenesis by both IODP and the U.S. MARGINS initiative, based on the wealth of geological and geophysical data available, a long historical record of great ($M > 8.0$) earthquakes, and the direct societal relevance of understanding tsunamis and earthquakes that have had, and will have, great impact on nearby heavily populated coastal areas.

The Nankai Trough region has a historical record of recurring great earthquakes that are typically tsunamigenic, including the 1944 Tonankai M 8.2 and 1946 Nankaido M 8.3 earthquakes (Ando, 1975; Hori et al., 2004). The rupture area and zone of tsunami generation for the 1944 event (within which this expedition is located) are now reasonably well understood (Ichinose et al., 2003; Baba et al., 2005) (Fig. **F1B**). Land-based geodetic studies suggest that the plate boundary thrust is currently strongly locked (Miyazaki and Heki, 2001), and the relatively low level of microseismicity near the updip limits of the 1940s earthquakes (Obana et al., 2001) implies significant interseismic strain accumulation on the megathrust. However, recent observations of VLF earthquakes within or just below the accretionary prism in the drilling area (Obara and Ito, 2005) demonstrate that some strain release occurs during interseismic periods between great earthquakes (Fig. **F1B**). Slow slip phenomena including episodic slow slip events and nonvolcanic tremor are also widely known to occur in the downdip part of the rupture zone (Ito et al., 2007).

The region offshore the Kii Peninsula on Honshu Island was selected for seismogenic zone drilling for several reasons. First, the rupture area of the most recent great earthquake, the 1944 Tonankai M 8.2 event, is well constrained by recent seismic and tsunami waveform inversions (e.g., Tanioka and Satake, 2001; Kikuchi et al., 2003). Slip inversion studies suggest that only in this region did past coseismic rupture clearly extend shallow enough for drilling (Ichinose et al., 2003; Baba and Cummins, 2005), and an updip zone of large slip has been identified and targeted (Fig. **F1B**). Notably, coseismic slip during events like the 1944 Tonankai earthquake may have occurred on the megasplay fault in addition to the plate boundary décollement (Ichinose et al., 2003; Baba et al., 2006). The megasplay fault is therefore a primary drilling target. Second, ocean-bottom seismometer (OBS) campaigns and onshore high-resolution geodetic studies (though of short duration) indicate significant interseismic strain accumulation (e.g., Miyazaki and Heki, 2001; Obana et al., 2001). Third, the region offshore the Kii Peninsula is generally typical of the Nankai margin in terms of heat flow and sediment on the incoming plate. This is in contrast to the area offshore Cape Muroto (the location of previous Deep Sea Drilling Project and Ocean Drilling Program [ODP] drilling) where both local stratigraphic variation associated with basement topography and anomalously high heat flow have been documented (Moore et al., 2001; Moore, Taira, Klaus, et al., 2001). Finally, the drilling targets are within the operational limits of riser drilling by D/V *Chikyu* (i.e., maximum of 2500 m water depth and 7000 m subseafloor penetration). In the seaward portions of the Kumano Basin, the seismogenic zone lies ~6000 m beneath the seafloor (Nakanishi et al., 2002).

Seismic studies/site survey data

A significant volume of site survey data has been collected in the drilling area over many years, including multiple generations of two-dimensional seismic reflection (e.g., Park et al., 2002), wide-angle refraction (Nakanishi et al., 2002), passive seismicity (e.g., Obara et al., 2004), heat flow (Yamano et al., 2003), side-scan sonar, swath bathymetry, and submersible and remotely operated vehicle (ROV) dive data (Ashi et al., 2002). In 2006, Japan and the United States conducted a joint, three-dimensional (3-D) seismic reflection survey over a ~11 km × 55 km area, acquired by PGS Geophysical, an industry service company (Fig. **F3**). This 3-D data volume is the first deep-penetration, fully 3-D marine survey ever acquired for basic research purposes and has been used to refine selection of drill sites and targets in the complex megasplay fault region, define the 3-D regional structure and seismic stratigraphy, analyze physical properties of the subsurface, and assess drilling safety (Moore et al., 2007, 2009).

Scientific objectives

Expedition 319 was noteworthy because it marked the first riser drill site in IODP history, as well as the first observatory installation for the *Chikyu*. Riser drilling allowed us to plan several measurements new to IODP, including measurement of in situ stress and pore pressure using the Modular Formation Dynamics Tester (MDT) wireline tool, real-time mud gas analysis, and analysis of drill cuttings. In addition, the operations plan included a leak-off test (LOT) at a casing set point for engineering purposes, which also provided a measurement of minimum stress magnitude. Our operational and scientific plan also included a long-offset (30 km) "walkaway" vertical seismic profile (VSP) and the first installation of long-term borehole monitoring instruments by the *Chikyu* using a simple instrument package ("smart plug") connected to a retrievable casing packer (Araki et al., 2009). Our objectives at Site C0009 were to drill, sample, log, and case the rocks and sediments above the locked portion of the coseismically active plate boundary thrust (Fig. **F4A;** see also Figs. **F1, F2, F3**). These operations also provide preparation for later observatory placement, which will monitor deformation, seismicity, pore pressure, and temperature. The scientific objectives at Site C0009 included:

1. Documenting the lithology, structural geology, physical properties, and fluid and rock composition of the upper ~1600 m of basin fill and possibly accreted sediments in the hanging wall of the plate boundary fault;

2. Collecting core at or near the depth of potential observatory installation, primarily to obtain samples for shore-based geotechnical and mechanical analyses;
3. Conducting downhole tests to measure in situ pore pressure and stress state; and
4. Conducting a two-ship VSP experiment to constrain the seismic velocity structure of the deep interior of the accretionary wedge and image the plate boundary below the drill site.

At Site C0010, our objective was to drill with measurement while drilling (MWD) and a basic suite of LWD tools (geoVISION resistivity tool [GVR] and gamma ray [GR]) to penetrate the megasplay fault at ~410 meters below seafloor (mbsf) and into the footwall to a total depth (TD) of 560 mbsf (Fig. **F4B**). The major scientific objectives at Site C0010 included:

1. Characterizing the lithology, structural geology, and physical properties of the hanging wall, megasplay fault zone, and footwall using logging data;
2. Correlating between Site C0010 and previously drilled IODP Site C0004 (~3.5 km along strike) to characterize variations in fault zone architecture and physical properties; and
3. Conducting observatory operations, including a "dummy run" of a seismometer and strainmeter package designed for placement in a future permanent observatory at this site and installation of a temporary monitoring package to monitor pore pressure and temperature within the fault zone accessed through a screened casing.

Operational strategy

Our drilling plan for Expedition 319 included one riser borehole in the Kumano Basin at proposed Site NT2-11B (drilled Site C0009; Fig. **F4A**) and one riserless hole at proposed Site NT2-01J (drilled Site C0010; Fig. **F4B**).

To meet the scientific and engineering objectives, primary operations at both sites were to drill and case to TD (Araki et al., 2009). Because of anticipated challenges and uncertainty in operations schedules with both riser and riserless operations, we also developed a detailed suite of contingency operations for the expedition. Our primary contingency operations included installing casing and a smart plug at IODP forearc basin Site C0002 (Araki et al., 2009) and drilling and coring sediment inputs Site NT1-01 proposed for Expedition 322 (Saito et al., 2009) (Fig. **F3**).

Planned operations at Site C0009 began with running and jetting-in a 36 inch conductor casing to 55 mbsf. Following this, the wellhead and blowout preventer (BOP) were to be set at the seafloor, and a 26 inch riserless hole drilled to 700 mbsf with MWD, including annular pressure while drilling (APWD). After installing and cementing 20 inch casing in the upper 700 m, the planned operations were to lower the BOP, connect it at the wellhead, drill a 12¼ inch riser hole from 700 to 1510 mbsf with MWD including recovery and analysis of cuttings, and then rotary core barrel (RCB) core from 1510 to 1600 mbsf. After coring and opening the cored hole to 12¼ inches, three wireline logging runs were planned from ~700 to ~1600 mbsf: (1) the Schlumberger Platform Express (PEX), including the Highly Integrated Gamma Ray Neutron Sonde, Three-Detector Lithology Density tool, and High-Resolution Laterolog Array (HRLA); (2) Formation MicroImager (FMI) and Sonic Scanner; and (3) MDT. After wireline logging, the hole was to be opened to 17 inches and cased to TD with 13⅜ inch casing. Drilling mud gas collection was planned during all riser drilling operations. After cementing the casing, a cement-bond log (CBL) was planned inside the casing, followed by a zero-offset VSP and a two-ship walkaway VSP experiment coordinated with the Japan Agency for Marine-Earth Science and Technology (JAMSTEC) R/V *Kairei*. The VSP experiment was planned for 2 or more days, but the duration depended on operational progress and the drilling schedule. Following the VSP, we planned to suspend the riser hole by setting a corrosion cap, with a contingency plan to hang a short (~100 m) thermistor string into the casing for later retrieval if time permitted.

We completed essentially all of the planned scientific and engineering objectives at Site C0009, with riser operations ending on 31 July (as scheduled, including contingency days). Because of time constraints at the time of casing and cementing, the CBL was eliminated from operations. In addition, because of the combination of time constraints on the drilling schedule and limitations on the availability of the *Kairei* (shooting vessel), the planned two-ship VSP experiment was shortened slightly. A total of 19 contingency days were included in the original schedule and were fully used, primarily because of recovery of a lost bottom-hole assembly (BHA)/drilling ahead tool (DAT) during riserless drilling, problems with the dynamic positioning system (DPS), mechanical problems related to riser system installation (riser tensioners and tensioner load ring), and weather. In other cases, operations were considerably faster than scheduled, including the retrieval of the riser system after completion of riser drilling operations and installation of the 20 inch casing string.

Planned operations at proposed Site NT2-01J (drilled Site C0010) included jetting-in a 20 inch casing string to 35 mbsf, followed by hole reentry and drilling of a 12¼ inch hole with MWD and a limited suite of LWD (GVR, including GR and azimuthal resistivity-at-the-bit [RAB] measurement) to TD at 560 mbsf. After drilling, 9⅝ inch casing with two screened casing joints (~11 m long each) spanning the megasplay fault would be installed to ~550 mbsf, leaving an ~10 m open "rathole." Based on seismic data, we estimated the depth of the megasplay fault at 410 mbsf; we anticipated adjusting the exact depth for the casing screens shortly before running the casing, using the newly acquired LWD/MWD data. After cementing the casing, we planned an observatory sensor dummy run to measure shock and acceleration experienced by highly sensitive strainmeter and seismometer instruments to assess operations for future reentry and installation, followed by a wireline temperature log inside the casing to identify the top of cement in the annulus. The hole was to be suspended by installing a retrievable casing packer (modified to include the smart plug instrument package below) at ~390 m and setting a corrosion cap. The smart plug is designed to thread to a crossover joint at the bottom of the bridge plug and includes a self-contained temperature sensor and data logger, as well as a pressure gauge and data logger package. These instruments will be in hydrologic communication with the fault zone at the screened interval and will monitor formation pore pressure and temperature from the time the bridge plug is set until it is retrieved at the beginning of future permanent riserless observatory installation operations.

We completed all of the planned operations at Site C0010, with the exception of the wireline temperature log, which we eliminated to preserve time for the anticipated challenges of running casing in the strong Kuroshio Current and after discussion with the operations group resolved that it would be of limited use to define the top of cement. In addition, drilling with LWD/MWD was suspended after reaching 482 m LWD depth below seafloor (LSF) (Table T1) in order to evacuate for a typhoon and resumed after ~2 days. Based on poor data quality related to ship heave and stick-slip, we reamed and relogged a critical interval near the megasplay fault zone from 348 to 418 m LSF before running down to the previous TD and drilling to a final TD of 555 m LSF.

In practice, our contingency options evolved during the expedition because of time constraints and the limited availability of personnel for coring operations. In response to these constraints, we developed additional contingency plans during the expedition, which would generate data of high value to the overall NanTroSEIZE drilling project. These operations included LWD/MWD at proposed Sites NT1-07 and NT1-01, which were the primary and contingency sites, respectively, for Expedition

322 (Saito et al., 2009). In the final 5 days of Expedition 319, we moved to Site C0011 (proposed Site NT1-07), dropped 6 transponders, and drilled with LWD/MWD to a TD of 952 m LSF. Data from Site C0011 are not described here but will be included in the *Expedition 322 Preliminary Report* along with results of planned coring, downhole measurements, and wireline logging.

Site summaries

Site C0009

Site C0009 marked the first riser drilling in IODP history. This allowed us to conduct several scientific operations new to IODP, including measurements of in situ pore pressure and stress using the MDT tool and LOTs, real-time mud gas analysis, and laboratory analyses of cuttings. In situ pore pressure, stress magnitude, and permeability are among the most central data for understanding the mechanics of active fault zones and testing the core NanTroSEIZE hypotheses, but they have previously been unavailable in IODP drilling. Analyses of mud gas and cuttings, although common in other riser drilling programs (e.g., Erzinger et al., 2006), were also conducted for the first time in IODP and will be essential for future riser-based drilling. Because there are no standard IODP procedures for shipboard measurements on cuttings, the scientific party developed several techniques for handling, sampling, and measurement of physical properties, rock chemistry, and sedimentological and structural description (see discussion in **"Insights from scientific riser operations"**).

Drilling at Site C0009 achieved all of the primary planned scientific objectives, although some operations were shortened slightly because of schedule constraints. After riserless drilling and installation of casing to 703.9 m drilling depth below seafloor (DSF), riser operations included collection of cuttings (from 1017 m mud depth below seafloor [MSF] to TD) and core (1509.7–1593.9 m core depth below seafloor [CSF]) to document stratigraphy and sediment composition, measure rock physical properties, and identify structures. Because of limited coring operations and limitations associated with cuttings analyses (see **"Insights from scientific riser operations"**), we defined a single integrated set of lithologic units based on the range of data available from cuttings, wireline logging data, and cores (Fig. **F5A, F5B**). We ran LOT and MDT experiments that provide direct measurements of in situ stress magnitude, as well as formation pore pressure and permeability. During all phases of riser drilling, we also collected mud gas for geochemical analyses, from 703.9 m drilling depth below rig floor (DRF) to TD (e.g., Wiersberg et al., 2007). A zero-offset and walkaway VSP experiment was conducted using a wireline array of seismometers within the borehole to define the seismic velocity and structure around the borehole and at the underlying plate boundary.

Lithology

Using the combination of data from wireline logs, cuttings, and limited core, we defined four distinct lithologic units composed of mud/mudstone with variable interbeds of sand, silt, and volcanic ash/tuff. The unit boundaries and lithologies are constrained by macroscopic description of cuttings and sediment from drilling mud and of cores, smear slide and thin section observations, bulk X-ray diffraction (XRD) and X-ray fluorescence (XRF) analyses, and wireline logging data including natural GR, caliper, density, photoelectric effect, spontaneous potential, resistivity (including resistivity images), and sonic velocity (Fig. F5A, F5B). Despite some chemical and physical artefacts in the cuttings and uncertainty in their depth of origin, lithologic boundaries defined by analysis of cuttings are generally consistent with boundaries defined by logging data:

- Unit I (Pleistocene–modern; 0–467 m wireline log matched depth below seafloor [WMSF]) is a mudstone with cyclical sand-rich layers ranging from ~10 to 50 m thick.
- Unit II (Pleistocene to ~1.5 Ma; 467–791 m WMSF) is a mudstone composed dominantly of silty clay, with some silt and sand interbeds and minor interbeds of volcanic ash.
- Unit III (Pliocene–Pleistocene: ~3.8 to ~1.5 Ma; 791–1285 m WMSF) is composed of silty clay and poorly lithified silty claystone, with interbeds of silt and fine sand layers. It is distinguished from Unit II by its overall finer grain size, higher wood/lignite content, slightly increased consolidation state, and higher organic content. On the basis of cuttings, we divided Unit III into two subunits, with Subunit IIIB distinguished from Subunit IIIA by increased wood/lignite and glauconite abundance.
- Unit IV (late Miocene: ~7.7–7.1 to ~5.59 Ma; 1285 WMSF to TD) is a silty claystone with silt interbeds and rare interbeds of fine vitric tuff. The Unit III/IV boundary is marked by changes in several logging data sets, increased lithification and sediment maturity, and several major compositional changes. It is also defined by a ~1.8 Ma age gap and an angular unconformity that can be traced across the Kumano Basin (Fig. F6).

Overall, we interpret the stratigraphic succession as a series of forearc basin–filling mudstones with varying sand and silt turbidite abundance underlain by older slope deposits and/or accretionary prism sediment. Unit I is significantly sandier than other units drilled at Sites C0009 and C0002 (20 km seaward). Unit II is characterized by turbidites that are coarser than those in underlying Units III and IV and the units drilled at Site C0002 but markedly thinner and finer grained than those in Unit I above. Unit III includes two subunits (IIIA and IIIB) containing thinly bedded fine-grained turbidites that were deposited above the carbonate compensation depth (CCD) in the early Kumano forearc basin. The lower subunit (IIIB) had an increased supply of terrigenous organic matter (i.e., wood fragments). The composition of detrital grains points to a source from exposed metamorphic rocks of the Shimanto Belt (e.g., Taira et al., 1988; Isozaki and Itaya, 1990) and is consistent for Units I, II, and III.

Unit IV is mudstone containing thin-bedded fine-grained turbidites. Depositional environment relative to the late Miocene CCD is not conclusive based on initial interpretations of calcareous microfossil test preservation (see **“Biostratigraphy”**); however, deposition may have been at depths close to the CCD. It resembles Unit IV at Site C0002 in terms of sedimentary facies (Expedition 315 Scientists, 2009). Unit IV at Site C0009, however, is less deformed and we observed no clear sedimentary, geochemical, or structural evidence (see below) to conclusively indicate that this unit is composed of highly deformed frontally accreted trench sediment. Thus, Unit IV could be interpreted as either a weakly deformed package of accreted trench sediments, slope deposits, or sediments deposited in the distal reaches of the early Kumano Basin.

Structural geology and geomechanics

At Site C0009, we documented geologic structures in cuttings from 1097.7 to 1512.7 m MSF, and in core from 1510.5 to 1593.9 m CSF. We also analyzed FMI borehole resistivity images from 710 to 1579.9 m WMSF. Although the FMI’s limited coverage of the borehole wall and reduced data quality in the deeper borehole (Unit IV) precluded clear identification of borehole breakouts in resistivity images, we were able to use the FMI caliper to measure borehole enlargement associated with breakouts. We also documented drilling-induced tensile fractures (DITF) in some portions of the hole. Both of these data sets are indicators of minimum and maximum horizontal stress orientation.

Vein structures identified in cuttings from the upper part of Unit IV are similar to those observed on previous drilling expeditions (e.g., Site C0002; Ashi et al., 2008) and in onshore exposures, and they are consistent with formation by dewatering or shaking-induced soft-sediment deformation. Faults identified in the cores exhibit two populations (one dipping at 10°–30° and the other at 50°–70°) reflecting both thrust and normal faults. Although most faults do not exhibit a clear sense of offset, we observed some cross-cutting relationships that indicate a complex deformation history in which faults exhibiting normal displacement both cut and are cut by faults having thrust displacement. We did not reorient structures identified in the cores because the cryogenic magnetometer was not on board during the expedition.

FMI images and caliper measurements provided additional structural data for Site C0009. In Subunit IIIA, beds dip gently north 10°–15°, whereas in Subunit IIIB, they dip gently north-northwest. A 3 m thick zone of deformation and increased bedding dip appears to distinguish Subunits IIIA and IIIB. Faults and fractures are also identified in Units III and IV and dip more steeply northwest than bedding planes, with a mean dip of ~60°. Within Unit IV, caliper measurements from the FMI indicate that the hole is significantly enlarged, with one caliper commonly measuring ≥16–18 inches in diameter and the other caliper typically close to 12 inches. The orientation of the largest caliper measurement (i.e., borehole enlargement) is stable even as the entire tool rotated in discrete 90° clockwise increments while being pulled uphole. The mean value of that orientation, weighted for the depth of borehole sampled in each interval, defines an alignment 58°–238° (northeast–southwest). We interpret this orientation as a series of breakouts, representing the direction of S_{hmin}. This indicates that the maximum stress in the horizontal plane (S_{Hmax}) is oriented at 148°–328° (southeast–northwest), which is similar to the orientation of S_{Hmax} at IODP Sites C0001, C0004, and C0006 seaward of the megasplay fault but nearly perpendicular to that at Site C0002 located 20 km to the southeast at the seaward edge of the Kumano Basin (Kinoshita, Tobin, Ashi, Kimura, Lallemant, Screaton, Curewitz, Masago, Moe, and the Expedition 314/315/316 Scientists, 2009) (Fig. F7).

Biostratigraphy

We established an age model for the drilled sequence at Site C0009 from calcareous nannofossil biostratigraphy, primarily utilizing cuttings samples (704–1610 m MSF) and augmented with core samples from 1509.7 to 1593.9 m CSF (Figs. F5A, F6). We analyzed 72 cuttings samples spaced at 5–30 m intervals, with the closest spacing near key lithologic and zonal boundaries. Calcareous nannofossils are generally abundant throughout the section, and preservation of fossils is moderate in the upper part but there is a trend toward poorer preservation below ~1290 m MSF within Unit IV. Except for a few samples from the top sand-rich interval in lithologic Unit II, most samples yielded abundant nannofossils and the major age-diagnostic taxa appear reasonably continuous throughout their ranges. Therefore, most of the important Neogene and Quaternary datums (summarized by Raffi et al., 2006) and hence the nannofossil zones of Martini (1971) were recognized. However, frequent downhole contaminations of species prevent the use of some important nannofossil datums based on first (or first common) occurrences.

Our results indicate that the sampled sequences range in age from late Miocene (>7.1 Ma) to Pleistocene (<0.43 Ma). Unit II and the upper half of Subunit IIIA are early Pleistocene, and the rest of Unit III is Pliocene (Fig. **F6A**). Unit IV is late Miocene, and we documented an unconformity spanning ~1.8 m.y. (5.6–3.8 Ma) between the late Pliocene (Subunit IIIB) and the late Miocene (Unit IV). The upper Miocene sequence continues to the base of the drilled section, with probable ages younger than 7.88 Ma.

Geochemistry

During riser drilling at Site C0009, we conducted scientific mud gas monitoring (e.g., Erzinger et al., 2006). The principal formation gases extracted from the returning drilling mud were hydrocarbons, mainly methane, with up to 14 vol% CH_4 detected during initial drilling of the 12¼ inch hole and up to 3 vol% detected during hole opening to 17 inches. We also detected traces of ethane (up to 16 parts per million by volume [ppmv]) and propane (up to 3 ppmv). During drilling of the 12¼ inch hole, methane concentrations were relatively low above ~800 m MSF. Methane concentrations were generally highest within Subunit IIIB from 1050 to 1220 m MSF. Below 1280 m MSF (approximately corresponding to the Unit III/IV boundary), methane concentrations decreased abruptly to ~4–5 vol%. During hole opening to 17 inches, a better depth resolution was achieved by modifying the gas extraction set-up; both data sets exhibit similar downhole trends.

The distribution of methane correlates directly with the presence of wood and lignite in cuttings, implying that they are the primary source of hydrocarbons (Figs. **F5A, F8**). The molecular composition of hydrocarbons clearly suggests a microbial source (the ratio CH_4/C_2H_6 was consistently >500 and typically ~1000), although this ratio might be somewhat biased by the greater solubility of methane in the drilling mud relative to ethane and propane. This interpretation is consistent with an estimated temperature of ~50°C at the base of the borehole, which is too low for thermogenic hydrocarbon generation. Based on the correlation between stratigraphic observations and mud gas distribution combined with the overall fine-grained nature of the sediments in Unit III, gas migration through permeable strata seems unlikely to play a significant role in the observed gas distribution. This interpretation is also consistent with the absence of gases indicating a contribution from greater source depth (i.e., helium or heavy hydrocarbons). Taken together with observations from physical property measurements (see **"Physical properties"**) these observations indicate a moderate gas saturation (Sw = ~10%) that was probably generated in place.

The total organic carbon (TOC) content of drill cuttings samples ranges from 0.93 to 8.7 wt%, with the highest values in Subunit IIIB between 1080 and 1240 m MSF. These values are consistent with the high abundance of wood/lignite observed in this unit and the occurrence of methane, as noted above. TOC and total nitrogen (TN) exhibit a very similar depth distribution. The TOC/TN ratio ranges from 13.8 to 74.5 with an average of 29.8; values are generally highest in Unit III and decrease in Unit IV. Marine organic matter typically exhibits TOC/TN ratios in the range of 6–9, whereas the ratio for terrestrial organic matter is typically >10. This suggests that the source of organic matter in much of the borehole is terrestrial, which is in agreement with the wood and coal fragments observed in drill cuttings.

Physical properties

We obtained a wide range of physical property data from wireline logs and measurements on cores and cuttings (Fig. **F5**). These data included bulk density and porosity, *P*- and *S*-wave velocity (V_P and V_S, respectively), magnetic susceptibility, electrical resistivity, and thermal conductivity (cores only). In general, bulk density gradually increases downsection and porosity (computed from bulk density and estimated from resistivity logs) decreases, which is consistent with a trend of increasing compaction with depth. *P*- and *S*-wave velocities increase with depth overall, but the *P*-wave velocity profile is marked by excursions to lower values within Unit III.

Most physical property measurements exhibit changes at the major lithologic unit boundaries. For example, the slope of the compaction trend increases slightly across the Unit III/IV boundary at 1285 m WMSF; we interpret this to reflect a change in either lithology or compaction history (i.e., secondary consolidation associated with the increased age of the sediment in Unit IV or possible lateral compression). In addition to the change in the slope of the porosity-depth trend, we observe a decrease in measured density (and concomitant increase in computed porosity) at the Unit III/IV boundary. We suggest this is an artifact of the higher clay content in Unit IV relative to overlying units; postexpedition XRD analyses of the clay-sized fraction will address this by quantifying the abundance of hydrous clay (i.e., smectite minerals).

On the basis of *P*-wave, *S*-wave, and resistivity logs, we identified four distinct zones of increased gas content in Unit III. Specifically, we observe intervals characterized by low V_P, low V_P/V_S ratio (and thus low Poisson's ratio), and increased resistivity that correlate clearly with depths of increased methane measured by mud gas analyses (Fig. **F8**). A preliminary calculation suggests a gas saturation of ~10%. We also observe a significant change in caliper at the Unit III/IV boundary. Above this, the hole remains in gauge, whereas below the boundary we observe significant enlargement with one caliper measuring up to 16–18 inches (see **"Structural geology and geomechanics"**). This enlargement, taken together with the decrease in Stoneley wave velocity in this interval, may be related to increased deformation in Unit IV.

Moisture and density (MAD) density and porosity data from cores are in good agreement with the wireline logging data. In contrast, measurements conducted on cuttings appear to significantly overestimate porosity (by as much as ~12%) and underestimate bulk density. This discrepancy may be related to the small size of the cuttings that led to swelling during washing or exposure to drilling mud in the borehole or water retention on the surfaces of small particles after washing. Although the absolute values of porosity measured on cuttings are most probably well in excess of true formation porosity, downhole trends may reflect real relative variations in formation bulk density and porosity. This and several other issues encountered in analysis of cuttings are discussed in more detail in **"Insights from scientific riser operations."**

Downhole measurements

Stress, pore pressure, and permeability

Measurement of in situ pore pressure and stress using the MDT wireline logging tool assembly was one of the new scientific operations for IODP conducted during Expedition 319. This wireline tool measures borehole pressure, formation pore pressure at the bed and meter scale, and least principal stress magnitude. We ran the MDT tool successfully 12 times at Site C0009. This included nine single probe tests to measure in situ pore pressure and fluid mobility and three dual packer tests in 1 m thick isolated intervals: one to measure formation permeability from a drawdown and recovery cycle and two to measure in situ stress (two of the single probe tests were conducted at the same depth stations as dual packer tests). The single probe test uses a circular probe sealed against the borehole wall to extract fluid and reduce formation pore pressure in a small volume and then records the subsequent pressure recovery. The dual packer test isolates an interval of the formation (configured for 1 m at Site C0009) to either draw down the pressure (again to estimate in situ pressure and permeability over a larger scale than the single probe test) or to increase the borehole pressure to create a hydraulic fracture and measure the least principal stress magnitude.

The nine in situ pore pressure measurements indicate that formation pore pressure is hydrostatic or elevated by only a few percent of the hydrostatic value to depths of at least 1463.7 m WMSF (the depth of the deepest reliable measurement) (Fig. **F9A**). The slight apparent overpressure could be due to pressurization of the formation by weighted drilling mud, an incorrect estimation of the hydrostatic pressure (e.g., if the integrated seawater density from mean sea level to the measurement point was slightly underestimated), or the presence of real but slight overpressure. The permeablities we measured with the single probe tests range from ~10^{-16} to 10^{-14} m^2 (Fig. **F9B**). Overall, the variation in permeability values is consistent with lithologic characteristics inferred from GR logs; the higher permeabilities correspond to zones of lower GR (i.e., sandier intervals). Analysis of the dual packer drawdown-recovery test at 1539.69 m WMSF in the clay-rich and fine-grained Unit IV yielded a permeability value of 1.3×10^{-17} m^2. It is important to recognize that the MDT tool is generally designed for use in formations with permeabilities > ~10^{-15} m^2. In low-permeability formations, both pore pressure and permeability estimates should be viewed with caution because the pressure recovery time may be considerably longer than the tool deployment time.

We conducted hydraulic fracturing (HF) tests near the top and bottom of the 12¼ inch open-hole section at 874.30 and 1462.3 m WMSF using the MDT dual packer tool. The deeper test did not yield reliable results. For the shallower test, we observed a repeatable and clear instantaneous shut-in pressure of 34.8 MPa, which we interpret as the least principal stress (S_3) (Fig. **F9A**). This value is smaller than the vertical stress (S_v). If the principal stresses are horizontal and vertical, then this implies $S_3 = S_{hmin}$; the measured value corresponds to an effective stress ratio (S'_{hmin}/S'_v) of 0.82. As part of standard riser drilling operations, we also conducted a LOT at the base of the 20 inch casing (708.6 m DSF). The leak-off pressures are 30.22–30.25 MPa, and as was the case for the MDT HF test, are less than S_v, also indicating that $S_3 = S_{hmin}$. However, the value of S_3 obtained from this test is considerably lower than from the MDT HF test, with $S'_{hmin}/S'_v = 0.44$. Although there is considerable uncertainty in determining the S_3 from this type of test (e.g., Zoback, 2007), the LOT was repeatable and appears reliable.

Vertical seismic profiling

We conducted a walkaway VSP experiment in Hole C0009A using an array of 16 seismometers within the Vertical Seismic Imager (VSI) wireline tool set inside the 13⅜ inch casing between 2989 and 3217 m DRF. The objective of the walkaway VSP experiment was to image the structure around the megasplay fault and master décollement below the borehole and evaluate seismic anisotropy of the basin sediment and accretionary prism around the borehole. The shooting vessel (*Kairei*) shot a single 53.4 km long offset transect in the dip direction of the subducting plate and a circular shooting offset of 3.5 km radius around the borehole. We obtained 880 shot records in the dip line and 275 shots in the circular line.

From the walkaway VSP records, we were able to identify direct wave arrivals, seismic phases associated with multiples in the water column, refractions from the accretionary prism, and reflections from interfaces below the seismometers within the accretionary prism as well as from the splay fault and probably from the plate boundary. The dense seismic array in the hole was sensitive enough that seismic waves traveling upward and downward were coherent and clearly distinguishable. We also observed subordinate seismic waves generated by direct waves hitting the structure of the borehole and traveling along the casing at ~6 km/s. These phases were prominent in the vertical component at frequencies higher than 20 Hz and make it difficult to see high-frequency phases from the formation. Therefore, deeper and weaker seismic phases appear clearer in horizontal component records because of smaller effects from such casing related phases.

Following the walkaway VSP experiment, we conducted a zero-offset VSP experiment using air guns deployed at 60 m offset from *Chikyu* and obtained by moving the seismic array upward from the depth of the walkaway VSP experiment in ~122 m intervals to obtain coverage around the entire length of the borehole. As was the case for the walkaway VSP, zero-offset VSP records also exhibited the subordinate seismic phases traveling vertically in the casing. We also observed acoustic waves propagating inside the casing, and those probably reflected back at the bottom of the casing (at the casing shoe or float collar). In horizontal component records, there are clear phases propagating downward with apparent velocities in good agreement with velocities from wireline sonic logs and with the velocities from precruise seismic processing. We picked these phases as *P*-waves propagating in the formation.

Cuttings–Core-Log-Seismic integration

We combined the zero-offset VSP (check shot) with wireline sonic velocities to derive a velocity-depth function at Site C0009 and used this velocity function to correlate the wireline, cuttings, and core data with time-based seismic data (Fig. **F5**). The velocities from the sonic log and check shot are lower than those used for 3-D seismic processing prior to this expedition. This is primarily due to a zone of low velocity and V_P/V_S ratio from ~1030 to 1200 m WMSF in the wireline sonic data that corresponds to a zone of increased free gas in Unit III (Figs. **F5A, F8**).

We identified several prominent seismic surfaces that can be traced regionally within the Kumano Basin (Unconformities UC1–UC4; Figs. **F4, F6**). The uppermost of these surfaces, Unconformity UC1, is a prominent reflector within Unit II at ~600 mbsf (Fig. **F6A**). Unconformity UC2 is located at ~750 m WMSF, 40 m above the interpreted Unit II/III boundary (Figs. **F5A, F6A**). Unconformity UC3 is a prominent positive polarity reflector and marks an angular unconformity at the base of the low-velocity zone in Subunit IIIB (Figs. **F5A, F6A**), and we interpret that it is caused by the strong increase in impedance at the base of the gas zone. Unconformity UC4 lies at the Unit III/IV boundary and is marked by a decrease in density and an increase in velocity; the net result is a positive increase in impedance (Fig. **F5A**).

Each lithologic unit is imaged as a distinct seismic facies. Lithologic Unit I is characterized by laterally continuous high-amplitude seismic reflections (Fig. **F6A**). These reflections are largely parallel; however, in the upper part of the section, they converge and onlap to the south-southeast (apparent direction in the plane of the seismic cross section shown in Fig. **F6B**) as Unit I thins. We interpret that the well-stratified and laterally continuous reflections are caused by abundant 10–50 m thick sand cycles as recorded in GR data that were deposited in deep water as turbidite deposits. Unit II is characterized by lower frequency reflections and slightly reduced amplitude relative to Unit I (Fig. **F6A**). The reflectors are generally not continuous; many intersect each other when traced laterally. The low amplitude in Unit II is broadly consistent with an interpretation of silty clay with few silt or sand interbeds. There are several bright reflections within Subunit IIIA, but the unit is generally less reflective than overlying units (Fig. **F6A**). The upper part of Subunit IIIB is relatively transparent and corresponds to a zone with uniformly low velocity abundant wood fragments identified in cuttings and elevated mud gas methane concentrations.

Unconformity UC3 lies near the base of Unit III and is interpreted as an angular unconformity. It truncates underlying reflectors and marks a transition from a transparent section (containing free gas) above to high-amplitude tilted reflectors in a statified basin below. GR values are slightly lower above than below Unconformity UC3, and we interpret this to record a lithologic change. Unconformity UC4 lies at the Unit III/IV boundary and separates reflective strata above from less reflective but more chaotic and discontinuous reflectors below. Reflections within Unit III onlap Unconformity UC4 with an apparent north-northwest–south-southeast direction.

Site C0010

Operations at Site C0010 included drilling with MWD/LWD across the megasplay fault to a TD of 555 m LSF, casing the borehole (with casing screens at the fault), conducting an observatory dummy run to test strainmeter and seismometer deployment procedures, and installation of a simple pore pressure and temperature monitoring system (smart plug). Although the smart plug is relatively simple, it marks the first observatory placement in NanTroSEIZE. All of the planned science objectives for Site C0010 were achieved; although casing operations were adjusted to fit hole conditions after drilling to TD (560 m DSF) with casing to 500 m DSF instead of the planned 525 mbsf outlined in the prospectus. MWD/LWD data (gamma ray and resistivity, including resistivity at bit images) were collected allowing (1) definition of major lithologic unit boundaries and of the shallow megasplay fault zone and (2) determination of the preferred placement of the screened joints interval within the fracture zone interval for the temporary observatory. Through comparison with previously drilled Site C0004 (Kinoshita, Tobin, Ashi, Kimura, Lallemant, Screaton, Curewitz, Masago, Moe, and the Expedition 314/315/316 Scientists, 2009) these data also provide insights into along-strike differences in the architecture of the megasplay fault and hanging wall.

After drilling the hole and in preparation for a future permanent observatory installation, a dummy sensor run was carried out to evaluate reentry operations during instrument deployment. After casing was completed and the borehole cemented, two dummy run tests were conducted, including adjustments for the effects of the Kuroshio Current, which reached speeds of 4.5 kt during the experiment. After the dummy run reentry simulations were completed, the smart plug was installed for short-term (1–2 y) data collection and storage to monitor temperature and pore pressure within the megasplay fault zone.

Lithology

We defined three logging units at Site C0010 on the basis of LWD/MWD measurements (GR and bit resistivity) (Fig. **F10**) and guided by previous results at nearby Site C0004 (Expedition 314 Scientists, 2009; Expedition 316 Scientists, 2009) (Fig. **F11**). Although in detail the sites are not identical (e.g., see **"Log-Seismic integration"**), the observations at Site C0004 provide valuable constraints on lithologic variations at Site C0010 (Kinoshita et al., 2008; Kimura et al., 2008). In particular, data from previous drilling at Site C0004 show that lithologic changes are best defined based on GR measurements.

We define three distinct lithologic packages at Site C0010. From top to bottom, these are slope deposits (Unit I, 0–182.5 m LSF), thrust wedge (Unit II, 182.5–407 m LSF), and overridden slope deposits (Unit III, 407 m LSF to TD). Logging Unit I is divided into two subunits. Subunit IA (0–161.5 m LSF) is characterized by GR and bit resistivity patterns similar to logging Unit I at Site C0004 (Figs. **F10, F11**) and we interpret it as hemipelagic slope sediments composed primarily of mud with minor distal turbidite interbeds. We interpret Subunit IB (161.5–182.8 m LSF) as slope sediments composed of material reworked from the underlying thrust wedge.

Logging Unit II (182.5–407 m LSF) is a thrust wedge comprising the hanging wall of the megasplay fault and is correlated with logging Unit II and lithologic Units II and III at Site C0004. The thrust wedge at Site C0010 has higher GR than at Site C0004, which may indicate higher clay content (Fig. **F11**). Logging Unit III (407 m LSF to TD) is composed of slope sediments overridden by the thrust wedge and correlates with logging Unit III and lithologic Unit IV at Site C0004. On the basis of the LWD data and coring results from Site C0004, we interpret Unit III as hemipelagic muds with minor turbidite interbeds and rare volcanic ash layers.

Structural geology and geomechanics

We measured the attitudes of faults, bedding, and breakouts from LWD resistivity image data. As a result of ship heave during logging operations, the resistivity image data exhibit variable quality. In most of the bedding data, we identified eastward dips of ~45°–60°. However, there is considerable scatter in both dip magnitudes and bedding orientations, and because of limited data quality there are a limited number of observations ($N = 11$). Faults dip to the west and south, with most dips ranging from ~40° to 80°. We observe the highest concentration of faults near the base of the thrust wedge. Notably, the two logging runs through the lowermost ~60 m of the thrust wedge (2900–2970 m LRF) are markedly different. The first logging run (during drilling) exhibits faults with a wide range of dips, generally to the south and west. The second run, which was conducted after reaming in an open hole, exhibits steeply dipping faults (>45° and mostly >60°), and shallowly dipping faults like those noted in the first logging run are not observed.

Borehole breakouts show that S_{Hmax} trends northwest–southeast, similar to other sites on the outer slope along the NanTroSEIZE transect (Sites C0001, C0004, and C0006) (Kinoshita et al., 2008; Tobin et al., 2009) (Fig. **F7**). A sharp discontinuity in stress orientation occurs across the base of the thrust wedge and is consistent with a fault discontinuity (Barton and Zoback, 1994). In contrast, the trend of breakouts at Site C0004 changes gradually downhole and is continuous across the base of the wedge (Kinoshita et al., 2008). The enlargement of breakouts during the interval between the two logging runs indicates that the breakouts grew with time in this environment, in contrast to observations from more lithified rocks (Zoback, 2007).

Physical properties

Physical properties from logging data collected at Site C0010 include GR, bit resistivity, shallow-, medium-, and deep-button resistivity, and ring resistivity (Fig. **F10**). In addition, we estimated porosity from resistivity. However, this approach is limited by the fact that there are no data from cores, cuttings, or logging to calibrate the transform from resistivity to porosity (e.g., Kinoshita et al., 2008; Conin et al., 2008).

Ring resistivity exhibits an overall increase downhole, ranging between 0.7 and 0.9 Ωm in the slope sediments of Unit I (0–182.5 m LSF). Resistivity in the stratified overridden slope deposits of Unit III (407–554 m LSF) below the thrust wedge (Unit II) follows the same trend, with values between 0.8 and 1.2 Ωm. Resistivity values in both Units I and III are similar to those for slope deposits at Site C0004 (Fig. **F11**). The thrust wedge (Unit II) is characterized by significantly higher overall resistivity than the slope deposits above and below. In the lower portion of Unit II (260–407 m LSF) we observe considerable scatter in resistivity, with fluctuations from 1.5 to 2.5 Ωm over distances of ~10–20 m.

The overall higher resistivity and the fluctuations in resistivity in the thrust wedge correlate tightly with increased overall GR values and excursions to lower GR values, respectively (Figs. **F10, F11**). The overall higher resistivity values may reflect increased compaction within the thrust wedge relative to the overlying and underlying slope sediments, increased clay content leading to increased tortuosity, or a combination of the two. We suggest that the large fluctuations superimposed on the overall trend reflect either interbedded coarser grained zones or more intensely faulted and fractured intervals.

We estimated porosity from resistivity using parameters for Archie's law derived at nearby Sites C0001 and C0004 that also penetrated slope sediments and the underlying wedge (Kinoshita et al., 2008; Kimura et al., 2008; Conin et al., 2008), where both logging and core data were available. For the slope apron (Unit I) and underthrust (Unit III) sediments at Site C0010, an exponential porosity-depth trend (Athy, 1930) fits the computed porosities well. In contrast, the estimated porosity of the thrust wedge is markedly lower because of its considerably higher resistivity, although as noted above the higher resistivity may be partly due to increased clay content. Preliminary calculations suggest that lithologic effects are unlikely to fully explain the magnitude of resistivity increase within the thrust wedge, indicating that it may reflect increased compaction state related to its burial history or increased in situ stress in the wedge relative to the slope sediments.

Log-Seismic integration

We used the time-depth data acquired at Site C0004 (Expedition 314 Scientists, 2009) to correlate the logs to the seismic data at Site C0010. The Unit I/II boundary marking the top of the thrust wedge is imaged with a weak positive polarity seismic reflection that is coincident with a sharp increase in resistivity (Figs. F10, F11). The Unit II/III boundary between the base of the thrust wedge and overridden slope sediment is recorded by a prominent negative polarity reflection. At this boundary, the resistivity drops markedly. We interpret that velocity and density also decrease at this boundary, resulting in the negative impedance contrast.

At Site C0010, GR values in the thrust wedge increase gradually from 65 API at the top to 120 API at the thrust wedge center and decrease to 80 API at the base (Fig. F10). Several fluctuations in GR values with depth are superimposed on this overall trend, with values ranging from 60 to 80 API units; resistivity cycles within the thrust wedge parallel decreases in GR values. We observe greater seismic reflection amplitudes within the thrust wedge at Site C0010 than at Site C0004 (Fig. F11; cf. Fig. F4B). We conclude that the fluctuations in composition or physical properties within the thrust wedge at Site C0010 recorded in GR and resistivity drive differences in velocity and density (impedance) that generate seismic reflections (see "Lithology" and "Physical properties"). These results suggest significant variation in composition or other properties in the thrust wedge over a scale of only a few kilometers. A striking feature of seismic profiles across the thrust wedge is that the negative polarity reflector is weak at the tip of the thrust wedge and increases where it is more deeply buried (Fig. **F4B**). The most likely explanation for this is that there is increasing consolidation in the thrust wedge relative to the underlying material.

Observatory

Sensor dummy run test

As part of our operations at Site C0010, we conducted two sensor dummy run tests to simulate future installation of long-term observatory instruments, with the goal of documenting vibration and shock associated with running the instrument package through the water column and reentering the borehole. During the first dummy run, two seismometers, an accelerometer-tiltmeter, a strainmeter, and nine miniature temperature loggers (MTLs) were attached to the sensor tree (Fig. **F12A, F12B**). In addition, two full joints and one pup joint of tubing were attached below the strainmeter to replicate the planned future installation procedure. Because of the high current in the area of Site C0010 (~4–5 kt surface current), we ran the instrument carrier to ~500 m DRF in a low-current area (LCA) and then drifted toward the drill site. Unfortunately, while drifting to the site for reentry, one seismometer was dropped from the instrument carrier, and the strainmeter was detached from the bottom of the carrier because the current caused strong vibrations of the drill pipe. After visual confirmation that these components were lost (by ROV at ~1650 meters below sea level [mbsl]), we retrieved the instrument carrier without reaching the seabed. However, acceleration, tilt, and temperature data in the water column were collected during this dummy run.

After the first run, we repaired the instrument carrier and conducted a second dummy run using the accelerometer-tiltmeter attached to the instrument carrier to evaluate shock, acceleration, and vibration during reentry. This run also included a dummy strainmeter, with similar dimensions and mass to a real strainmeter, and two full joints of 3½ inch tubing attached below the instrument carrier. The bottom of the sensor tree was reentered into the wellhead three times to 5–7 m DSF. The reentry operations were generally very smooth; during the third reentry, the tubing below the sensor tree hit against the reentry cone two times. After the sensor tree was recovered, the accelerometer-tiltmeter was checked. Unfortunately, the recording stopped because of damage sustained by vibration in the water column and no acceleration and tilt data were obtained for the reentry test.

Smart plug installation

After the observatory dummy runs were completed, we suspended Hole C0010A by installing a smart plug instrument package below a mechanically set retrievable casing packer (Fig. **F12C, F12D**). The retrievable packer was set inside casing above two screened casing joints; the smart plug and screen placement in the casing were configured to continuously monitor pore pressure and temperature in an isolated interval of formation including the splay fault and also monitor hydrostatic pressure as a reference (Fig. **F12C**). The smart plug contains two high-precision pressure transducers with period counters and four temperature sensors (one as part of each pressure gauge for compensation, one platinum chip thermistor, and one stand-alone MTL) in a shock-proof housing (Fig. **F12D**). The self-contained instrument has a recording lifetime of ~7 y.

The smart plug is designed to thread onto the casing packer. Based on difficulties with the dummy run caused by the strong Kuroshio Current, we further secured the smart plug to the crossover below the packer by tack-welding prior to running it into the water column (Fig. **F12D**). The smart plug safely entered the hole and the packer was set at 364 m DSF. Retrieval of the bridge plug and instrument package is anticipated for 2010 or 2011 when a more sophisticated long-term monitoring system will be deployed at Site C0010 (Fig. **F13**).

Key results and implications

Geomechanics: structures and stress state

We collected several data sets at Sites C0009 and C0010 that provide constraints on present-day in situ stress orientation and magnitude, as well as on past deformation. At Site C0009, borehole breakouts inferred from wireline calipers in Unit IV (1285–1579.9 m WMSF) indicate that S_{Hmax} is oriented 148°–328° (northwest–southeast). DITF tentatively interpreted from borehole resistivity images in Unit II (~800–1000 m WMSF) are also compatible with a northwest–southeast oriented S_{Hmax}. This orientation is ~90° to that at Site C0002, located ~20 km seaward in the Kumano Basin (Fig. **F7**). At Site C0010, breakouts observed in RAB images indicate a S_{Hmax} orientation of 145°–325° (northwest–southeast), consistent with that seen at previously drilled Sites C0001, C0004, and C0006 on the outer continental slope between the seaward edge of the Kumano Basin and the subduction trench (Tobin et al., 2009). The emerging picture of stress conditions (see also Kinoshita et al., 2008; Tobin et al., 2009) across the margin from borehole observations and seismic reflection data is one in which S_{Hmax} is slightly oblique to the plate convergence direction (but approximately perpendicular to the trench) in the outer accretionary wedge (Fig. **F7**). Near the seaward portion of the Kumano Basin, there is active northwest–southeast extension (approximately perpendicular to the trench) but within an ~15–20 km wide zone. Landward of this, S_{Hmax} rotates back to an orientation nearly perpendicular to the trench and similar to that on the outer slope.

We also obtained two independent direct measurements of S_3 at Site C0009 from an MDT hydraulic fracturing test at 879 m WMSF and a LOT at 704 m DSF (Fig. **F9**). In both cases, the S_{v}, or overburden, is greater than the measured S_3. Under the assumption that the principal stresses are horizontal and vertical, we conclude that S_3 is horizontal ($S_{\mathrm{hmin}} = S_3$) and the vertical stress is either the maximum or intermediate principal stress (S_1 or S_2). Taken together, the results from resistivity imaging (breakouts and DITF) and direct stress measurement (MDT and LOT) at Site C0009 indicate either a normal or strike-slip faulting regime in which S_{Hmax} is oriented northwest–southeast. In the case of normal faults, the dominant strike would be northwest–southeast. The effective stress ratio ($S'_{\mathrm{hmin}}/S'_{\mathrm{v}}$, where effective stress is given by the total stress minus the pore fluid pressure, assumed to be hydrostatic) is significantly greater for the MDT measurement ($S'_3/S'_{\mathrm{v}} = 0.82$) than for the LOT ($S'_3/S'_{\mathrm{v}} = 0.44$) (Fig. **F9A**). We consider the MDT measurement to be slightly more reliable (see **"Downhole measurements"**). The effective stress ratio obtained in the LOT is consistent with active normal faulting for a friction coefficient of $\mu = \sim 0.4$, whereas the differential stress obtained from the MDT measurement is considerably smaller and insufficient to drive active normal faulting unless $\mu < \sim 0.15$ (e.g., Zoback, 2007).

In addition to in situ stress indicators, we documented fault types and orientations from resistivity images, seismic reflection data, and cores to gain insight into deformation history and the associated stress conditions when these structures were active. The relative timing of different phases of faulting can be determined in some cases but recent fault activity cannot be confirmed except where faults cut the seafloor in seismic reflection data. However, it is important to note that these still may not reflect present-day stress conditions. Fractures in resistivity images, including one documented normal fault, trend northeast–southwest and most dip to the northwest (average dip = 45°; modal dip = 60°–70°). Cores exhibit a range of fault types, crosscutting relationships, and orientations. In seismic reflection data close to Site C0002, we observe recently active normal faults trending northeast–southwest and a second, less prevalent set trending northwest–southeast (Kinoshita, Tobin, Ashi, Kimura, Lallemant, Screaton, Curewitz, Masago, Moe, and the Expedition 314/315/316 Scientists, 2009). In the landward part of the Kumano Basin near Site C0009, normal faults are sparse overall and the northwest–southeast trending set becomes slightly more common relative to the northeast–southwest trending set. The presence and orientation of normal faults in the seismic reflection data are generally consistent with in situ stress magnitude and orientation data. However, the predominant northeast–southwest strike of faults and fractures documented in borehole FMI images at Site C0009 is not; if they are normal faults, they are inconsistent with the orientation of S_{Hmax}, whereas if they are thrusts they are inconsistent with the fact that $S_{\mathrm{hmin}} < S_{\mathrm{v}}$.

There are several potential explanations for this range of observations. One possibility is that the structures identified in FMI images are not presently active and therefore are not consistent with present-day stress regime at Site C0009 (northeast–southwest extension, parallel to the margin). This hypothesis is consistent with the fact that the faults and fractures measured by FMI data are resistive, suggesting that they may not be currently active (e.g., Barton et al., 1995). The discrepancy between past and in situ stress states could be related to variations in stress during the earthquake cycle or to longer term processes related to the migration of deformation, resulting in migration of deformation patterns within the basin. At Site C0002, however, fault orientations and present-day stress indicators are in agreement and indicate northwest–southeast extension normal to the margin (Tobin et al., 2009). This state of stress could have existed at Site C0009 previously and could explain the fault orientations in FMI data.

Alternatively, it is possible that measurements of stress state and those of long-term strain taken at different depths in the borehole represent real changes in the stress regime with depth. In this case, the stress regime would be consistent with normal faulting in the upper ~900–1200 m and transition to one of lateral compression below this, perhaps across the boundary into Unit IV. A third possibility is that the two horizontal principal stresses are close in magnitude in the landward portion of the basin (i.e., near Site C0009), such that $S_{\mathrm{hmin}} \approx S_{\mathrm{Hmax}} < S_{\mathrm{v}}$ (i.e., $S_3 \approx S_2 < S_1$). This stress state would permit normal faulting on structures as observed in seismic reflection data and borehole FMI images, while honoring the MDT and LOT stress measurements indicating $S_{\mathrm{hmin}} < S_{\mathrm{v}}$. However, the latter hypothesis does not explain the observation of only one dominant (northeast–southwest) trend for structures in the FMI resistivity data.

Forearc basin development and correlation with Site C0002: depositional and tectonic environment

Our interpretation of new data from Site C0009, evaluated in the context of previous results from drilling in the Kumano Basin (Ashi et al., 2008), parallels the interpretation of geological and tectonic evolution initiated by the Expedition 314 and 315 scientists (Expedition 314 Scientists, 2009; Expedition 315 Scientists, 2009). Four lithologic units were described at both drill sites. These units (Units I and II taken together, Unit III, and Unit IV) comprise three unconformity-bounded depositional sequences (Fig. **F6**). Unit IV, deposited below Unconformity UC4, represents either frontally accreted prism material or slope sediment deposited prior to formation of the modern Kumano Basin (Fig. **F6B, F6C**). We interpret Unit III, which is bounded above and below approximately by Unconformities UC2 and UC4, respectively, as early stage forearc basin fill or slope deposits, some of which may be associated with transport from out of the plane of the cross section shown in Figure **F6B, F6C.** Above Unconformity UC2, deposition of Unit II and Unit I record the Quaternary infilling of the Kumano Basin.

At both Sites C0009 and C0002, drilling penetrated through Pliocene–Quaternary aged basin fill and across a basin-wide unconformity identified in seismic reflection data into finer grained, tilted, and variably deformed late Miocene sediments below. At both sites, this lower unit (Unit IV) is composed of mudstone with thin-bedded fine-grained turbidites. At Site C0002, sediments of this lower unit are significantly deformed and have undergone carbonate dissolution, suggesting deposition below the CCD. This unit was interpreted as accretionary prism material by Expedition 314 and Expedition 315 scientists (Ashi et al., 2008; Tobin et al., 2009). In contrast, at Site C0009, Unit IV is weakly deformed and shows inconclusive evidence for carbonate dissolution and depth relative to the CCD. From the data collected at Site C0009 and comparison with previous drilling results at Site C0002, we interpret Unit IV as weakly deformed accreted trench sediments, as trench-slope deposits overlying accreted trench sediments, or as sediments deposited within the earliest Kumano forearc basin. Above Unit IV, Unconformity UC4 exhibits more than 1000 m of relief between Sites C0009 and C0002 and marks a hiatus of approximately equal age and duration at both sites (~5.6–3.8 Ma) (Fig. **F6**). This suggests a tectonic event of regional significance, possibly related to the onset of out-of-sequence thrusting in the prism or to basement ridge subduction.

Unit III at Site C0009 is approximately coeval with Unit III at Site C0002 (~1.6–3.8 Ma) but it is ~5 times thicker at Site C0009 and highly variable in thickness throughout the basin (Fig. **F6B**). At Site C0002, ~20 km farther seaward in the basin, it is interpreted as a condensed section of early forearc basin or slope basin/apron mudstones (Ashi et al., 2008). At Site C0009, this unit is distinguished from its lateral equivalent at Site C0002 by the presence of silt and ash beds and by abundant terrigenous input including wood and lignite (Figs. **F5A, F8**). We suggest that Unit III at Site C0009 represents early (unconformable) forearc basin or slope deposits.

Unconformity UC2 separates laterally continuous high-amplitude reflections above from a more acoustically transparent unit of variable thickness below. Seismic Surfaces S1a and S2a downlap Unconformity UC2 near Site C0009 (Fig. **F6B, F6C**). Units I and II are a conformable package of sediments grading upward from mudstone (Unit II) to interbedded mudstone and sandstone (Unit I). This conformable succession was deposited at both Sites C0009 and C0002. However, it is greatly expanded at Site C0009, with sedimentation rates of ~700–800 m/m.y. We suggest that these strata record infilling of the Kumano Basin and the progressive landward (northwestward) migration of the depocenter, likely caused by slip on the megasplay and resulting uplift of the seaward edge of the basin (e.g., Moore et al., 2007).

Plate boundary structure from walkaway VSP experiment

A collaborative effort between IODP-Center for Deep Earth Exploration (CDEX) and JAMSTEC enabled a long-offset two-ship walkaway VSP experiment using an air gun source towed by the *Kairei,* along with a zero-offset VSP using a source at the drillship, in both cases shooting to receivers within the borehole. The walkaway VSP tracklines included a single line crossing over the location of the borehole with offsets up to 30 km and a circular trackline around the borehole with ~3.5 km radius to investigate anisotropy. The long offsets allowed refractions and reflections from the accretionary wedge, plate boundary, and subducting plate to be recorded at the wireline tool within the borehole to ~1200 mbsf. Recording arrivals in the borehole environment provides a higher resolution image than surface ship acquisition because the seismometers are coupled to the stiff and less attenuative formation; this configuration also allows high-fidelity measurement of shear waves converted from *P*-waves at subsurface boundaries. The data will allow seismic analyses of the velocity structure of the subduction zone forearc and the seismic attributes of the plate boundary in the region beneath the borehole at ~10–12 km.

Architecture and along-strike variation of the megasplay fault

Although we drilled Site C0010 with only a limited suite of LWD/MWD tools, the resistivity and GR data sets provide a useful basis for comparison with the nearby Site C0004 located ~3.5 km along strike to the northeast. Based on the two penetrations of the thrust wedge, along with observations from 3-D seismic reflection data, it is clear that the character and physical properties of the megasplay fault system vary markedly along strike, even over short distances (Fig. **F11**).

At Site C0010, both GR values and resistivity are higher in the thrust wedge than in the slope sediment above and below (Figs. **F10, F11**). In contrast, at Site C0004 GR values and resistivity within the thrust wedge are only very slightly higher than in the overlying and underlying units and are considerably lower than in the thrust wedge at Site C0010 (Kinoshita et al., 2008). Both GR and resistivity logs are also characterized by fluctuations to lower values in the thrust wedge at Site C0010 that are not observed at Site C0004. The values for the minima in GR and resistivity at Site C0010 are similar to those for the entire thrust wedge at Site C0004.

The base of the thrust wedge at Site C0010 is marked by a negative polarity seismic reflection. In contrast, the base of the thrust wedge at Site C0004 is marked by a positive polarity reflection, consistent with an increase in impedance as expected from observed *P*-wave velocity and bulk density from LWD and core data (Kinoshita et al., 2008; Kimura et al., 2008). The thrust wedge in the vicinity of Site C0004 is seismically transparent in character, whereas at Site C0010 there are several clear reflectors, which likely correlate with variations in GR and resistivity (Fig. **F11**). From both LWD azimuthal resistivity images and seismic data, the base of the thrust wedge is sharper at Site C0010 than at Site C0004, where coring documented a ~50 m thick fault zone (or “fault-bounded package”) (Kimura et al., 2008). This is consistent with the observation that at Site C0010 the mean borehole breakout orientation changes abruptly by ~20°–30° across the base of the thrust wedge, whereas at Site C0004 it does not (Kinoshita, Tobin, Ashi, Kimura, Lallemant, Screaton, Curewitz, Masago, Moe, and the Expedition 314/315/316 Scientists, 2009).

We suggest that the overall higher values of GR and resistivity reflect increased compaction in the thrust wedge at Site C0010 relative to the sediment above and below and relative to the thrust wedge at Site C0004, although it is also possible that these data could reflect a higher clay content. In the latter case, resistivity would be higher due to increased tortuosity associated with fine grain size and surface area. Similarly, the fluctuations in GR and resistivity in the thrust wedge at Site C0004 could reflect variations in porosity or fracture density (with lower values associated with zones of increased fracturing or lower porosity), compositional layering, or a combination of the two.

The negative polarity reflection at the base of the thrust wedge at Site C0010 also suggests that it has a lower porosity than the overridden slope sediments below. However, based on the compaction trend for the slope sediments above and below the thrust wedge inferred from resistivity data (Conin et al., 2008), the overridden slope sediments do not appear to be underconsolidated, as might be the case for compaction disequilibrium (Hart et al., 1995; Saffer, 2003). Thus we conclude that the thrust wedge at Site C0010 is overcompacted, meaning that its porosity is anomalously low for its burial depth. This could result from increased mean effective stresses in the thrust wedge or from uplift of the wedge along the megasplay from greater depth. In contrast, at Site C0004 the thrust wedge exhibits porosity similar to the slope sediments and there is no evidence for enhanced compaction. Downdip from Site C0004, the seismic reflection polarity at the base of the thrust wedge becomes negative, most likely indicating increased compaction of the thrust wedge. Overall, we suggest that in the area of Site C0010 the thrust wedge comprises a consolidated and fractured package that probably originated at greater depth than the thrust wedge sampled at Site C0004, where it may primarily be composed of reworked and deformed slope deposits. This interpretation is consistent with the location of Site C0010 on the flank of a lateral ramp on the megasplay fault (Fig. **F11**).

Insights from scientific riser operations

Expedition 319 marked the first riser drilling in IODP history. As noted above, this allowed us to conduct several scientific operations for the first time in IODP, including measurement of in situ stress, permeability, and pore pressure using the MDT tool, real-time analysis of mud gases, and analysis of cuttings for sedimentological, chemical, structural, and physical property data. Here, we briefly discuss some of the key insights gained from each of these new endeavors.

Stress, permeability, and pore pressure from MDT and LOT measurements

During Expedition 319, we deployed the MDT wireline logging tool in riser Hole C0009A to measure in situ formation pore pressure, formation permeability (often reported as mobility = permeability/viscosity), and S_3 at several isolated depth intervals. This was the first time that the tool had been used in IODP drilling because it is currently not usable with the small-diameter riserless drill pipe used by IODP. We conducted nine single probe tests to measure formation pore pressure and fluid mobility and three dual packer tests (one drawdown test to measure formation hydraulic properties and two hydraulic fracturing tests to measure the least principal stress magnitude) (cf. Fig. F9). Successful deployment of this tool to measure in situ pore fluid pressure and stress magnitude deeper within the accretionary prism and in the vicinity of major fault zones in future riser holes will constitute a major breakthrough in understanding subduction zone fault mechanics and is a critical part of the NanTroSEIZE program. However, there are limitations in using the MDT tool successfully that warrant consideration, most notably that pore pressure and permeability measurements may be unreliable in low-permeability formations ($k < \sim10^{-15}$ m^2) because the time required for pressure equilibration can greatly exceed the deployment time. This also highlights the value of obtaining FMI or other borehole imaging data prior to running the MDT in order to select measurement targets that will yield meaningful data.

Sampling and analysis of cuttings and mud gas

We collected samples from the riser drilling mud, including cuttings, mud, and mud gas, during riser drilling at Site C0009. The results of shipboard analyses may provide guidance for future IODP riser drilling by serving as a blueprint for handling, treatment, and analysis approaches and by demonstrating the types and quality of data that can be obtained from these materials, especially for poorly lithified shallow sediments and sedimentary rocks. In addition to basic lithological description, for sufficiently lithified cuttings (deeper than ~1000 m MSF in ~2.5 Ma claystones at Site C0009) we were able to analyze microfossils to define ages, document deformation features preserved in cuttings, measure physical properties including porosity and density, and quantify composition by XRD, XRF, and carbonate analyses. We also conducted several experiments on cuttings and core samples to investigate the sensitivity of shipboard measurements to cuttings processing techniques (including the composition of fluid used for washing and the soaking time), to the cuttings size fraction(s) used for measurements, and to different drilling modes and mud compositions.

One concern in using drilling mud and cuttings for scientific analysis centered on the ability to obtain intact cuttings from shallow (<2000 m MSF) sediments and sedimentary rock and on uncertainty about the material's depth of origin. Comparisons between cuttings (collected from 5 m depth intervals) and wireline log data at Site C0009 indicate a likely depth uncertainty of ~10 m, but mixing during mud ascent and/or cavings from uphole may occur over larger distances. A second concern was that cuttings may be preferentially preserved from particular lithofacies (i.e., more lithified or cohesive claystones) and thus provide a biased sampling of the formation. Initial results suggest that this is likely the case. We conclude that sedimentological and geochemical data from cuttings (at least over the depth range we encountered) are useful for some applications, including the definition of overall lithofacies from relative abundance of lithic fragments, mudstone cuttings, and disaggregated sands or the characterization of mudrock chemistry, provenance, and compositional variations. Data from cuttings may be less meaningful for other applications such as quantitative grain size assessment, detailed lithofacies characterization, chemical analyses if there are effects from interaction with drilling mud, and physical property measurements.

Based on comparison between cuttings, cores, and logs, we also noted that the absolute values for some measurements on cuttings samples may not accurately reflect formation properties, although trends in these data sets generally show good agreement with equivalent log (or in some cases core) data. This is particularly true for physical properties and some geochemical analyses. For example, the high pH of the drilling mud appears to strongly affect carbonate, calcium, and carbon content. This chemical contamination correlates with the time the cuttings were exposed to drilling mud in the borehole. Similarly, porosity values from cuttings are anomalously high, both with respect to their depth of origin and in comparison to log and core data; the discrepancy varies with sample handling and washing procedures and with soaking time. Thus it appears that the absolute values of compositional and physical property data from cuttings should be treated with caution but that overall downhole trends are likely to be reliable.

We also monitored mud gas chemistry in real time throughout riser drilling operations to document the composition and concentration of gas released from the pore spaces of the formation as it was drilled. This method, used previously during International Continental Scientific Drilling Program scientific continental drilling (e.g., Erzinger et al., 2006), was used in scientific ocean drilling for the first time during Expedition 319. One example of the value and reliability of these data comes from comparison of the drilling mud gas, cuttings, and wireline logging data in Subunit IIIB (Figs. F5, F8). Increased mud gas methane concentrations are clearly correlated with increased wood content in cuttings; gas concentrations are also tightly correlated with several intervals of low V_P/V_S and Poisson's ratio observed in sonic velocity logs (Fig. F8). Because pore water geochemical analyses are not possible on cuttings and are difficult on strongly lithified or low-porosity core samples, mud gas analysis offers a promising approach for characterizing formation fluids in future riser drilling. These data are important for understanding hydrologic and geochemical processes associated with faulting and fluid flow.

Observatory installation and preparation

Dummy run

The dummy run test in Hole C0010A simulated operational procedures for installation of planned permanent future observatories. The permanent observatories include three major components: bottom-hole instruments, tubing to provide mechanical support for downhole cables and capillary tubes, and a circulation obviation retrofit kit (CORK) wellhead (Becker and Davis, 2005), which lands at the casing hanger and suspends the instruments below (Fig. **F12A, F12B**). In this test, we successfully confirmed operational procedures to make up the bottom-hole instruments and lower them into the water, which went very smoothly. We were initially concerned that the weak surface of the strainmeter might hit the guide funnel below the rotary table as the tubing below the strainmeter entered the ocean and was exposed to the Kuroshio Current, but by adjusting the length of tubing prior to assembly we were able to solve this problem by trial and error.

The instruments were subjected to significant vibration on the drill string as the *Chikyu* drifted to the site for reentry because of the high-velocity Kuroshio Current. This resulted in damage to the accelerometer and loss of a seismometer and strainmeter during the two dummy runs. Before the experiment, vibration on the drill string was acknowledged as a potential issue but not emphasized as the primary concern. The tubing and the instrument string are much weaker than drill pipe, and therefore vibration was amplified in these weak sections through resonance. Effects were so strong that it is unlikely that some vital parts of instruments (such as hinges and pivots in the seismometers) could maintain their performance after installation in the hole, even if we could modify design of the instrument carrier to maintain its integrity during installation. In addition, we did not test the entire planned instrument string, which will include a CORK head and >500 m of hydraulic tubing and cables. This experience necessitates a more complete evaluation of the observatory installation and design.

Evaluation and modifications are necessary to address several issues, including: (1) sensor integrity under vibration, (2) resonance effects and stress in sections of the observatory under vibration, and (3) tolerance of downhole cable and capillary tubes to stress and vibration. Acceleration data from the dummy run test in this expedition will provide invaluable information to conduct these evaluations.

There are also other options for installation of long-term observatories that should be considered. The smart plug installed in this expedition (see **"Temporary monitoring system"**) offers one encouraging option for intermediate to long-term emplacement of robust but simple retrievable observatories. In a modified smart plug incorporating a seismometer, continuous seismic observations for a period of 2 y would be possible in conjunction with pressure and temperature observations. Such an installation would still require evaluation of effects from vibration on seismometers and pressure gauges because like the bottom-hole instrument string for the dummy run test, the smart plug is also run into the borehole by drill pipe. Another option would be to separate the tasks of lowering sensors into the hole from lowering the observatory to the seafloor in order to reduce effects from the current-induced vibration during lowering to the seafloor. In this case, an observatory package that houses a bottom-hole sensor and downhole cable wound in a winch could be landed on the reentry funnel of the borehole without severe vibration to sensors and cables. The sensor could then be lowered to the bottom of the hole by wireline using the winch. Such an observation system has been developed for logging (Amitani et al., 2002) but is not used routinely in boreholes. Installation of cabled sensors into a borehole by controlled wireline has also been achieved (Stephen et al., 2003). In this case, the downhole cable was payed out under the seafloor station before reentry. This raises risks of damaging the cable by heave of the ship when the cable is lowered into the borehole. For any of these options, it is necessary to implement assessment of risks in each stage of deployment.

Temporary monitoring system

After LWD, casing, and the dummy run test at Site C0010, we suspended the hole by installing a sensor package (smart plug) attached below a retrievable casing packer (Fig. **F12C, F12D**). The smart plug is a robust, retrievable, stand-alone instrument package designed with relatively short lead time in order to make use of suspended boreholes prior to final observatory installation. Although it is relatively simple, the smart plug at Site C0010 represents the first long-term monitoring in the NanTroSEIZE project and the first observatory element installed by the *Chikyu*. If successful, it will provide another tool for long-term hydrologic and/or thermal monitoring in scientific ocean boreholes.

For the installation at Site C0010, the retrievable casing packer was placed above two screened casing joints that provide hydraulic communication with the megasplay fault zone (Fig. **F12C**). In this configuration, the smart plug will monitor pore pressure and temperature within the megasplay fault and will also record the hydrostatic pressure (overlying ocean) as a reference (Fig. **F12C**). The hole completion relies on cement at the base of the casing shoe and in the annulus (a planned top of cement at ~40 m DSF), and on collapse of soft sediment and thrust wedge material against the casing over the ~400 m of annulus above the screens, to achieve hydraulic isolation from the sediments above and below, respectively. Upon recovery of the instruments (planned for 2010 or 2011), we will assess the efficacy of hydraulic isolation by comparison of the fault zone and hydrostatic pore pressure time series and by the response of the fault zone pore pressure to tidal loading (e.g., Wang and Davis, 1996). We also anticipate conducting a CBL as part of future operations to define the top of cement and to constrain the extent of formation collapse against the casing above the screens.

Despite strong ocean currents (up to 4.5 kt and persisting to a depth of several hundred meters below sea level), the smart plug was successfully run to the wellhead and set inside the casing. However, even for installation of this relatively simple and short sensor package, we encountered problems with the Kuroshio Current; upon running the drill pipe to the surface, the running tool sheared off from the drill pipe at a 3½ inch tubing connection, presumably as a result of vibration in the water column. One key difference between the smart plug and many previous hydrologic observatory installations in ODP (e.g., Becker and Davis, 2005) is that data cannot be downloaded from the sensor package until it is retrieved with the packer using a drillship. Thus, we cannot assess whether damage to the electronics or pressure sensors was sustained during running to the wellhead or hole reentry prior to instrument recovery.

Preliminary scientific assessment

Riser drilling at Site C0009 during Expedition 319 allowed a number of new techniques and measurements. These included measurement of gas from drilling mud; analysis of sediment and rock cuttings; and measurement of in situ stress magnitude, formation pressure, and permeability. Important outcomes of Expedition 319 were an assessment of the scope and limitations of these new techniques and improved cuttings sample handling and processing methodologies. In addition, experience gained from riser drilling with weighted mud during Expedition 319 will be valuable in planning and executing future deep riser drilling. At the riserless Site C0010, the first observatory installation by the *Chikyu* was conducted during the expedition. In addition, future observatory instruments and an instrument carrier were tested during run-in to evaluate the current design. Knowledge gained from this expedition, in terms of both operations and science, will be invaluable for future riser drilling expeditions and for observatory installation.

The goals of this expedition were numerous and involved a wide range of different drilling operations, including coring, drilling mud sampling, wireline logging, LWD/MWD, a VSP experiment involving a second vessel, and observatory installation operations. The aim was to drill at two primary sites over a period of 114 days including 27 contingency days: one site using riserless and riser drilling within the forearc basin above the seismogenic part of the active plate boundary, and the other site using riserless drilling in the shallow part of the major megasplay fault system. The scientific objectives were to further understand the processes and properties of the forearc and fault systems while also preparing for and installing observatory systems for long term monitoring of temperature, pore pressure, deformation, and seismicity at these sites.

Success relative to planned objectives

Site C0009 within the landward part of the Kumano forearc basin was successfully drilled to the planned drilling depth of 1600 mbsf, the proposed site of future observatory sensors. Cuttings were collected for the entire riser drilled interval, with multiple sets in certain intervals. Core recovery was limited in the upper part of the cored section but overall provides sample material for shipboard analysis and postexpedition geotechnical studies at the depth of planned future observatory installation and to calibrate cuttings samples and wireline logs. The three planned wireline logging runs were successfully completed to TD including, for the first time in IODP, the successful deployment of the MDT tool for in situ pore pressure and stress magnitude measurement. A late addition to the operational plan, a zero-offset and walkaway VSP experiment, was incorporated into the operational plan (although with a slightly reduced experiment) despite complex scheduling logistics. Ultimately, the walkaway VSP will provide improved resolution of seismic velocity around the borehole and probably image the plate boundary and other structures beneath the borehole. The borehole was cased to 1540 m DSF, preserving the hole for future observatory installation.

Site C0010 was drilled through the shallow megasplay thrust fault near its updip terminus and overlying the hypothesized updip limit of the seismogenic plate boundary to 560 m LSF with an MWD/LWD (gamma ray and resistivity only) data set collected down the borehole and across the megasplay fault, including relogging an interval because of poor data quality during bad weather. We were able to define major unit boundaries and the fault zone on the basis of the limited MWD/LWD data sets, guided by observations from LWD and coring at nearby Site C0004. The borehole was cased with a screened interval across the megasplay fault zone and cemented as planned. Running of the dummy observatory sensor package to test conditions and adapt engineering design for future installations was hindered by current vibrations and loss of part of the package prior to reentry. Therefore, shock and acceleration data are available in the water column but not from reentry into the borehole. A temporary monitoring package (smart plug) was successfully installed to measure formation pore pressure and temperature within the megasplay fault zone and is programmed to record data until retrieval in the coming 1–2 y.

The integration of core, cuttings, log, and seismic data at and between the two sites, combined with NanTroSEIZE Stage 1 sites provides sediment properties, lithology, and structure at a wide range of sites and depths across the forearc basin and prism; allows interpretation of structure and development of the Kumano basin and forearc from the late Miocene to present; indicates hydrological state of the basin and upper prism sediments from in situ measurements; and provides a comprehensive view of in situ stress variability (primarily orientation) across the forearc.

Additional time at the end of the expedition allowed the planned contingency operations to be assessed and MWD/LWD drilling of future coring Site NT1-07 (Site C0011), the primary coring target for Expedition 322, was chosen as the best science for the time and personnel available. This data set provided an important advance data set to guide the coring, downhole measurements, and sampling plan for Expedition 322. This is a contribution to the overall NanTroSEIZE program and also constitutes an example of successful operational and scientific flexibility that allowed the best use of contingency time. Site C0011 was drilled to 980 m DSF, collecting gamma ray and resistivity data (including resistivity images). These data will be formally reported in Expedition 322 publications.

Problems and challenges

The wide range of different and new drilling operations during Expedition 319 involving different personnel, equipment, and potential problems resulted in a very long and complex planning process. It is therefore unsurprising that operations and logistics were complex during this expedition. At Site C0009, several operational problems were encountered during riser preparations and drilling resulting in lost time. These included recovery of a lost BHA/DAT, riser system installation problems, and DPS issues. However, with specific operations taking both more and less time than anticipated, Site C0009 drilling ultimately ended on schedule but used all allocated contingency time. The constantly changing drilling operations schedule also made planning and conducting the walkaway VSP experiment with *Kairei* very complicated and almost impossible. The flexibility of schedules and vessel availability will need to be reviewed carefully when planning future experiments of this kind.

An additional operational challenge we faced was in cementing both the riser and riserless boreholes. Successful cementing is essential to ensure sealing and good coupling between the casing and formation for both operations (i.e., successful deepening of the borehole and continued control of borehole pressure) and scientific objectives (e.g., integrity of observatory installations and obtaining high-quality VSP data). We encountered some problems in cementing both the 13⅜ inch casing at Site C0009 and the 9⅝ inch casing at Site C0010. In the case of the riser hole, cement loss and low cementing efficiency may be related to mud losses during drilling; merging of data from scientific measurements and operations may be useful in evaluating this possibility. For the riserless site, some uncertainty in the cement job resulted from problems with running and landing the cement dart. In both cases, the outcomes also highlight the value of running CBLs in future operations to define the top of cement and evaluate coupling of casing to the formation.

Riserless drilling of Site C0010 was more simple operationally and took less time than originally scheduled, despite the high velocity of the Kuroshio Current (up to 5 kt) during operations and temporary evacuation during a typhoon. Vibrations induced by the current resulted in the destruction of one instrument and the loss of two others within the sensor package during the dummy run observatory installation at Site C0010. This reduces the amount of data available for future observatory installation planning but importantly indicates the potential impact of the current on the drill string. The significant vibration sustained while running the instruments in the water column and through the Kuroshio Current may prompt a significant redesign of the observatory systems and deployment strategies.

This expedition was the first to process and analyze drilling mud samples, including gas and cuttings. Therefore, considerable preplanning was undertaken and patience and versatility on the part of the science and technical team were needed to analyze samples and maximize scientific achievements. In both cases, all groups have worked extremely hard to provide valuable experimental guidelines for future IODP drilling mud sample handling. This expedition was also unusual in splitting the Science Party into two groups but working continuously and collectively on shipboard data analysis and report preparation with four co-chief scientists and specialty coordinators working together across the halves of the expedition to unify the two groups and the scientific results. This aspect of Expedition 319 was extremely challenging for the co-chiefs, expedition project managers, and also for the science party members and required patience, cooperation, and scientific involvement both before and after shipboard participation. Improved Internet bandwidth for file sharing between shore-based and shipboard science groups will be essential to ensure the success of similar future expeditions. Experiences during this expedition indicate that the entire science party should meet prior to the expedition to reduce the split of the party into two groups and the importance of communication cannot be underestimated. This model will be required for future riser drilling operations; therefore, the experience and lessons learned during Expedition 319 will be invaluable in guiding and planning these efforts.

Operations

Shingu, Japan port call

Loading for Expedition 319 began on 8 May 2009 at Shingu, Japan, a few days later than the originally planned sailing date because of bad weather in the area. A "prespud" meeting was held aboard the *Chikyu* on 9 May 2009. The *Chikyu* departed Shingu at 0930 h on 10 May 2009 to Site C0009 (proposed Site NT2-11B). The Expedition 319 operations summary is shown in Table T2.

Transit to Site C0009

The *Chikyu* departed Shingu for Site C0009 at 0930 h on 10 May 2009. Upon arrival at the site, the ship was set in dynamic positioning mode, the Big Head transducers were lowered, and a detailed seabed survey began at 1700 h on 12 May, finishing on 15 May. Official water depth at the site is 2082.3 m DRF (2054 m mud depth below sea level [MSL]). Two arrays of 10 transponders were deployed on 16 and 17 May and were immediately calibrated. The 36 inch conductor pipe, gamma ray attenuation (GRA)/Mudmat, and DAT were rigged up and the vessel moved 5 nmi upstream to lower the 36 inch conductor through the GRA and Mudmat on 17 May.

Hole C0009A

Initial operations began with a run in the hole and jet-in after the ROV seafloor survey.

Spudding in Hole C0009A (33°27.4704′N, 136°32.1489′E) took place at 0930 h on 19 May, followed by jetting-in the 36 inch conductor. The 36 inch conductor was successfully installed to 2136.8 m DRF (54.5 m DSF) by 1730 h on 19 May. However, the top connection of the 36 inch DAT sheared because of excessive slackoff and bending of the pipe above the DAT. A successful fishing run was completed on 23 May and the 26 inch drilling BHA reentered the 36 inch wellhead at 0700 h on 24 May. Drilling with the 26 inch BHA and MWD continued to 2795 m DRF (712.7 m DSF) and successfully reached the target depth on 25 May. A DPS malfunction occurred on 26 May, the investigation of which continued until 30 May, when the DPS was fixed and carefully observed in order to evaluate repairs, while 20 inch casing was prepared for installation. A final decision regarding the DPS failure was made on 31 May and planned operations resumed.

Preparations for running the 20 inch casing began on 1 June and the casing was installed to 2786.2 m DRF (703.9 m DSF) on 2 June with cement operations concluding on 3 June. Rigup for running riser pipe and BOP installation continued until 7 June. Meanwhile, a thruster failure occurred on 4 June and investigations into the cause continued until 8 June. Running down the BOP with riser pipe began on 8 June, with fairings being attached to the uppermost 11 sections of the riser pipe. Problems with the riser tensioner Riser Anitrecoil System (RARS) valves were discovered on 13 June and troubleshooting continued until 17 June. The rotating telescopic joint load ring became stuck on 19 June; however, the BOP was successfully connected to the wellhead on 21 June.

Following the BOP pressure test, the 17 inch drill out cement assembly was run into the hole on 24 June and drilled out 3 m of cement to 2798 m DRF (715.7 m DSF) by 25 June. After this, two LOTs were conducted at the casing shoe on 26 June (see **"Leak-off test"** below). Following the LOTs, the hole was drilled with a 12¼ inch drill BHA with MWD tools, including Power-V and MWD, beginning on 28 June. Cuttings and drilling mud gas were continuously collected during drilling. Including several short trips and circulation from bottoms up, 12¼ inch drilling reached TD at 3592 m DRF (1509.7 m DSF) on 2 July. The first two cores had very poor recovery because of equipment problems and other issues. Cuttings and drilling mud gas were collected during this phase. After coring, the RCB cored section was reamed with the 12¼ inch drilling assembly to open the hole and collect additional cuttings. Opening the hole with the 12¼ inch drilling assembly continued to a final TD of 3686 m DRF (1603.7 m DSF). During this time, lost circulation material was added to drilling mud to address lost circulation in the hole. On 12 July, two wireline logging runs were conducted: the first run with Environmental Measurement Sonde (EMS)-HRLA-PEX-GR, the second one with electromagnetic interference (EMI)-Hostile Natural Gamma Ray Spectrometry Cartridge (HNGC)-Sonic Scanner-EMS-Power Positioning Device and Caliper Tool (PPC). Prior to the third wireline logging run with the MDT, a 12¼ inch wiper trip assembly was run to clean the hole. After the wiper trip, MDT logging was conducted on 14 and 15 July.

Soon after MDT operations finished and the tools were pulled out of the hole, the hole was opened to 17 inches on 16 July. Drilling mud gas was collected during this hole opening phase. Hole-opening operations continued until the hole was reamed to 3650 m DRF (1567.7 m DSF) on 19 July. Several wiper trips and circulation bottoms ups were conducted to clean the hole prior to installing 13⅜ inch casing. Preparations for running began on 21 July and the casing was successfully installed into the hole on 22 July. The 13⅜ inch casing shoe was set at 3624.3 m DRF (1542 m DSF). Cementing the 13⅜ inch casing took place on 23 July. During cementing operations, landing of the second cement plug could not be confirmed, and cement loss was observed (84% efficiency for the cement job). Upon pulling the cementing assembly to the surface, cement was found on the ports of the tool, indicating the possibility of a cement leak from the tool at the casing hanger. A junk basket with a 12¹⁄₁₆ inch gauge ring was run into the hole to determine if any cement was left inside the 13⅜ inch casing. The junk basket run encountered resistance at 2075–2080 m DRF (near the wellhead). After several attempts, the junk basket was rerun with an 8¼ inch gauge ring, and the casing was found to be sufficiently clear to run the VSI tool string. This plan modification, of running the junk basket rather than the scraper, as well as the cancellation of the CBL, was made in part to adjust the VSP operation time to match the availability of the shooting vessel, *Kairei*. Five VSI sensor arrays were rigged up on 24 July, and a check shot test was performed. There was a problem found in the VSP cables, so the sensor arrays were retrieved and checked. Four arrays of VSP tools (a total of 16 shuttles) were put back into the hole after finding a communication problem between Number 4 and Number 5 arrays. The walkaway VSP experiment with *Kairei* was started at ~2000 h on 24 July. One line and one circle shooting transect for the walkaway VSP experiment was finished on 25 July, followed by a zero-offset VSP on the same day (see **"VSP operations"**). Preparations to retrieve the BOP started on 26 July, and all riser pipes and the BOP were safely retrieved on 30 July. Retrieving transponders via ROV was completed early on 31 July, and the ROV set the corrosion cap into the wellhead on the same day. All operations for Hole C0009A were completed at 2400 h on 31 July. The *Chikyu* started moving to Site C0010 (proposed Site NT2-01J) at 0000 h on 1 August.

Leak-off test

After 20 inch casing was run to 703.9 m DSF and cemented to 708.6 m DSF, the hole was deepened to 715.7 m DSF. The hole was circulated and cleaned. Preparations for the LOT started at 2315 h on 25 June. From ~0000 to 0200 h on 26 June, there were various problems with a valve (the upper inline blowout preventer [IBOP]): the lower IBOP kill line was flushed and tested at 1000 pounds per square inch (psi).

The first LOT began at 0215 h, with 1.08 g/cm^3 of KNPP mud at a pump rate of 0.25 bbl/m. Pumping stopped when the pump pressure reached 116 psi. The total volume pumped was 2.2 bbl. The leak-off pressure was 105 psi, or an equivalent mud weight (EMW) of 1.106 g/cm^3 at the casing shoe. The maximum pressure was recorded as 116 psi (EMW = 1.109 g/cm^3). After pumping stopped there was a flowback volume of 0.5 bbl.

Preparation for the second LOT started at 0306 h. Both mud tanks were filled for a line pressure test. Pressure was held at 272 psi. At 0322 h, the LOT proceeded with a 1.08 g/cm^3 KNPP mud at a pump rate of 0.25 bbl/m. The pump was stopped when pressure reached 135 psi, for a total pumped volume of 3.6 bbl. The leak-off pressure was 105 psi, or an equivalent mud weight of 1.106 g/cm^3. The maximum pump pressure was 133 psi, or an EMW = 1.113 g/cm^3. After pumping stopped there was a flowback volume of 0.5 bbl.

VSP operations

The VSP experiment was divided into two parts: a walkaway VSP in conjunction with the research vessel *Kairei* and a zero-offset VSP conducted by the *Chikyu* alone. Operations for the walkaway VSP were adjusted from the precruise plans because of scheduling uncertainties and delays with expedition operations. One line of air gun shooting, combined with one circuit around *Chikyu,* was achievable in the time available. Before OBS deployment, synchronization of radio signals between the *Kairei* and the *Chikyu* was checked and confirmed. The *Kairei* began operations by dropping eight OBSs, in conjunction with four broadband OBSs, which had been placed in 2008. After pulling out of the hole following the junk basket run, the VSI tool string, consisting of 20 seismometers, was lowered into the hole to 2085.5 m DRF at 0730 h on 24 July. Caliper checks on each seismometer, used to couple the tools to the formation, thereby improving data collection, indicated that a short circuit had occurred somewhere along the string. Therefore, the VSI string was pulled from the hole at 1030 h and the 4 seismometers were removed to reduce risks of further cable problems, leaving 16 seismometers remaining on the VSI tool for the walkaway VSP. The VSI tool was again lowered into the hole at 1600 h and locked in the casing from 2999.2 to 3227.8 m DRF. *Kairei* deployed four air gun strings, and after a check shot at 1951 h, it was determined that the formation coupling was poor at this interval, so the VSI tool was raised to 2963.7–3222.3 m DRF and anchored in preparation for a shaker test, which tests the connection of the seismometers to the casing and, in turn, the casing to the formation. *Kairei* began moving along the linear transect, shooting at 2018 h, and recorded the first position at ~24.1 km, with a 60 m shot interval. When the *Kairei* reached a point 1 nmi from the *Chikyu* on 25 July at 0311 h, she made a slight deviation from course and then at 0327 h, an intermission in shooting until the circle (clockwise around the *Chikyu*) transect began at 0405 h. The shooting interval for the circle transect was 30 s at a distance from the *Chikyu* of 3.5 km; shooting finished at 0632 h. The *Kairei* then returned to the line transect and resumed shooting the linear transect at 0713 h. At 10.7 km from Hole C0010A, the Number 3 gun array on *Kairei* unexpectedly stopped firing; however, firing continued with the remaining 3 arrays. The line transect ended at 0847 h on 25 July, when the *Kairei* reached a point 29.3 km from Hole C0009A.

Preparations for the zero-offset VSP experiment began immediately; the *Chikyu* deployed a set of air guns suspended from a crane off the port side of the ship. These were shifted to a point farther from the *Chikyu* to avoid causing any damage to the azimuth thrusters from the underwater shocks. A delay of ~4 h occurred because of repeated failures of the shear pin on the compensation line. An additional delay was caused by the use of faulty shackles on the air gun assembly—the crane operator noticed that condemned shackles had been used and called for their replacement before deploying the air gun at 1145 h. The zero-offset VSP began with the VSI array in the same position it was for the walkaway VSP, but between shootings the array was moved upward in the casing at 122 m intervals. Shooting and recording began at 1620 h, and it was soon discovered that Seismometers 9 and 10 were malfunctioning, and it was decided to run the zero-offset VSP with only the Seismometers 1–8 ($N = 8$). At 1916 h, pulling out of the hole for the VSI tool string began, finishing rigdown at 0100 h on 26 July.

Transit to Site C0010

After operations were completed at Site C0009, the *Chikyu* moved to Site C0010 (proposed Site NT2-01J). While in transit, the drill pipe was set up and racked in preparation for running into the hole. The location was reached at 0100 h on 5 August 2009, and the ROV engaged in a seabed survey.

Hole C0010A

The *Chikyu* moved to the new location after completing operations in Hole C0009A, and Schlumberger engineers and technicians prepared the Schlumberger MWD and LWD tools for assembly prior to drilling Hole C0010A (target depth = 560 mbsf, water depth = 2523.7 m). The BHA included a 12¼ inch bit, RAB-8, TeleScope, stabilizer, crossover subs, 11 drilling collars, and a mechanical jar. The mud cart and jet-in tools were prepared and hung below the *Chikyu* in the LCA prior to drifting to the site. The ROV was again deployed for the jet-in, which occurred on 5 August at 0745 h. The jetting-in included placing a Mudmat and 20 inch casing to 41 m DSF.

The BHA was made up of a 12¼ inch bit, with an 8¼ inch LWD GVR measuring natural GR and resistivity, and the MWD-PowerPulse measuring direction and inclination, torque, and weight on bit. After MWD and LWD drilling to 402 m DSF, operations were suspended on 9 August to move the *Chikyu* to safety, out of the path of Typhoon "Etau," and wait on weather. Although the winds and wave predictions were not very severe (21–31 m/s winds and 5.9–9.5 m swells), the heave prediction was of greater concern. Heave had a detrimental influence on the LWD data quality, and the Co-Chief Scientists and Operations Superintendent (OSI) decided to ream and relog the hole from 2900 to 2970 m DRF, in order to improve the data quality around the fault zone target and to better define locations for screen joint placement. After the storm passed, the *Chikyu* returned to Site C0010 to resume drilling operations to TD, arriving on the morning of 12 August at 0200 h. Reaming operations began at 0300 h and included relogging the 2900–2970 m DRF section. TD (3107 m DRF, 555.00 m DSF) was reached on 12 August at 1715 h, when circulation and Hi-Vis mud was pumped into the hole. Operations continued with a wiper trip to the 20 inch casing shoe at 41 m DSF and then running back to the bottom of the hole. Because the wiper trip exhibited tightness in one section of the hole below 2995 m DRF even after reaming, reaming continued from 2995 to 3107 m DRF. After spotting with kill mud, pulling out of the hole to 2584 m DRF, and then washing to 2543 m DRF to clean the wellhead, pulling out of the hole continued to surface while recovering the ROV in preparation for moving the *Chikyu* to a LCA. At 1700 h, the BHA was back on the drill floor.

The *Chikyu* moved upcurrent, and then 13 nmi northwest of Site C0010 to an LCA to run the casing pipe, finishing preparations on 13 August. After examining the LWD data from Runs 1 and 2, the bottom depth of the screen casing joints was set at 2959 m DRF (407.59 m DSF). Casing was run into the water column, and the *Chikyu* started drifting to Hole C0010A on 14 August. At 1120 h on 15 August, the casing was run into Hole C0010A and reached 500 m DSF at ~1443 h. At 2130 h pulling out of the hole began, and at 2230 h the stinger was out of the hole. There was no signal from the cement dart to show that it had landed/seated properly, so a scraper run was planned. There was a break while the ROV umbilical was under repair, during which the 8½ inch drill collar was made up for a scraper run. The scraper run was cancelled after the cement dart was found when the BHA was disassembled. Instead, a drift in from 2 nmi above Site C0010 for a sweep entered the hole at 1210 h on 17 August and finished at 1400 h, reaching deck at 1621 h. With the sweep finished, the dummy run could begin. On 19 August, OBSs used in conjunction with VSP operations at Site C0009 were acoustically released and recovered by the supply ship, *Kaiko,* at 2020 h on 20 August.

Dummy run

The dummy run began in the LCA at 0830 h on 18 August and involved testing whether it could be run through the 9⅝ inch casing, since it was discovered that the dummy run sensor carrier was warped. After confirming that it could pass though the casing unimpeded at 0900 h on 18 August, the entire array was made up beginning at 1215 h and run into the hole at 1500 h. During these operations, the smart plug was tested in preparation for installation in Hole C0010A. There was considerable vortex-induced vibration from the strong current (4.5 kt) during drifting in to location, and the carrier was held at 1650 mbsl for ROV inspection. At 1750 h on 19 August, the ROV was deployed and at 2045 h reached the carrier. Visual inspection revealed that the strainmeter and tubing below were lost, as well as one of the two seismometers. The remaining seismometer and accelerometer remained attached, and at 2130 h, after meeting with the OSI, the Co-Chief Scientists decided to recover the carrier to the surface for further inspection. As *Chikyu* moved north 9 nmi to the LCA, the carrier was pulled up, reaching deck at 0400 h on 20 August. The carrier showed signs of polishing and cracking and required around 4 h for the ship's welder to repair. The second dummy run carrier used only the accelerometer and a dummy strainmeter with two tubing joints below the seismometer, and it was decided to stab the reentry cone 2–3 times with no attempt to pass the carrier into the hole. The carrier was returned to the water at 1500 h on 20 August and lowered below the Kuroshio Current, and the *Chikyu* drifted back to Hole C0010A. At 0915 h on 21 August, the *Chikyu* returned to the site and jumped the ROV in preparation for stabbing the wellhead. At 0955 h the carrier was ready for stabbing into Hole C0010A, which began at 1010 h, followed by the second stab and the third at 1025 h. Pulling out of the hole began at 1040 h, and the carrier reached the drill floor at 1630 h.

Smart plug

The smart plug was made up and welded to the crossover sub at 0525 h on 22 August and then run into the hole. Drifting to Site C0010 began, and at 1350 h, 4 nmi from the site, the ROV was deployed. At 1709 h, the *Chikyu* was still 9.2 nmi from Hole C0010A, arriving at 0110 h on 23 August. There was another delay as the ROV umbilical needed work to fix another broken strand. The smart plug and packer were run into Hole C0010A at 0404 h, and the packer was set at 0850 h. The drill string was removed at 0930 h while the *Chikyu* moved again to the LCA, this time only 3 nmi from Site C0010. Upon recovery, it was discovered that the running tool had sheared off of the drill pipe in the water column at a 3½ inch tubing connection. The corrosion cap was attached to the ROV carrier, in preparation for setting in at the wellhead. At 1800 h, the ROV was launched but experienced problems with the umbilical again at 2030 h. After troubleshooting was completed, the corrosion cap was finally set at 1015 h on 24 August. The ROV began recovery of the transponders but again ran into trouble and was recovered on deck. It was decided to recover the remaining three transponders with the *Kaiko,* after acoustically releasing them from the seafloor. By 1200 h on 25 August, with all transponders recovered, the *Chikyu* began moving toward Site C0011 (proposed Site NT1-07).

Transit to Site C0011

After operations were completed at Site C0010, the *Chikyu* moved to Site C0011 (proposed Site NT1-07). While recovering the transponders at Site C0010, the drill pipe was set up and racked in preparation for running into the hole. The location was reached at 1700 h on 25 August 2009.

Hole C0011A

The *Chikyu* moved to the new location after completing operations in Hole C0010A, and Schlumberger engineers and technicians prepared the Schlumberger MWD and LWD tools for assembly, prior to drilling Hole C0011A (target depth = as deep as possible or 900 mbsf, water depth = 4049 m). Because the water depth was too great for ROV placement of transponders and the ROV was under repair, the six transponders were dropped from the surface. All transponders were dropped by 0400 h on 26 August. At 0845 h on 26 August, the 12¼ inch bit LWD/MWD BHA was run into the hole, and a calibration check was conducted between the Big Head transducers on the ship and the transponders deployed on the bottom. At 1900 h on 26 August, a prespud meeting was held to determine target depth (900 m LSF), jet-in program, and conditions for stopping drilling. Spud-in of Hole C0011A was achieved at 2239 h on 26 August, and the water depth was confirmed by MWD GR measurement at 4049 m. After jetting in to 41 m DSF, drilling the 12¼ inch hole commenced from this depth. There were short wiper trips and sweeps to ensure that the borehole condition remained good and to prevent getting the BHA stuck in the hole when the available drilling time ran out. We reached TD (952 m LSF) at 2400 h on 29 August, spotted 121 m^3 of 1.30 g/cm^3 kill mud, and began pulling out of the hole. The BHA reached the surface at 1300 h on 30 August, and the tools were laid down for LWD data recovery. In the meantime, the *Chikyu* moved to the rendezvous point for the supply ship, the *Kairei,* to load and backload cargo for Expedition 322.

Transit to Yokkaichi

After finishing laydown of the BHA and drill pipe and finishing cargo loading with the *Kairei,* the supply ship was released and the *Chikyu* continued moving to Ise Bay to dock at the port of Yokkaichi, Japan, reaching the headlands at 1600 h on 30 August.

References

Abbas, R., Jarouj, H., Dole, S., Junaidi, E.H., El-Hassan, H., Francis, L., Hornsby, L., McCraith, S., Shuttleworth, N., van der Plas, K., Messier, E., Munk, T., Nødland, N., Svendsen, R.K., Therond, E., and Taoutaou, S., 2004. A safety net for controlling lost circulation. *Oilfield Rev.,* Winter 2003:20–27.

Amitani, Y., Kyo, M., Hashimoto, K., Shimura, T., and Sawa, T., 2002. Borehole Reentry System "BENKEI". *Proc. Int. Offshore Polar Eng. Conf.,* 12:116–121.

Ando, M., 1975. Source mechanisms and tectonic significance of historical earthquakes along the Nankai Trough, Japan. *Tectonophysics,* 27(2):119–140. **doi:10.1016/0040-1951(75)90102-X**

Araki, E., Byrne, T., McNeill, L., Saffer, D., Eguchi, N., Takahashi, K., and Toczko, S., 2009. NanTroSEIZE Stage 2: NanTroSEIZE riser/riserless observatory. *IODP Sci. Prosp.,* 319. **doi:10.2204/iodp.sp.319.2009**

Ashi, J., Kuramoto, S., Morita, S., Tsunogai, U., Goto, S., Kojima, S., Okamoto, T., Ishimura, T., Ijiri, A., Toki, T., Kudo, S., Asai, S., and Utsumi, M., 2002. Structure and cold seep of the Nankai accretionary prism off Kumano—outline of the off Kumano survey during YK01-04 Leg 2 cruise. *JAMSTEC J. Deep Sea Res.,* 20:1–8. (in Japanese, with abstract in English)

Ashi, J., Lallemant, S., Masago, H., and the Expedition 315 Scientists, 2008. NanTroSEIZE Stage 1A: NanTroSEIZE megasplay riser pilot. *IODP Prel. Rept.,* 315. **doi:10.2204/iodp.pr.315.2008**

Athy, L.F., 1930. Density, porosity, and compaction of sedimentary rocks. *AAPG Bull.,* 14:1–24.

Baba, T., and Cummins, P.R., 2005. Contiguous rupture areas of two Nankai Trough earthquakes revealed by high-resolution tsunami waveform inversion. *Geophys. Res. Lett.,* 32(8):L08305. **doi:10.1029/2004GL022320**

Baba, T., Cummins, P.R., and Hori, T., 2005. Compound fault rupture during the 2004 off the Kii Peninsula earthquake (M 7.4) inferred from highly resolved coseismic sea-surface deformation. *Earth, Planets Space,* 57(3):167–172.

Baba, T., Cummins, P.R., Hori, T., and Kaneda, Y., 2006. High precision slip distribution of the 1944 Tonankai earthquake inferred from tsunami waveforms: possible slip on a splay fault. *Tectonophysics,* 426(1–2):119–134. **doi:10.1016/j.tecto.2006.02.015**

Barton, C.A., Zoback, M.D., and Moos, D., 1995. Fluid flow along potentially active faults in crystalline rock. *Geology,* 23(8):683–686. **doi:10.1130/0091-7613(1995)023<0683:FFAPAF>2.3.CO;2**

Barton, C.A., and Zoback, M.D., 1994. Stress perturbations associated with active faults penetrated by boreholes: possible evidence for near-complete stress drop and a new technique for stress magnitude measurement. *J. Geophys. Res., [Solid Earth],* 99(B5):9373–9390. **doi:10.1029/93JB03359**

Becker, K., and Davis, E.E., 2005. A review of CORK designs and operations during the Ocean Drilling Program. *In* Fisher, A.T., Urabe, T., Klaus, A., and the Expedition 301 Scientists, *Proc. IODP,* 301: College Station, TX (Integrated Ocean Drilling Program Management International, Inc.). **doi:10.2204/iodp.proc.301.104.2005**

Byrne, D.E., Davis, D.M., and Sykes, L.R., 1988. Loci and maximum size of thrust earthquakes and the mechanics of the shallow region of subduction zones. *Tectonics,* 7(4):833–857. **doi:10.1029/TC007i004p00833**

Conin, M., Bourlange, S., Henry, P., and the IODP Expedition 314/315/316 Scientific Party, 2008. Interpretation of LWD resistivity from Nankai accretionary wedge in the light of clay physico-chemical properties. *Eos, Trans. Am. Geophys. Union,* 89(53)(Suppl.):T31B–1999. (Abstract) **http://www.agu.org/meetings/fm08/waisfm08.html**

Erzinger, J., Wiersberg, T., and Zimmer, M., 2006. Real-time mud gas logging and sampling during drilling. *Geofluids,* 6(3):225–233. **doi:10.1111/j.1468-8123.2006.00152.x**

Expedition 314 Scientists, 2009. Expedition 314 Site C0004. *In* Kinoshita, M., Tobin, H., Ashi, J., Kimura, G., Lallemant, S., Screaton, E.J., Curewitz, D., Masago, H., Moe, K.T., and the Expedition 314/315/316 Scientists, *Proc. IODP,* 314/315/316: Washington, DC (Integrated Ocean Drilling Program Management International, Inc.). **doi:10.2204/iodp.proc.314315316.116.2009**

Expedition 315 Scientists, 2009. Expedition 315 Site C0002. *In* Kinoshita, M., Tobin, H., Ashi, J., Kimura, G., Lallemant, S., Screaton, E.J., Curewitz, D., Masago, H., Moe, K.T., and the Expedition 314/315/316 Scientists, *Proc. IODP,* 314/315/316: Washington, DC (Integrated Ocean Drilling Program Management International, Inc.). **doi:10.2204/iodp.proc.314315316.124.2009**

Expedition 316 Scientists, 2009. Expedition 316 Site C0004. *In* Kinoshita, M., Tobin, H., Ashi, J., Kimura, G., Lallemant, S., Screaton, E.J., Curewitz, D., Masago, H., Moe, K.T., and the Expedition 314/315/316 Scientists, *Proc. IODP,* 314/315/316: Washington, DC (Integrated Ocean Drilling Program Management International, Inc.). **doi:10.2204/iodp.proc.314315316.133.2009**

Flemings, P.B., Behrmann, I., Davies, T., John, C., and the Expedition 308 Project Team, 2005. Gulf of Mexico hydrogeology—overpressure and fluid flow processes in the deepwater Gulf of Mexico: slope stability, seeps, and shallow-water flow. *IODP Sci. Prosp.,* 308. **doi:10.2204/iodp.sp.308.2005**

Hart, B.S., Flemings, P.B., and Deshpande, A., 1995. Porosity and pressure: role of compaction disequilibrium in the development of geopressures in a Gulf Coast Pleistocene basin. *Geology,* 23(1):45–48. **doi:10.1130/0091-7613(1995)023<0045:PAPROC>2.3.CO;2**

Heki, K., 2007. Secular, transient and seasonal crustal movements in Japan from a dense GPS array: implication for plate dynamics in convergent boundaries. *In* Dixon, T., and Moore, C. (Eds.), *The Seismogenic Zone of Subduction Thrust Faults:* New York (Columbia Univ. Press), 512–539.

Hickman, S., Zoback, M., and Ellsworth, W., 2004. Introduction to special section: preparing for the San Andreas Fault Observatory at depth. *Geophys. Res. Lett.,* 31(12):L12S01. **doi:10.1029/2004GL020688**

Hori, T., Kato, N., Hirahara, K., Baba, T., and Kaneda, Y., 2004. A numerical simulation of earthquake cycles along the Nankai Trough in southwest Japan: lateral variation in frictional property due to the slab geometry controls the nucleation position. *Earth Planet. Sci. Lett.,* 228(3–4):215–226. **doi:10.1016/j.epsl.2004.09.033**

Ichinose, G.A., Thio, H.K., Somerville, P.G., Sato, T., and Ishii, T., 2003. Rupture process of the 1944 Tonankai earthquake (M_s 8.1) from the inversion of teleseismic and regional seismograms. *J. Geophys. Res.,* 108(B10):2497. **doi:10.1029/2003JB002393**

Isozaki, Y., and Itaya, T., 1990. Chronology of Sanbagawa metamorphism. *J. Metamorph. Geol.,* 8(4):401–411. **doi:10.1111/j.1525-1314.1990.tb00627.x**

Ito, Y., Obara, K., Shiomi, K., Sekine, S., and Hirose, H., 2007. Slow earthquakes coincident with episodic tremors and slow slip events. *Science,* 315(5811):503–506. **doi:10.1126/science.1134454**

Kikuchi, M., Nakamura, M., and Yoshikawa, K., 2003. Source rupture processes of the 1944 Tonankai earthquake and the 1945 Mikawa earthquake derived from low-gain seismograms. *Earth, Planets Space,* 55(4):159–172.

Kimura, G., Screaton, E.J., Curewitz, D., and the Expedition 316 Scientists, 2008. NanTroSEIZE Stage 1A: NanTroSEIZE shallow megasplay and frontal thrusts. *IODP Prel. Rept.,* 316. **doi:10.2204/iodp.pr.316.2008**

Kinoshita, M., Tobin, H., Ashi, J., Kimura, G., Lallemant, S., Screaton, E.J., Curewitz, D., Masago, H., Moe, K.T., and the Expedition 314/315/316 Scientists, 2009. *Proc. IODP,* 314/315/316: Washington, DC (Integrated Ocean Drilling Program Management International, Inc.). **doi:10.2204/iodp.proc.314315316.2009**

Kinoshita, M., Tobin, H., Moe, K.T., and the Expedition 314 Scientists, 2008. NanTroSEIZE Stage 1A: NanTroSEIZE LWD transect. *IODP Prel. Rept.,* 314. **doi:10.2204/iodp.pr.314.2008**

Kobayashi et al., 2009. *CDEX Technical Report. Volume 7: Drilling Program NanTroSEIZE Stage 2: IODP Expedition 319 and 322:* Yokohama (CDEX JAMSTEC).

Lay, T., Kanamori, H., Ammon, C.J., Nettles, M., Ward, S.N., Aster, R.C., Beck, S.L., Bilek, S.L., Brudzinski, M.R., Butler, R., DeShon, H.R., Ekström, G., Satake, K., and Sipkin, S., 2005. The great Sumatra-Andaman earthquake of 26 December 2004. *Science,* 308(5725):1127–1133. **doi:10.1126/science.1112250**

Ma, K., 2005. Slip zone and energetic of a large earthquake from seismological modeling and fault core of TCDP. *Eos, Trans. Am. Geophys. Union,* 86(52):T43D-02. (Abstract)

Martini, E., 1971. Standard Tertiary and Quaternary calcareous nannoplankton zonation. *In* Farinacci, A. (Ed.), *Proc. 2nd Int. Conf. Planktonic Microfossils Roma:* Rome (Ed. Tecnosci.), 2:739–785.

Miyazaki, S., and Heki, K., 2001. Crustal velocity field of southwest Japan: subduction and arc-arc collision. *J. Geophys. Res.,* 106(B3):4305–4326. **doi:10.1029/2000JB900312**

Moore, G.F., Bangs, N.L., Taira, A., Kuramoto, S., Pangborn, E., and Tobin, H.J., 2007. Three-dimensional splay fault geometry and implications for tsunami generation. *Science,* 318(5853):1128–1131. **doi:10.1126/science.1147195**

Moore, G.F., Park, J.-O., Bangs, N.L., Gulick, S.P., Tobin, H.J., Nakamura, Y., Sato, S., Tsuji, T., Yoro, T., Tanaka, H., Uraki, S., Kido, Y., Sanada, Y., Kuramoto, S., and Taira, A., 2009. Structural and seismic stratigraphic framework of the NanTroSEIZE Stage 1 transect. *In* Kinoshita, M., Tobin, H., Ashi, J., Kimura, G., Lallemant, S., Screaton, E.J., Curewitz, D., Masago, H., Moe, K.T., and the Expedition 314/315/316 Scientists, *Proc. IODP,* 314/315/316: Washington, DC (Integrated Ocean Drilling Program Management International, Inc.). **doi:10.2204/iodp.proc.314315316.102.2009**

Moore, G.F., Taira, A., Klaus, A., Becker, L., Boeckel, B., Cragg, B.A., Dean, A., Fergusson, C.L., Henry, P., Hirano, S., Hisamitsu, T., Hunze, S., Kastner, M., Maltman, A.J., Morgan, J.K., Murakami, Y., Saffer, D.M., Sánchez-Gómez, M., Screaton, E.J., Smith, D.C., Spivack, A.J., Steurer, J., Tobin, H.J., Ujiie, K., Underwood, M.B., and Wilson, M., 2001. New insights into deformation and fluid flow processes in the Nankai Trough accretionary prism: results of Ocean Drilling Program Leg 190. *Geochem., Geophys., Geosyst.,* 2(10):1058. **doi:10.1029/2001GC000166**

Moore, G.F., Taira, A., Klaus, A., et al., 2001. *Proc. ODP, Init. Repts.,* 190: College Station, TX (Ocean Drilling Program). **doi:10.2973/odp.proc.ir.190.2001**

Moore, J.C., and Saffer, D., 2001. Updip limit of the seismogenic zone beneath the accretionary prism of southwest Japan: an effect of diagenetic to low-grade metamorphic processes and increasing effective stress. *Geology,* 29(2):183–186. **doi:10.1130/0091-7613(2001)029<0183:ULOTSZ>2.0.CO;2**

Nakanishi, A., Takahashi, N., Park, J.-O., Miura, S., Kodaira, S., Kaneda, Y., Hirata, N., Iwasaki, T., and Nakamura, M., 2002. Crustal structure across the coseismic rupture zone of the 1944 Tonankai earthquake, the central Nankai Trough seismogenic zone. *J. Geophys. Res.,* 107(B1):2007. **doi:10.1029/2001JB000424**

Nelson, E.B., and Guillot, D., 1990. *Well Cementing:* Sugar Land, TX (Schlumberger Educational Services).

Obana, K., Kodaira, S., Mochizuki, K., and Shinohara, M., 2001. Micro-seismicity around the seaward updip limit of the 1946 Nankai earthquake dislocation area. *Geophys. Res. Lett.,* 28(12):2333–2336. **doi:10.1029/2000GL012794**

Obara, K., Hirose, H., Yamamizu, F., and Kasahara, K., 2004. Episodic slow slip events accompanied by nonvolcanic tremors in southwest Japan subduction zone. *Geophys. Res. Lett.,* 31:L23602. **doi:10.1029/2004GL020848**

Obara, K., and Ito, Y., 2005. Very low frequency earthquakes excited by the 2004 off the Kii Peninsula earthquakes: a dynamic deformation process in the large accretionary prism. *Earth, Planets Space,* 57(4):321–326.

Park, J.-O., Tsuru, T., Kodaira, S., Cummins, P.R., and Kaneda, Y., 2002. Splay fault branching along the Nankai subduction zone. *Science,* 297(5584):1157–1160. **doi:10.1126/science.1074111**

Raffi, I., Backman, J., Fornaciari, E., Pälike, H., Rio, D., Lourens, L., and Hilgen, F., 2006. A review of calcareous nannofossil astrobiochronology encompassing the past 25 million years. *Quat. Sci. Rev.,* 25(23–24):3113–3137. **doi:10.1016/j.quascirev.2006.07.007**

Ruff, L., and Kanamori, H., 1983. Seismic coupling and uncoupling at subduction zones. *Tectonophysics,* 99(2–4):99–117. **doi:10.1016/0040-1951(83)90097-5**

Saffer, D.M., and Marone, C., 2003. Comparison of smectite- and illite-rich gouge frictional properties: application to the updip limit of the seismogenic zone along subduction megathrusts. *Earth Planet. Sci. Lett.,* 215(1–2):219–235. **doi:10.1016/S0012-821X(03)00424-2**

Saffer, D.M., 2003. Pore pressure development and progressive dewatering in underthrust sediments at the Costa Rican subduction margin: comparison with northern Barbados and Nankai. *J. Geophys. Res.,* 108(B5):2261–2276. **doi:10.1029/2002JB001787**

Saito, S., Underwood, M.B., and Kubo, Y., 2009. NanTroSEIZE Stage 2: subduction inputs. *IODP Sci. Prosp.,* 322. **doi:10.2204/iodp.sp.322.2009**

Seno, T., Stein, S., and Gripp, A.E., 1993. A model for the motion of the Philippine Sea Plate consistent with NUVEL-1 and geological data. *J. Geophys. Res.,* 98(B10):17941–17948. **doi:10.1029/93JB00782**

Stephen, R.A., Spiess, F.N., Collins, J.A., Hildebrand, J.A., Orcutt, J.A., Peal, K.R., Vernon, F.L., and Wooding, F.B., 2003. Ocean seismic network pilot experiment. *Geochem., Geophys., Geosyst.,* 4(10):1092. **doi:10.1029/2002GC000485**

Taira, A., Katto, J., Tashiro, M., Okamura, M., and Kodama, K., 1988. The Shimanto Belt in Shikoku, Japan: evolution of Cretaceous to Miocene accretionary prism. *Mod. Geol.,* 12:5–46.

Tanioka, Y., and Satake, K., 2001. Detailed coseismic slip distribution of the 1944 Tonankai earthquake estimated from tsunami waveforms. *Geophys. Res. Lett.,* 28(6):1075–1078. **doi:10.1029/2000GL012284**

Tobin, H., Kinoshita, M., Ashi, J., Lallemant, S., Kimura, G., Screaton, E.J., Moe, K.T., Masago, H., Curewitz, D., and the Expedition 314/315/316 Scientists 2009. NanTroSEIZE Stage 1 expeditions: introduction and synthesis of key results. In Kinoshita, M., Tobin, H., Ashi, J., Kimura, G., Lallemant, S., Screaton, E.J., Curewitz, D., Masago, H., Moe, K.T., and the Expedition 314/315/316 Scientists, Proc. IODP, 314/315/316: Washington, DC (Integrated Ocean Drilling Program Management International, Inc.). **doi:10.2204/iodp.proc.314315316.101.2009**

Tobin, H.J., and Kinoshita, M., 2006a. Investigations of seismogenesis at the Nankai Trough, Japan. *IODP Sci. Prosp.,* NanTroSEIZE Stage 1. **doi:10.2204/iodp.sp.nantroseize1.2006**

Tobin, H.J., and Kinoshita, M., 2006b. NanTroSEIZE: the IODP Nankai Trough Seismogenic Zone Experiment. *Sci. Drill.,* 2:23–27. **doi:10.2204/iodp.sd.2.06.2006**

Wang, K., and Davis, E.E., 1996. Theory for the propagation of tidally induced pore pressure variations in layered subseafloor formations. *J. Geophys. Res.,* 101(B5):11483-11496. **doi:10.1029/96JB00641**

Wang, K., and Hu, Y., 2006. Accretionary prisms in subduction earthquake cycles: the theory of dynamic Coulomb wedge. *J. Geophys. Res.,* 111(B6):B06410. **doi:10.1029/2005JB004094**

Wiersberg, T., and Erzinger, J., 2007. A helium isotope cross-section study through the San Andreas Fault at seismogenic depths. *Geochem., Geophys., Geosyst.,* 8(1):Q01002. **doi:10.1029/2006GC001388**

Yamano, M., Kinoshita, M., Goto, S., and Matsubayashi, O., 2003. Extremely high heat flow anomaly in the middle part of the Nankai Trough. *Phys. Chem. Earth,* 28(9–11):487–497. **doi:10.1016/S1474-7065(03)00068-8**

Zoback, M.D., 2007. *Reservoir Geomechanics:* Cambridge (Cambridge Univ. Press).

Table T1. Expedition 319 drilling depth terms. (**See table note.**)

Depth term	Depth term explanation
mbsf	Meters below seafloor
DRF	Drilling depth below rig floor (rotary table)
DSF	Drilling depth below seafloor
CSF	Core depth below seafloor
MRF	Mud depth below rig floor (used for drilling mud cuttings and gas)
MSF	Mud depth below seafloor (used for drilling mud cuttings and gas)
WRF	Wireline log depth below rig floor
WMSF	Wireline log matched depth below seafloor
LRF	LWD depth below rig floor
LSF	LWD depth below seafloor

Note: Depth terms are derived from IODP Depth Scales (**www.iodp.org/program-policies/**). LWD = logging-while-drilling.

Table T2. Expedition 319 coring summary. (**See table notes.**)

Hole	Latitude	Longitude	Water depth (mbsl)	Cores (*N*)	Interval cored (m)	Core recovered (m)	Recovery (%)	Drilled interval (m)	Total penetration (m)	Time on site (days)
C0009A	33°27.4704′N	136°32.1489′E	2054	9	84.20	57.87	68.7	1591.8	1603.7	76
			Site C0009 totals:	9	84.20	57.87	68.7	1591.8	1603.7	76
C0010A	33°12.5981′N	136°41.1924′E	2552	0	Set casing/observatory testing			560.0	560.0	21
			Site C0010 totals:	0	0.00	0.00	0.0	560.0	560.0	21
C0011A	32°49.73′N	136°52.89′E	4049	0	LWD/MWD			952.0	952.0	5
			Site C0011 totals:	0	0.00	0.00	0.0	952.0	952.0	5
			Expedition 319 totals:	9	84.20	57.87	68.7	3021.7	3105.9	102

Notes: *N* = number. LWD = logging while drilling, MWD = measurement while drilling.

Figure F1. A. Map of study area showing drill sites. Green squares = Expedition 319, red circles = NanTroSEIZE Sate 1, black box = location of 2006 three-dimensional seismic reflection data acquisition, black line = KR0108-5 two-dimensional seismic profile, yellow arrows = estimated far-field vectors between Philippine Sea plate and Japan (Seno et al., 1993; Heki, 2007), stars = epicentral location of great earthquakes. Inset shows location of Nankai Trough around the drill sites. (**Continued on next page.**)

A

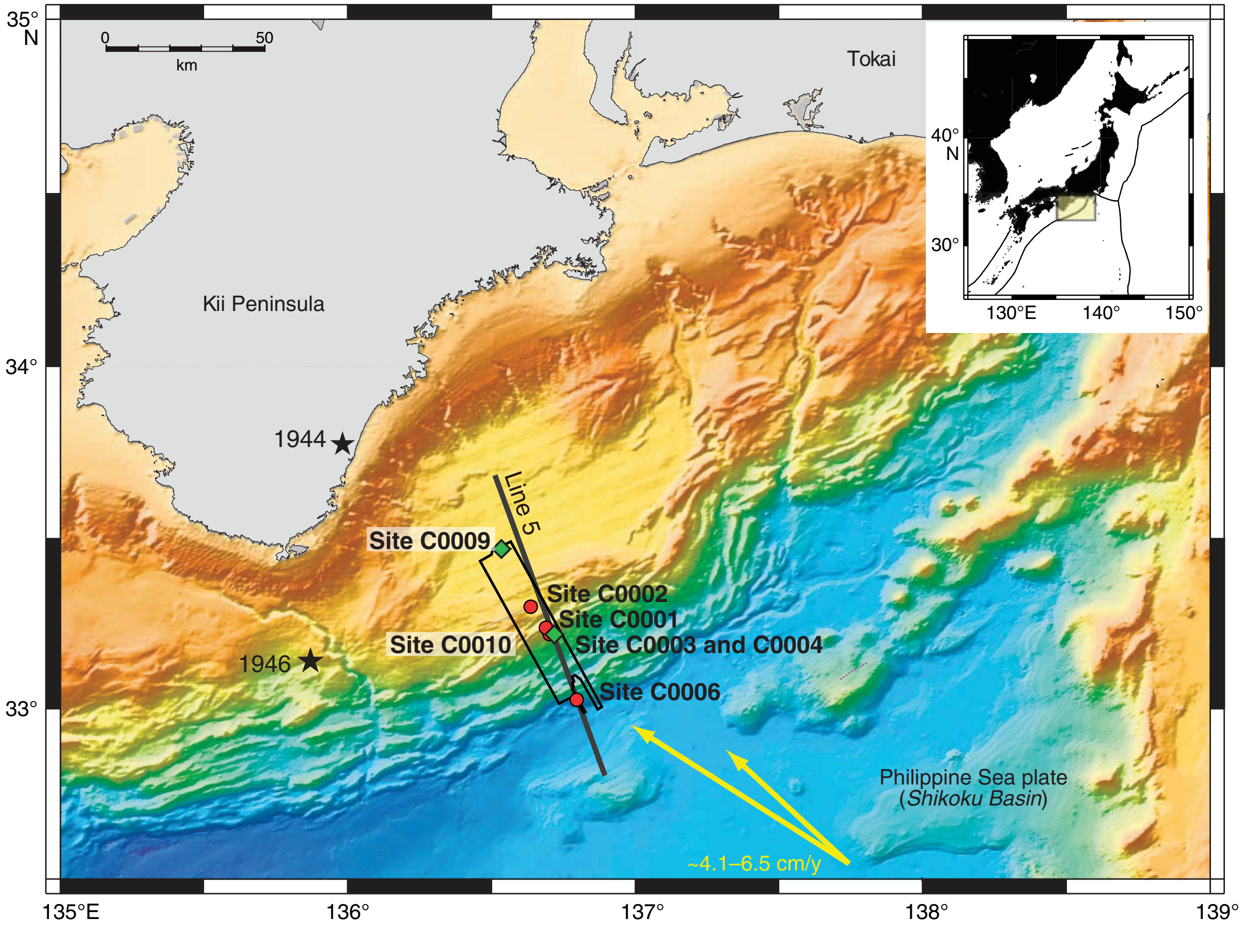

Figure F1 (continued). B. Map of drill sites, details of 1944 earthquake slip, and coseismic very low frequency earthquakes (VLFs). Contours = estimated slip during the 1944 event (0.5 m intervals) (Kikuchi et al., 2003), red box = region of recorded VLFs (Obara and Ito, 2005).

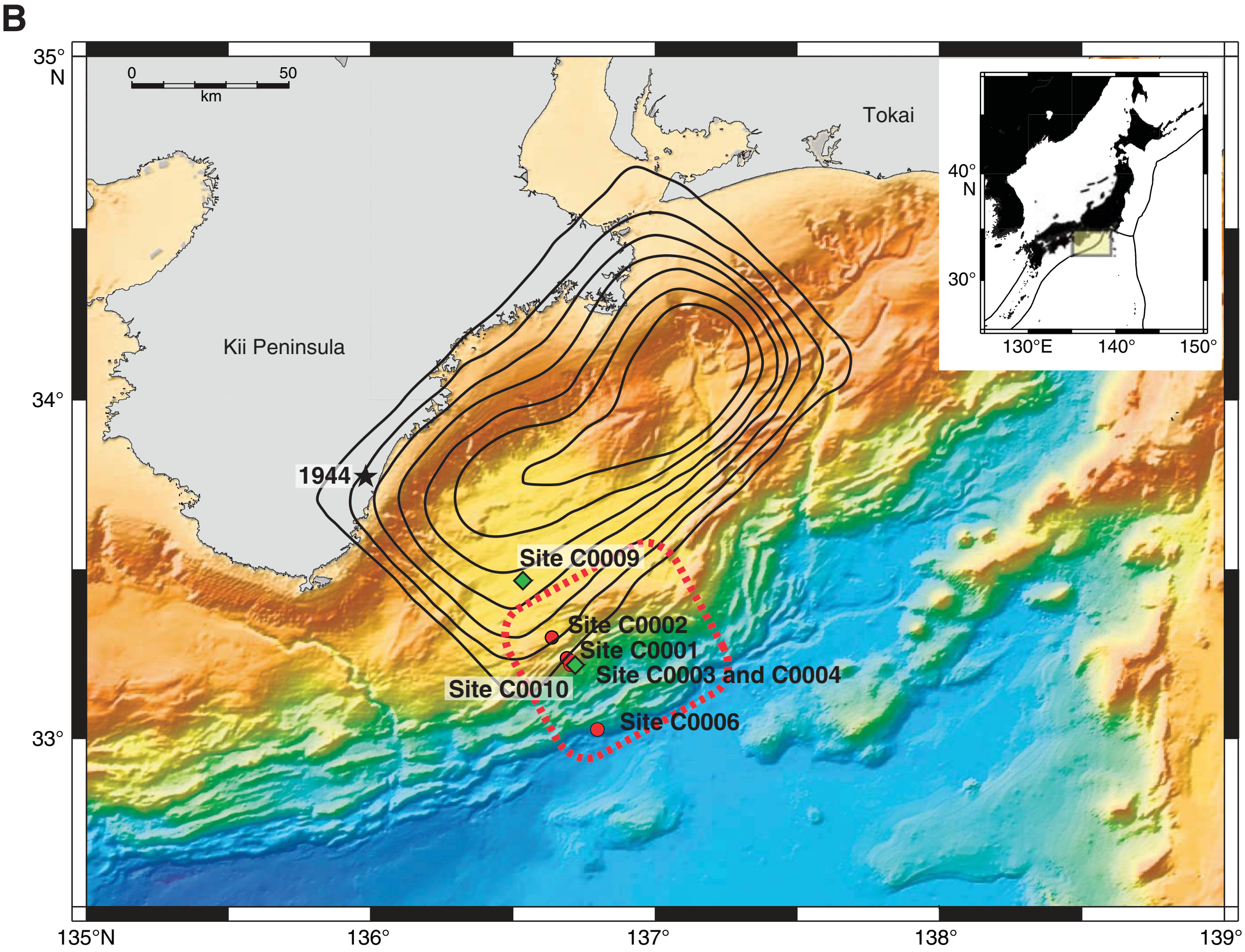

Figure F2. Interpreted seismic line from Park et al. (2002) showing drill site locations. Location shown in Figure F1A.

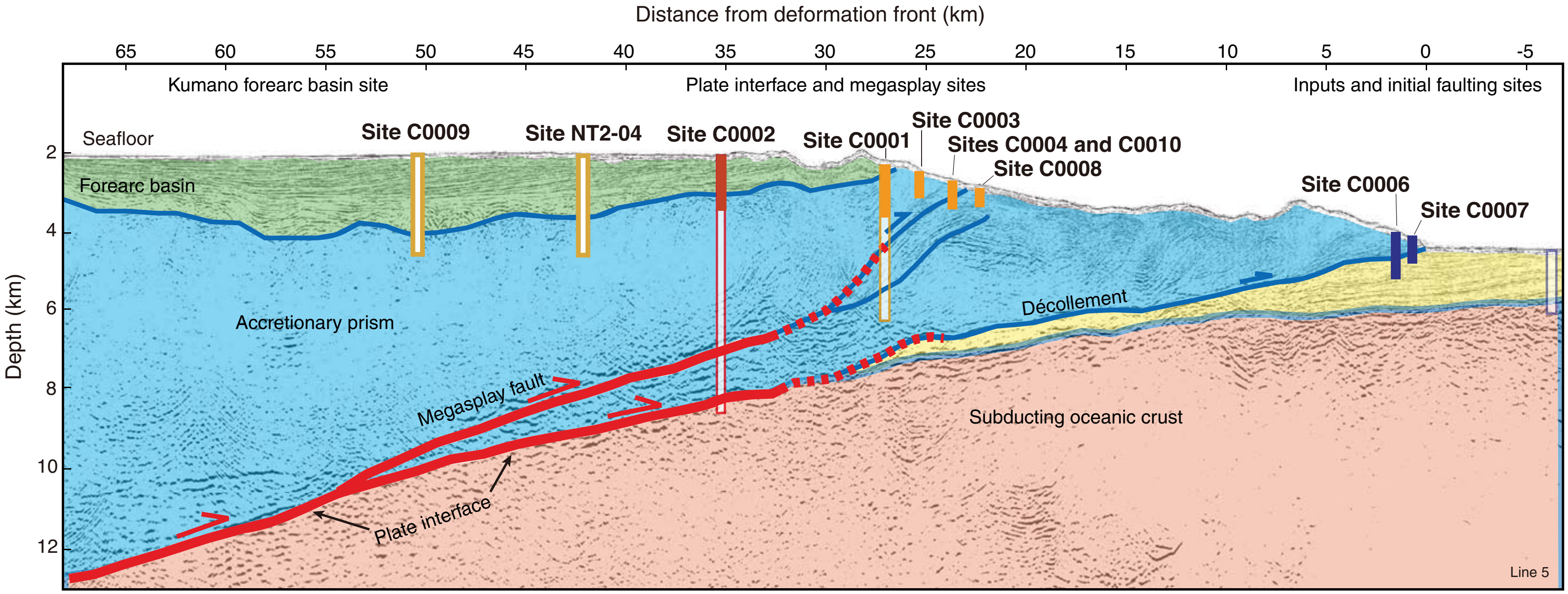

Figure F3. Seismic line from three-dimensional volume showing drill site locations (Araki et al., 2009).

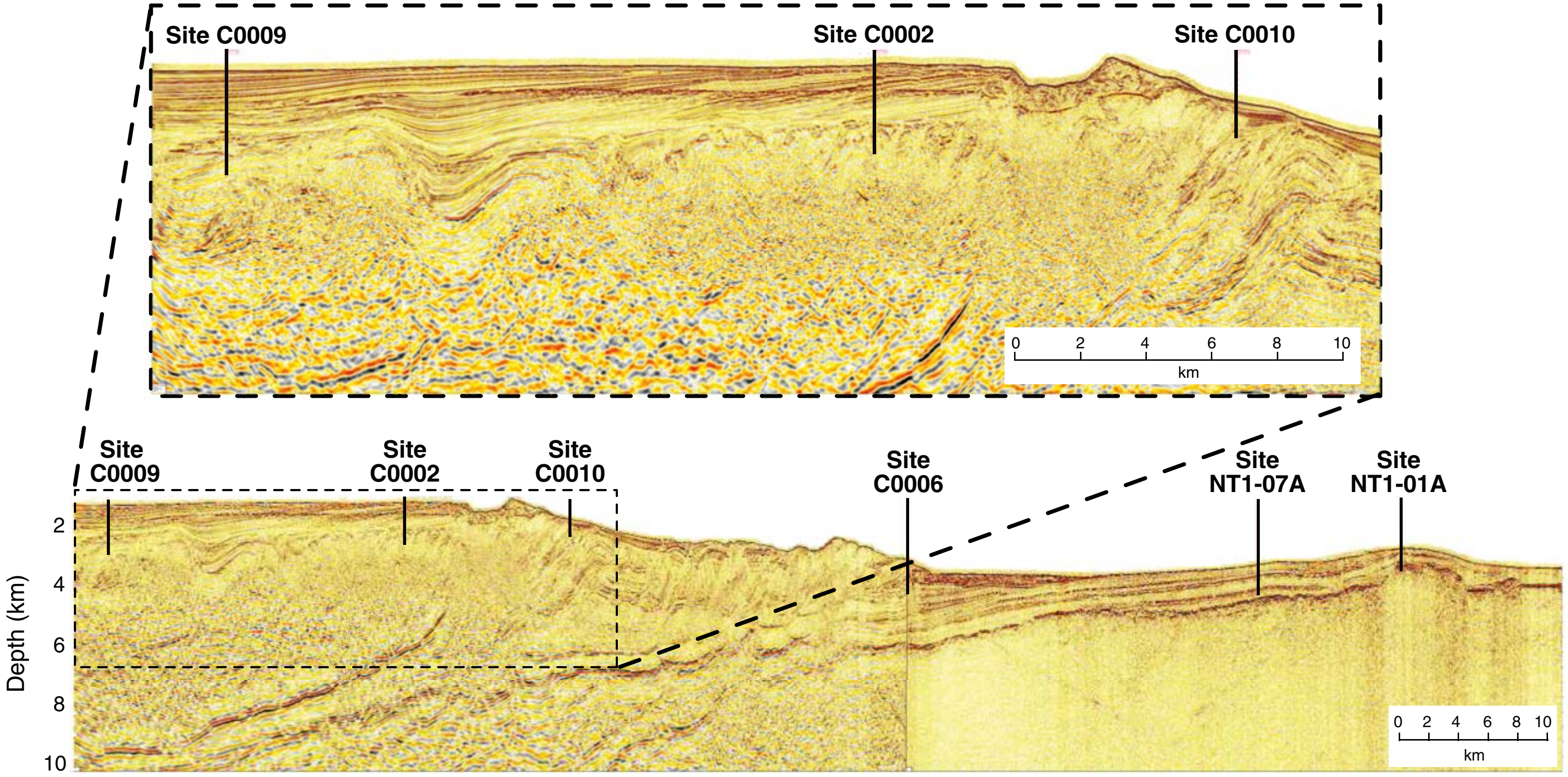

Figure F4. A. Seismic section showing location of Site C0009, including several regional surfaces interpreted within the Kumano Basin (see text for discussion). (**Continued on next page.**)

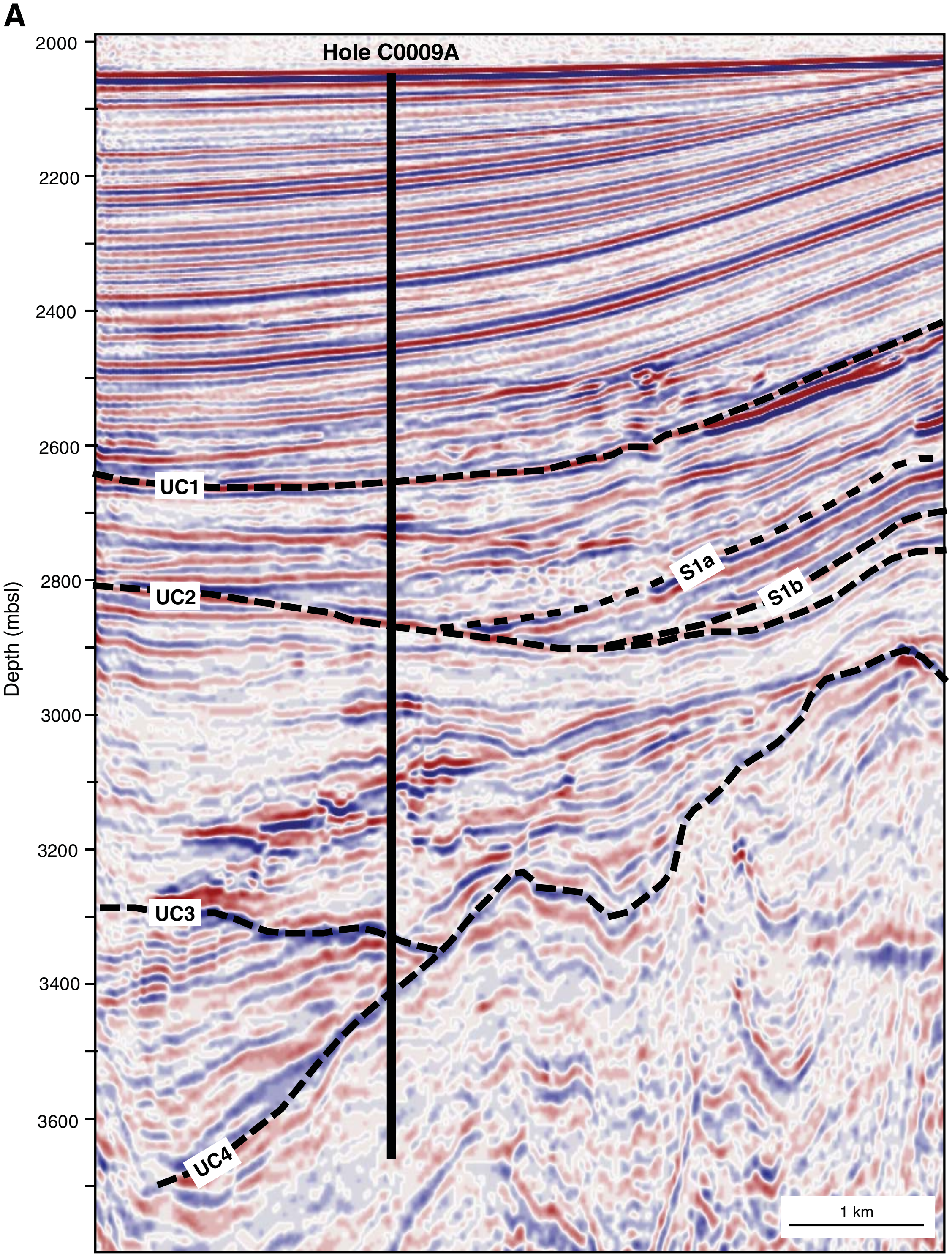

Figure F4 (continued). B. Seismic section showing location of Site C0010.

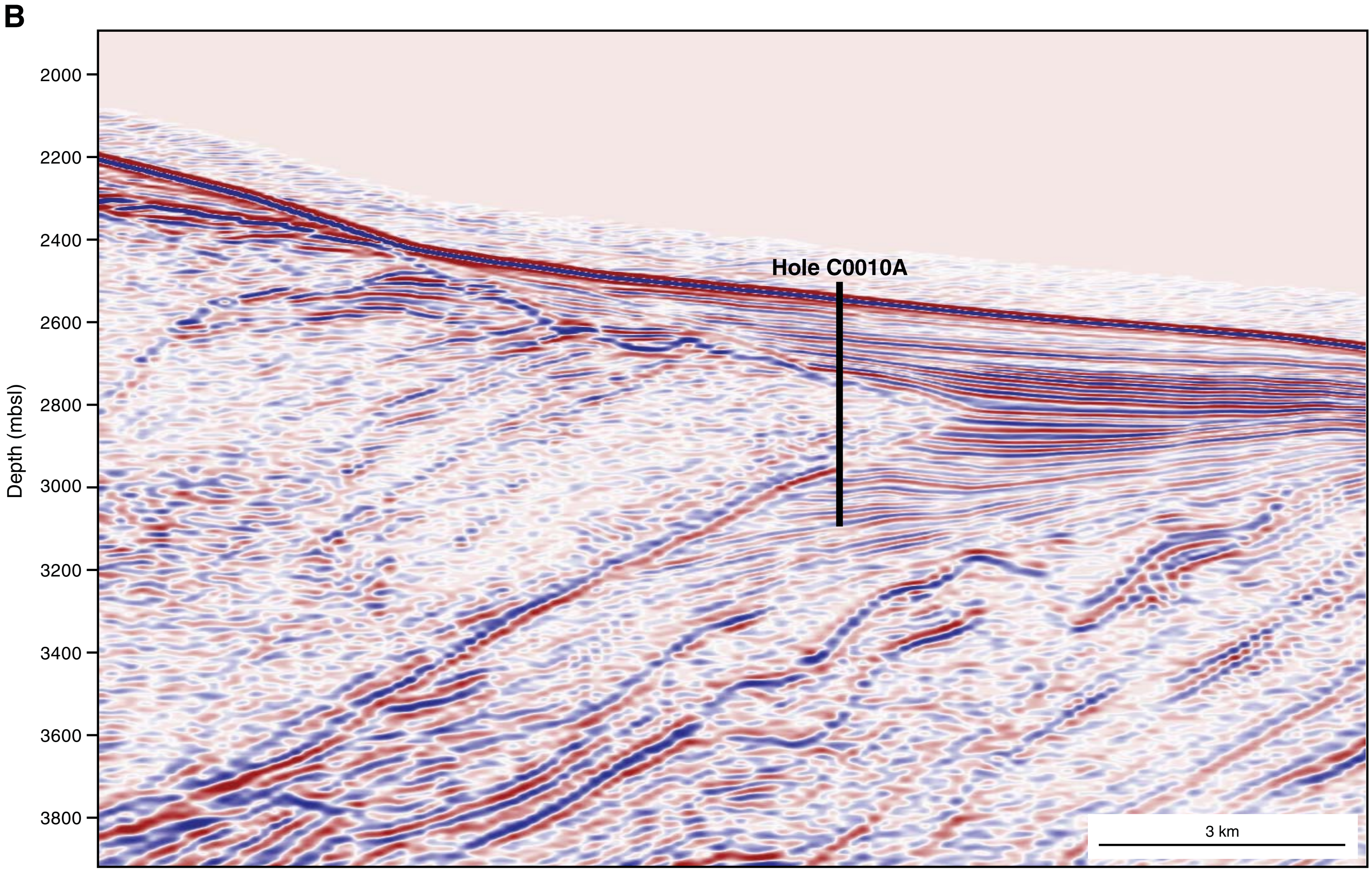

Figure F5. A. Site summary diagram for Site C0009 showing wireline logs and cuttings/core from 700 to 1600 mbsf. SP = spontaneous potential, LOI = loss on ignition, FMI = Formation MicroImager. (Continued on next page.)

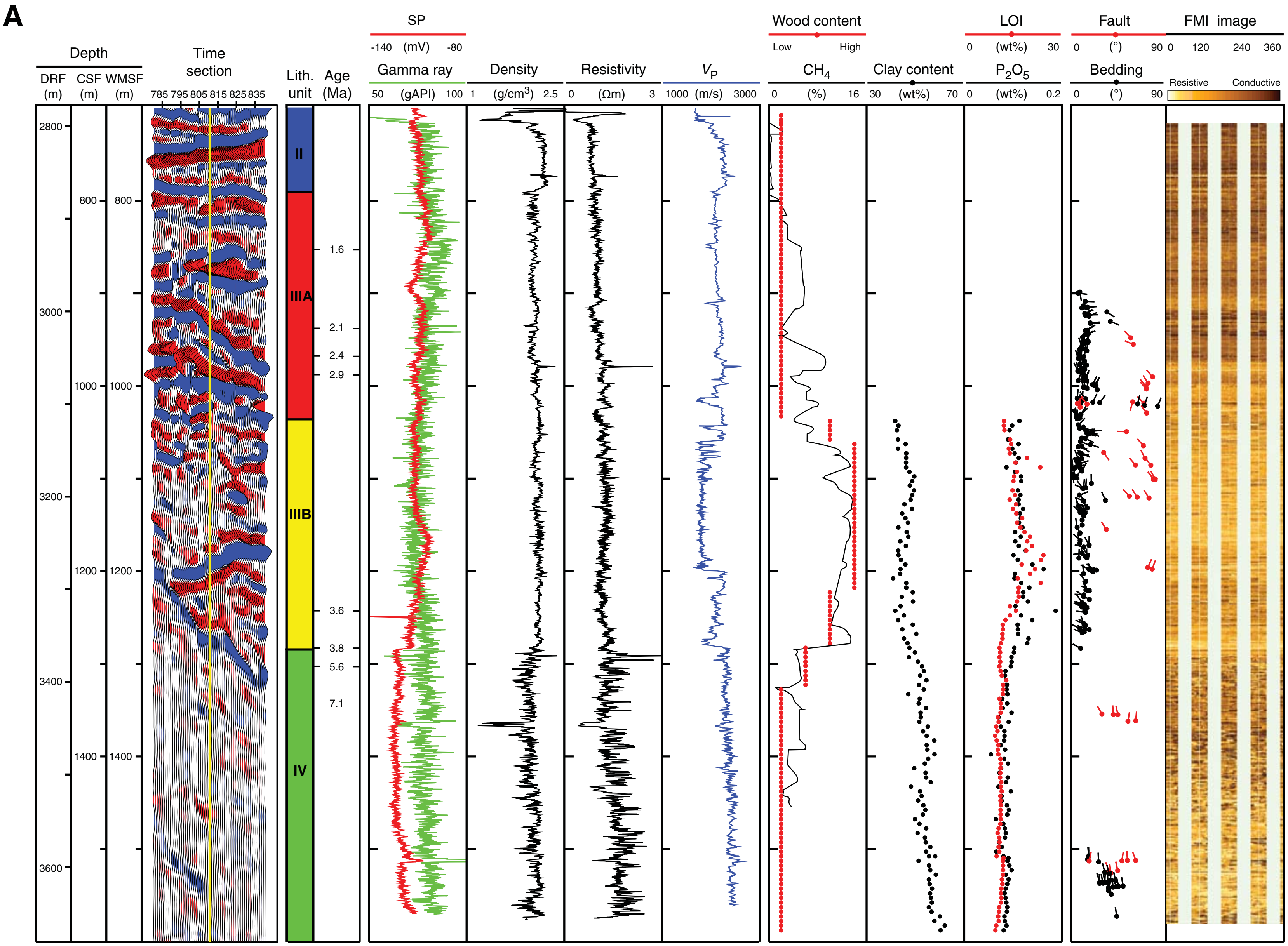

Figure F5 (continued). B. Site C0009 site summary diagram from 1510 to 1594 m CSF. PEF = photoelectric effect, MAD = moisture and density.

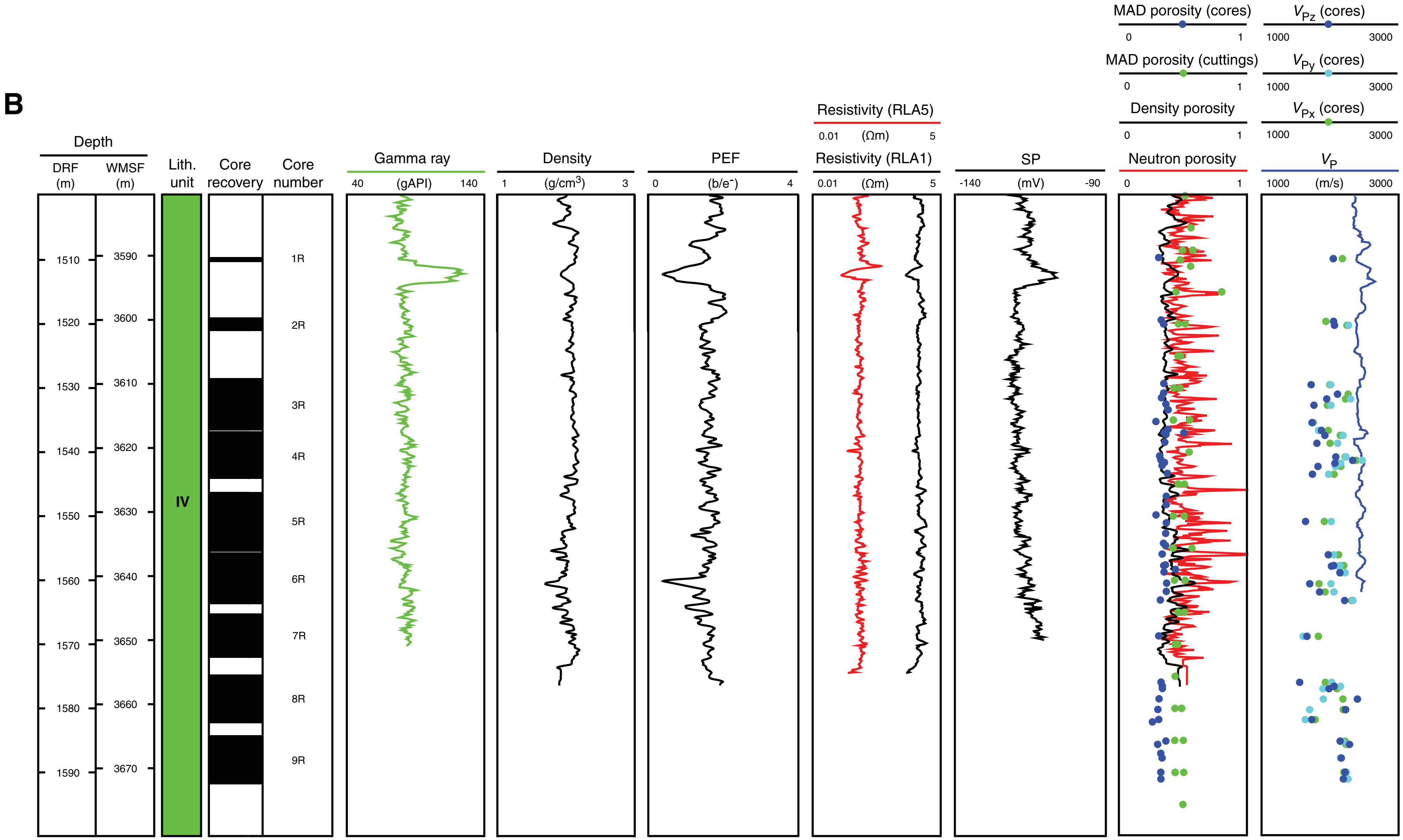

Figure F6. A. Detailed seismic line at Site C0009 as in Figure F4, with lithologic units and ages overlain. (Continued on next two pages.)

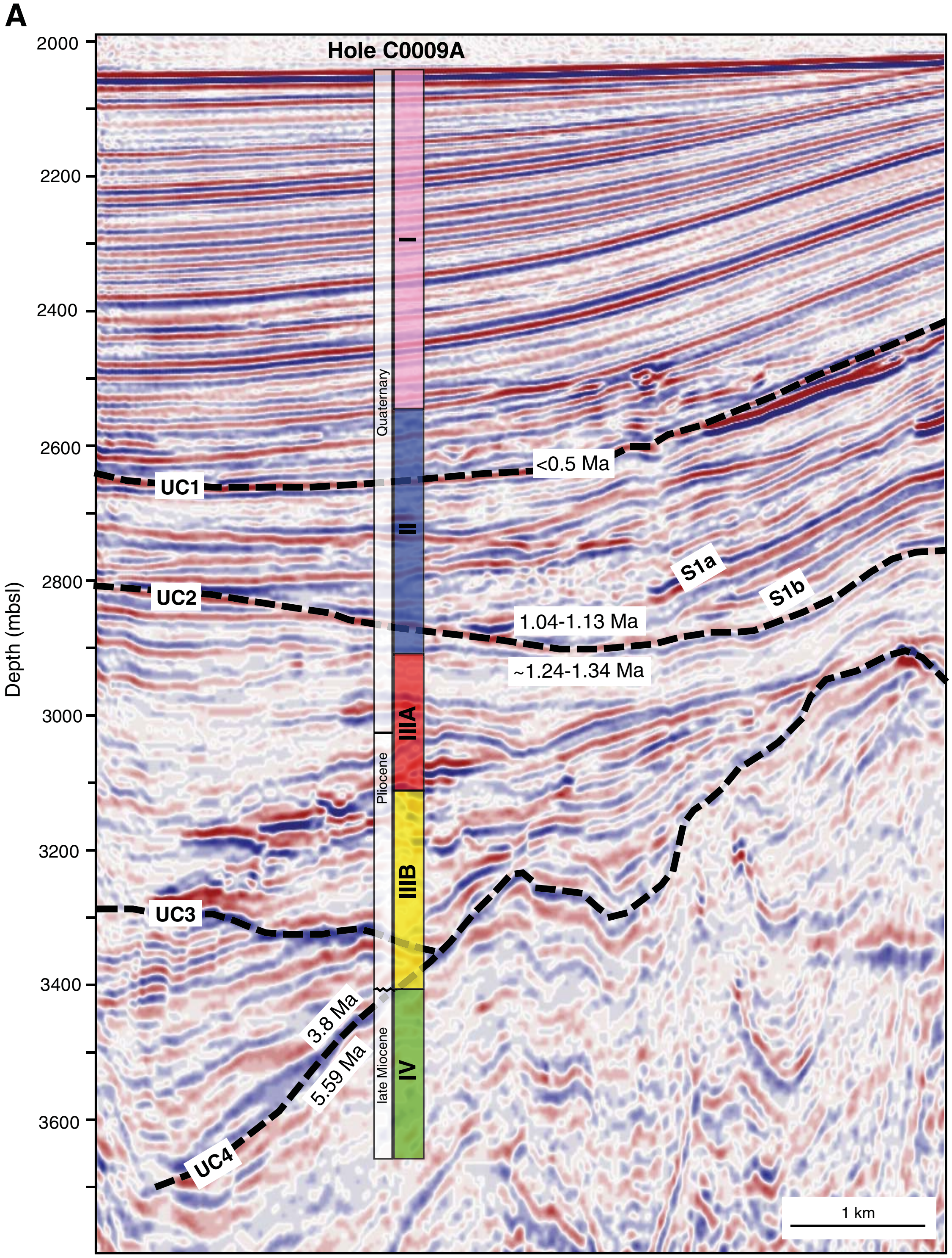

Figure F6 (continued). B. Regional seismic line showing correlation between Sites C0009 and C0002, including stratigraphic columns. (**Continued on next page.**)

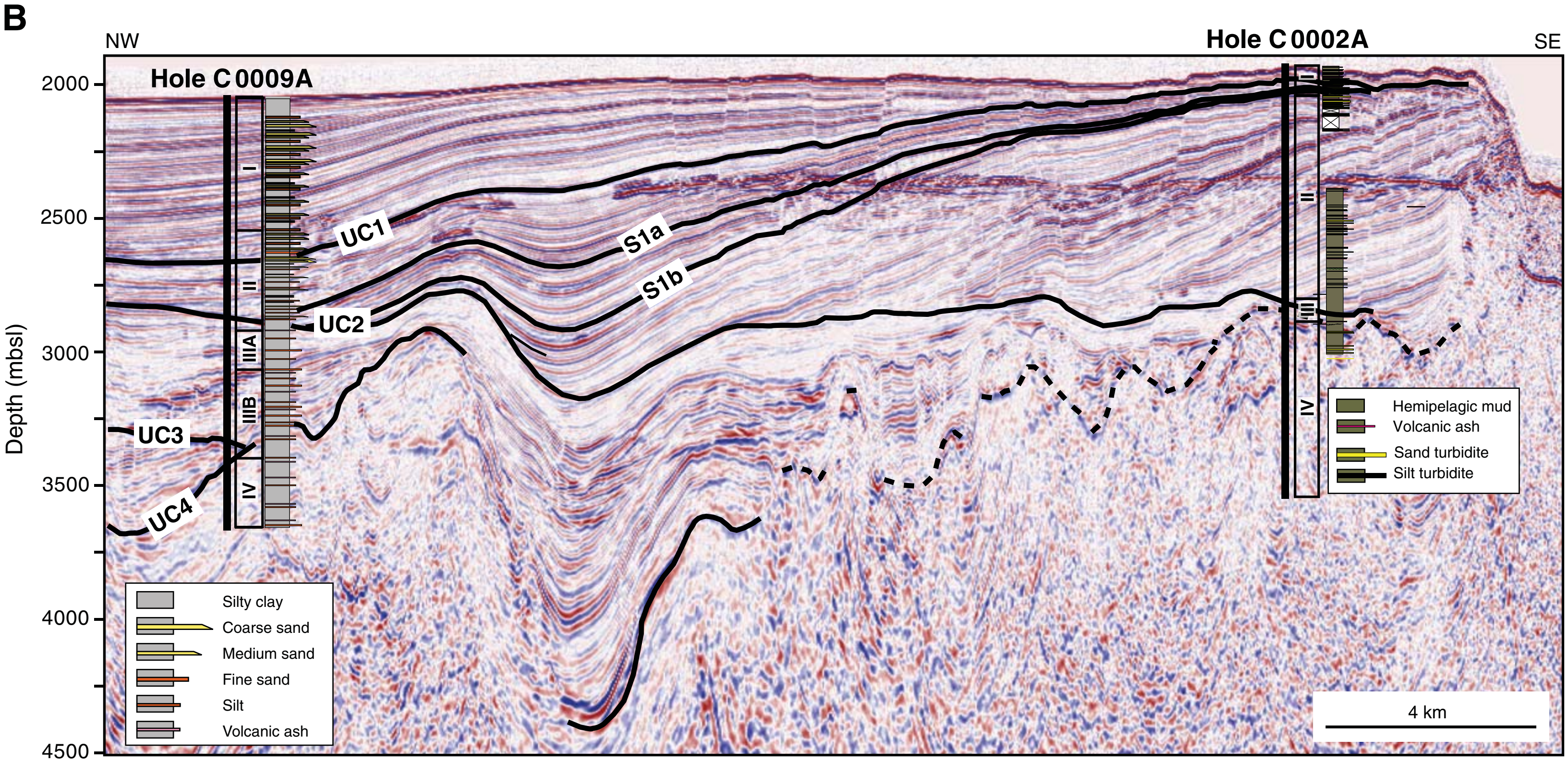

Figure F6 (continued). **C.** Interpretation of seismic profile in Figure F6B, showing lithologic units and ages. Inset shows detail of Units III–IV at Site C0002.

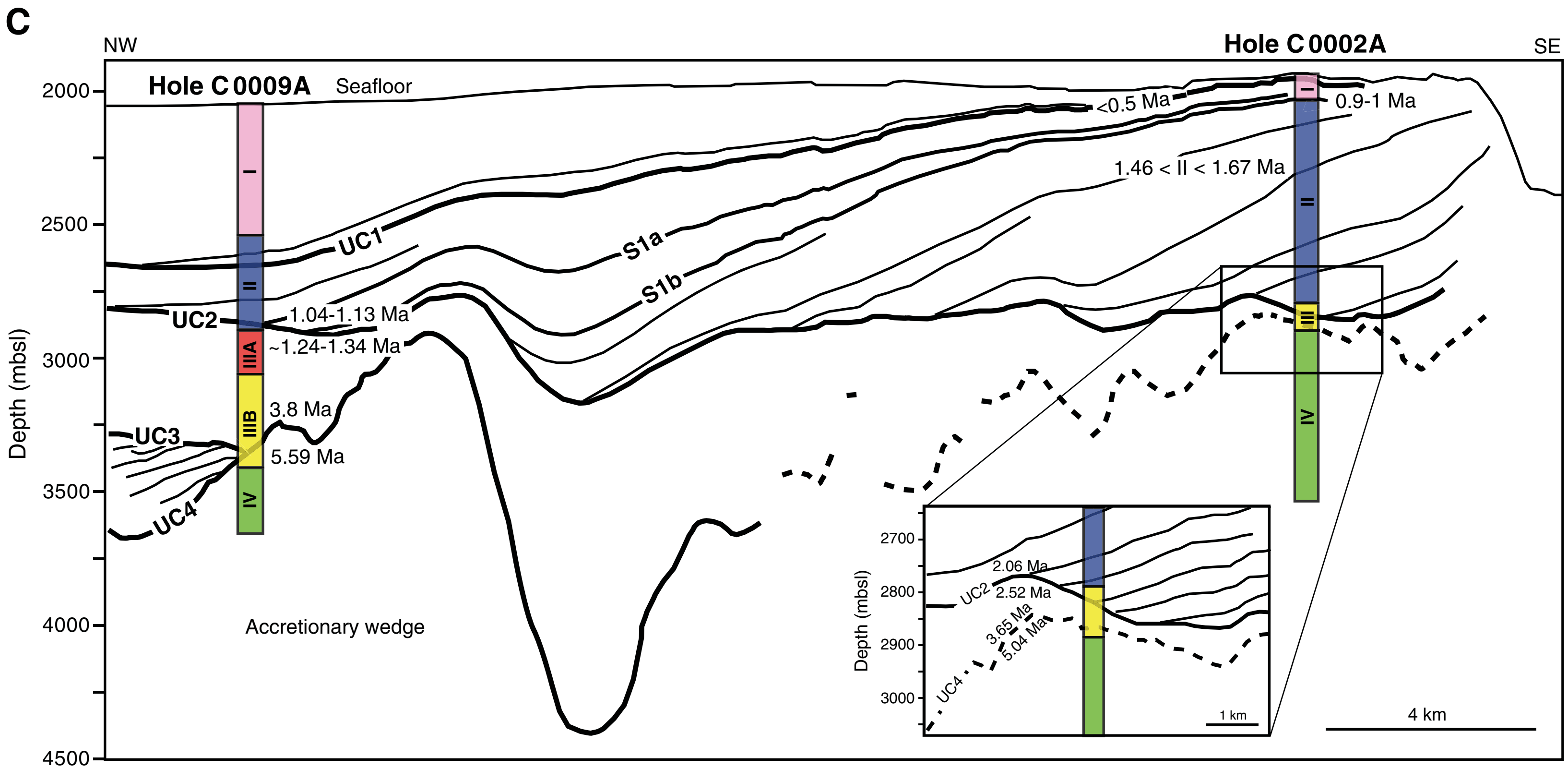

Figure F7. Map showing orientations of maximum horizontal stress (S_1) inferred from borehole breakouts (see also Kinoshita et al., 2008). At Site C0002, red line = orientation in forearc basin sediments, blue line = orientation in underlying accretionary prism. GPS = Global Positioning System.

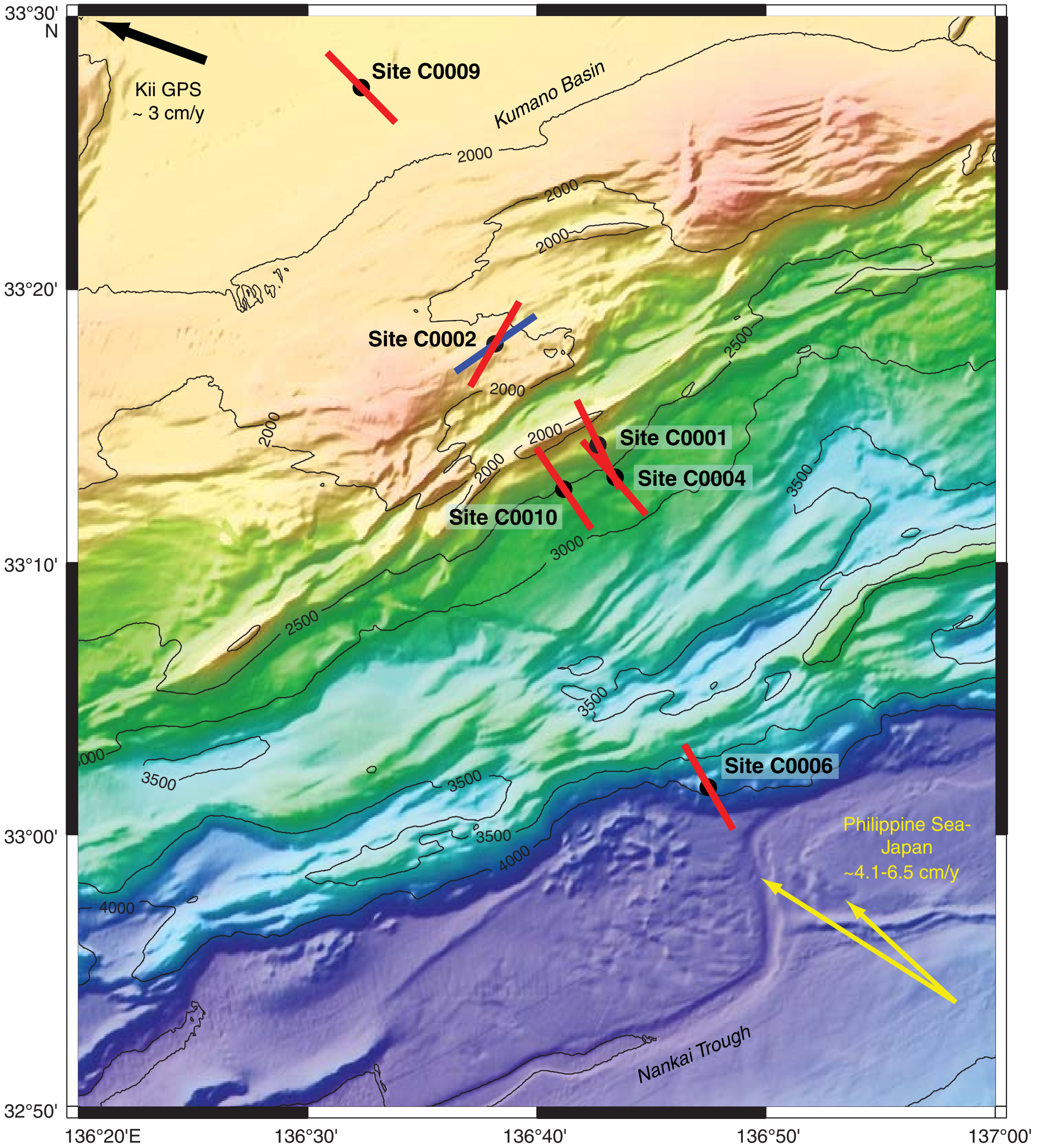

Figure F8. V_P/V_S ratio, P-wave velocity and resistivity, and mud gas concentrations at Site C0009.

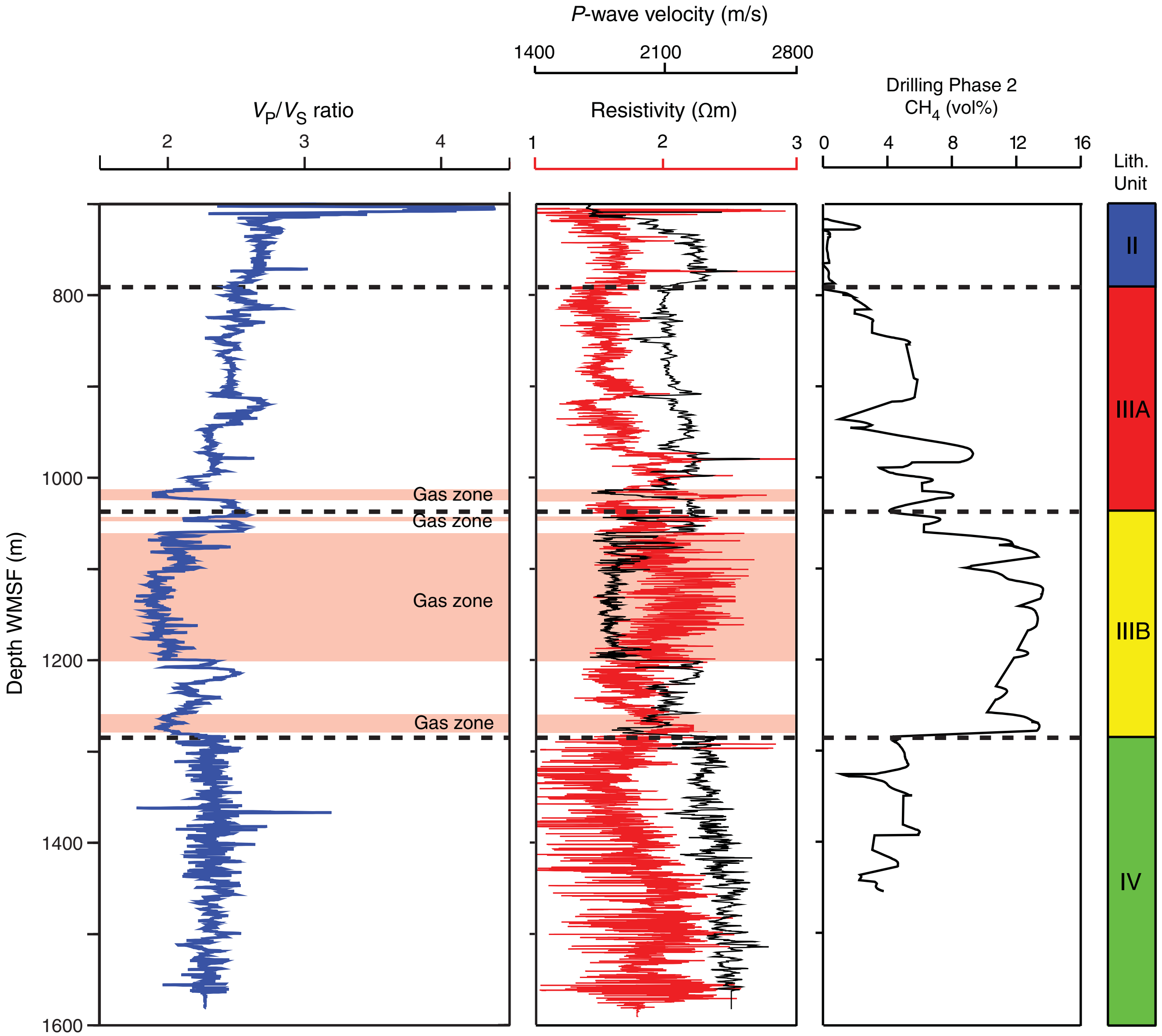

Figure F9. A. Summary of pressure and stress measurements, Site C0009. Blue triangles = pore pressure measurements, orange circles = static mud pressure measurements in the borehole, open square = minimum stress measured by LOT, solid square = MDT hydraulic fracturing tests. **B.** Summary of fluid mobility (defined as permeability/fluid viscosity) from single probe MDT tests.

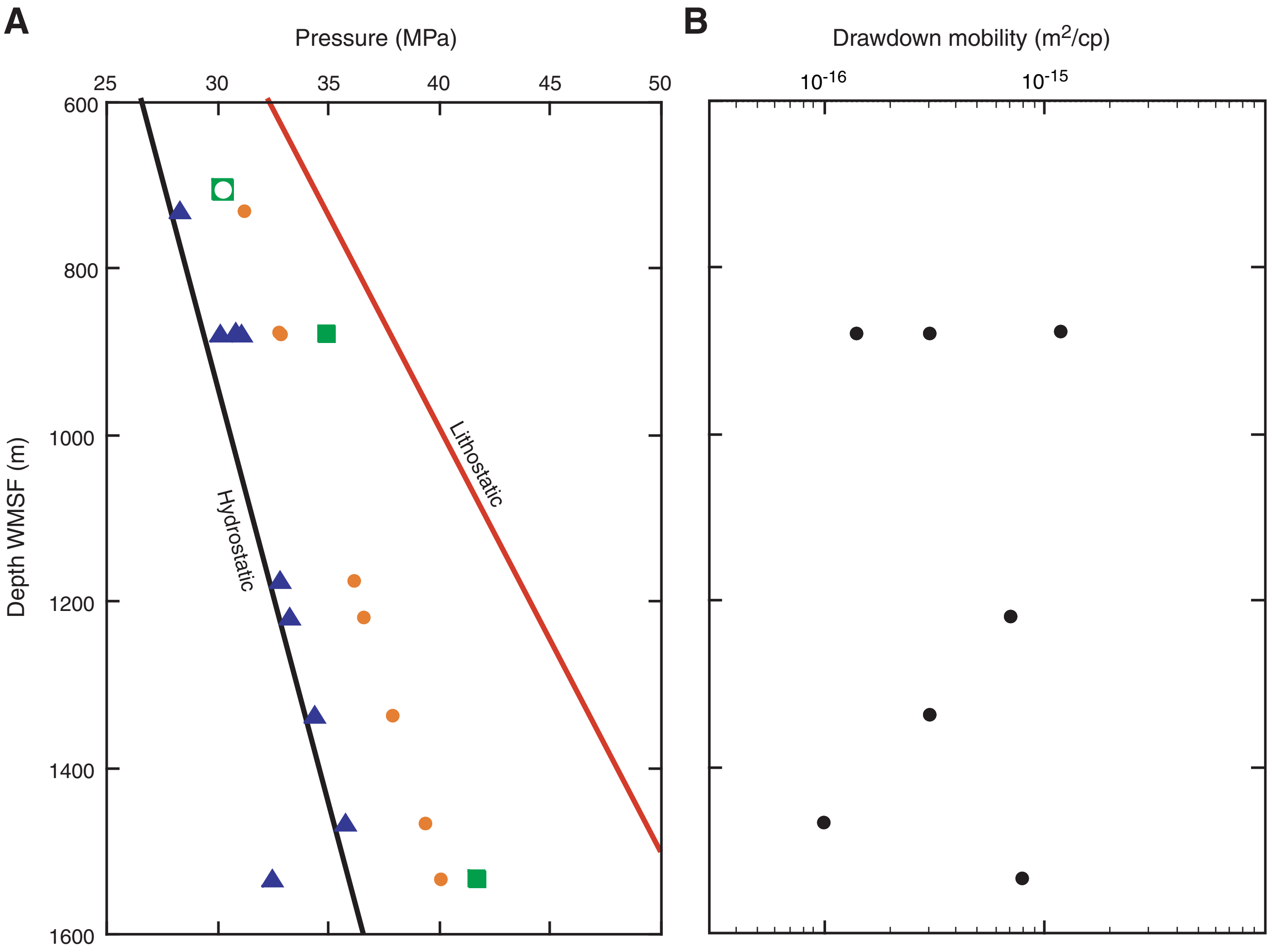

Figure F10. Summary diagram showing LWD/MWD and seismic data at Site C0010. Key elements of casing and hole suspension are shown at right: blue = casing screens, black = casing shoe, thin black = retrievable packer, thin red = smart plug.

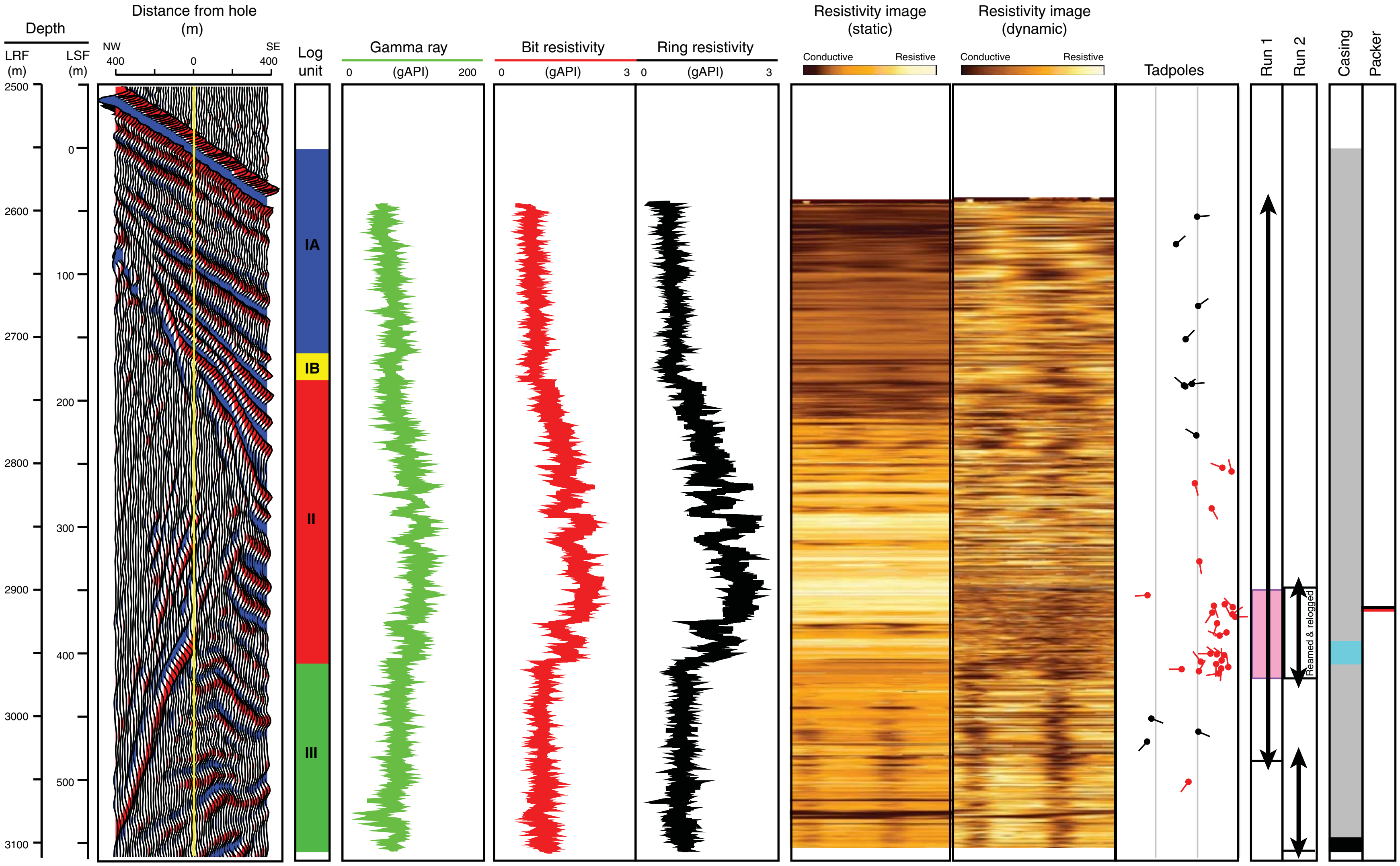

Figure F11. A. Seismic section correlating between Sites C0004 and C0010. **B.** Basic interpretation of seismic line. Solid line = seafloor, dashed lines = top and base of the thrust wedge, vertical black lines = borehole locations, gray lines = gamma ray (GR) logs, red lines = resistivity logs. For Site C0010, logging units are shown; for Site C0004, both logging units (left) and lithologic units defined by coring (right) are shown. Note that the vertical exaggeration (VE) is greater in the interpretation.

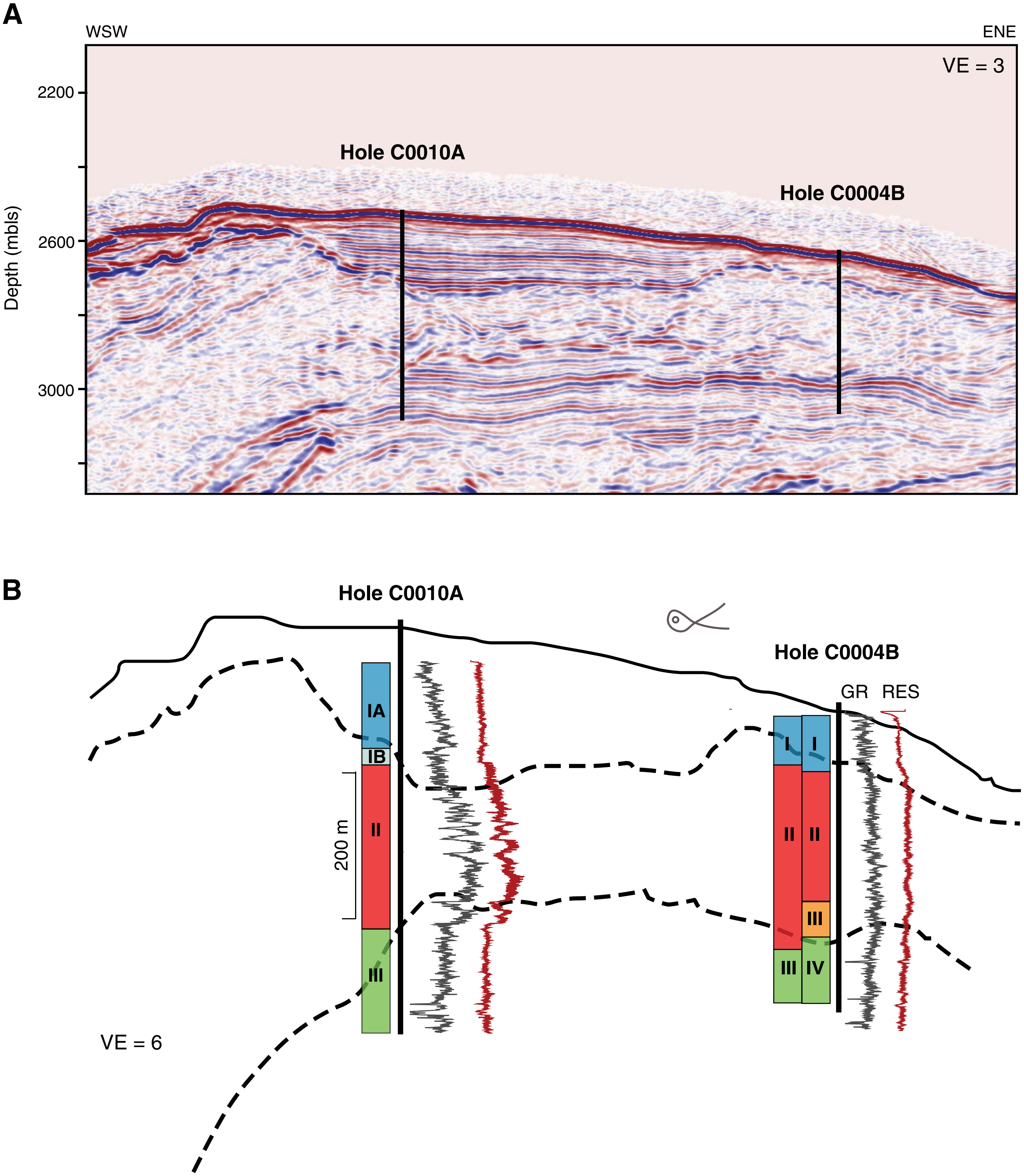

Figure F12. **A.** Schematic diagram showing dummy run test sensor tree instrument configuration. **B.** Photos of the dummy run assembly on the rig floor. (**Continued on next two pages.**)

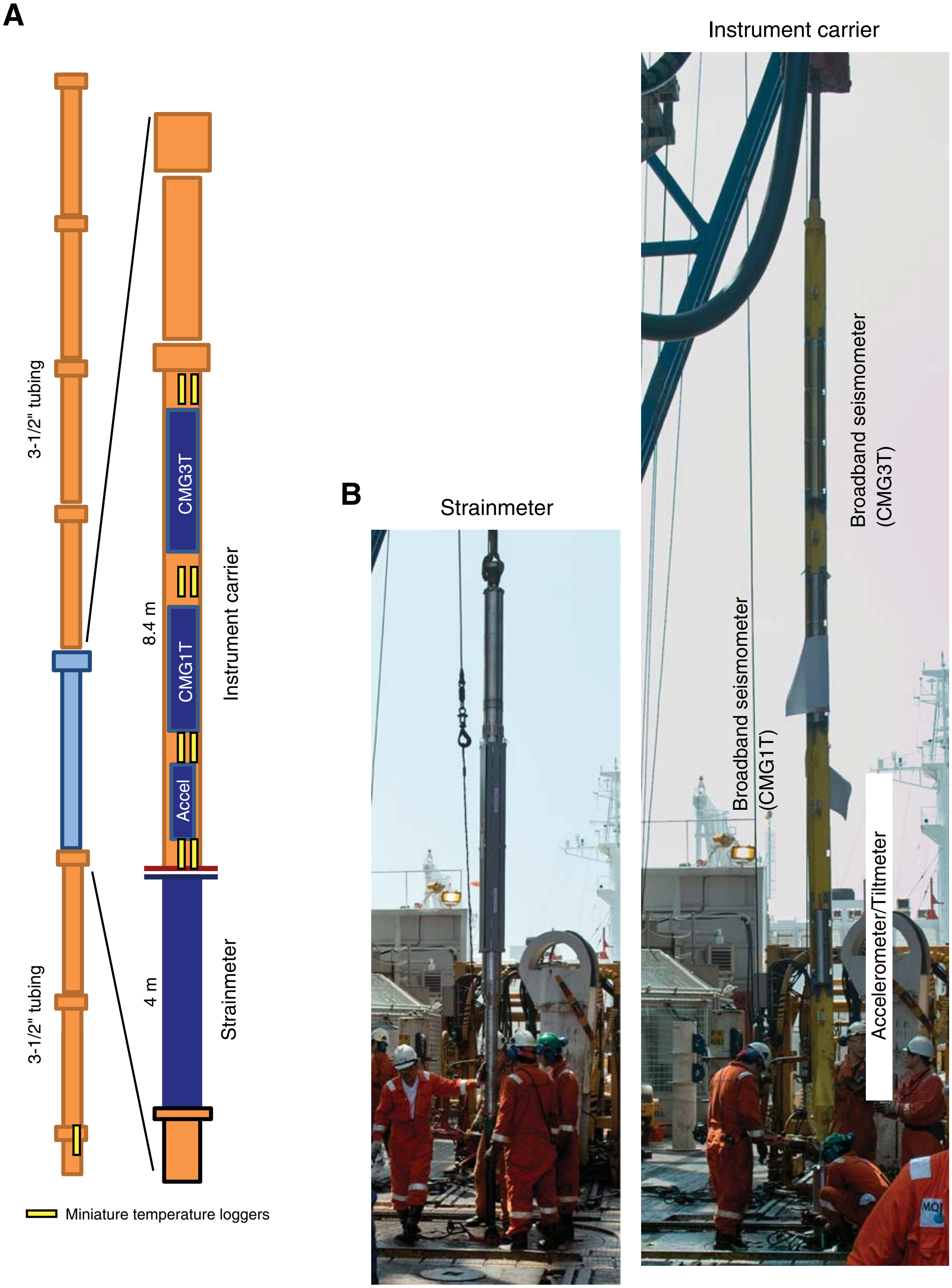

Figure F12 (continued). C. Schematic showing the configuration of screens and sensors for hole suspension with the smart plug sensors. (**Continued on next page.**)

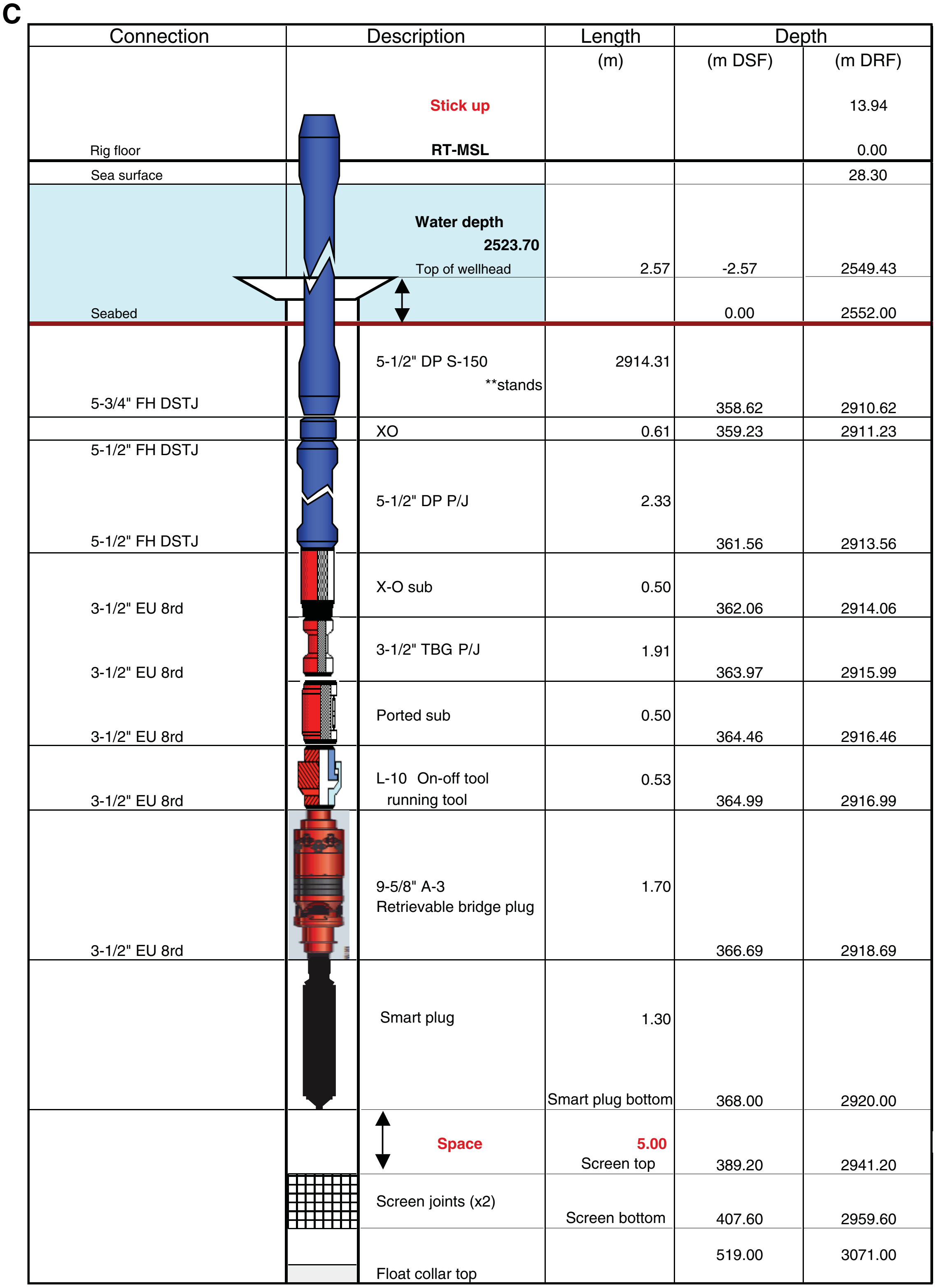

Connection	Description	Length	Depth	
		(m)	(m DSF)	(m DRF)
	Stick up			13.94
Rig floor	RT-MSL			0.00
Sea surface				28.30
	Water depth 2523.70			
	Top of wellhead	2.57	-2.57	2549.43
Seabed			0.00	2552.00
5-3/4" FH DSTJ	5-1/2" DP S-150 **stands	2914.31	358.62	2910.62
	XO	0.61	359.23	2911.23
5-1/2" FH DSTJ 5-1/2" FH DSTJ	5-1/2" DP P/J	2.33	361.56	2913.56
3-1/2" EU 8rd	X-O sub	0.50	362.06	2914.06
3-1/2" EU 8rd	3-1/2" TBG P/J	1.91	363.97	2915.99
3-1/2" EU 8rd	Ported sub	0.50	364.46	2916.46
3-1/2" EU 8rd	L-10 On-off tool running tool	0.53	364.99	2916.99
3-1/2" EU 8rd	9-5/8" A-3 Retrievable bridge plug	1.70	366.69	2918.69
	Smart plug	1.30 Smart plug bottom	368.00	2920.00
	Space	5.00 Screen top	389.20	2941.20
	Screen joints (x2)	Screen bottom	407.60	2959.60
	Float collar top		519.00	3071.00

Figure F12 (continued). D. Photo of the smart plug (bottom) and retrievable casing packer (top) shortly before running it to the seafloor for reentry.

D

Figure F13. Schematic showing planned long-term observatory configuration. ROV = remotely operated vehicle.